NRL REPORT R-3412

PRELIMINARY DESIGN OF THE AN/SPS-2 (XDQ) ANTENNA

R. J. Adams, K. S. Kelleher and C. R. Lundquist

February 4, 1949

APPROVED FOR PUBLIC
RELEASE - DISTRIBUTION
UNLIMITED

Approved by:

Dr. R. C. Guthrie, Head, Search Radar Section
Mr. L. A. Gebhard, Superintendent, Radio Division II

NAVAL RESEARCH LABORATORY
CAPTAIN F. R. FURTH, USN, DIRECTOR
WASHINGTON, D.C.

DISTRIBUTION

BuShips	
Attn: Code 916	10
CNO	
Attn: Op-413-B2	5
Attn: Operational Evaluation Group	1
ONR	
Attn: Code N-482	2
CO, ONR, Boston	1
OinC, NRL Field Station, Boston	
Attn: Dr. H. Krutter	2
Dir., USNEL	2
Attn: Code 323	1
Cdr., USNOTS	
Attn: Reports Unit	2
SNLO, USNELO	2
Ch. of Staff, USAF	1
OCSigO	
Attn: Ch. Eng. & Tech. Div., SIGTM-S	1
CO, SCEL	
Attn: Dir. of Engineering	2
Dir., ESL, Belmar, N. J.	2
BAGR, CD, Wright-Patterson Air Force Base	
Attn: BAU-ADD	1
CG, AMC, Wright-Patterson Air Force Base	
Attn: Eng. Div., Electronics Subdiv., MCREEO-2	1
Attn: Code MCREEP	1
Attn: Engineering Div., Project RAND	1
CO, 4151st Air Force Base Unit, Red Bank	
Attn: Ch. Eng. Div., WLENG	1
CO, 4153rd Air Force Base Unit, Cambridge	
Attn: ERCAJ-2	1
CO, AMC, Electronics Research Lab., Cambridge	
Attn: Dr. R. C. Spencer	1

DISTRIBUTION (Cont.)

OinC, USNEU, NBS	
Attn: Electronics Division	1
INSMAT, Brooklyn for Airborne Instruments Lab.	
Attn: Mr. M. Chaffee	1
RDB	
Attn: Library	2
Attn: Navy Secretary	1
Science and Technology Project	
Attn: Mr. J. H. Heald	2

CONTENTS

Abstract vi

Problem Status vi

Authorization vi

INTRODUCTION 1

Coverage 1
Antenna Specifications 1
Modified Specifications 2

REFLECTOR VERSUS LENS ANTENNA 2

Electrical Considerations 2
Mechanical Considerations 9

SYMMETRICAL VERSUS ASYMMETRICAL REFLECTOR 10

Effect of Feed Obstruction on Pattern 10
Effect of Reflector on Mismatch 10
Disadvantages of Asymmetrical Reflector 11
Pattern Evaluation 11
Feed Problem 16

MULTIPLE-FEED PROBLEM 19

Illumination-Taper Problem 19
Space Attenuation 19
Dependence of Horn Size on f/D Ratio 20
Primary Patterns Versus Horn Aperture 21
Illumination Taper as a Function of f/D Ratio 25

HORN DESIGN AND THE MULTIPLE-FEED PROBLEM 25

Horn Designs for Improved Directivity 25
Methods of Improving Aperture Efficiency 26
Methods of Overlapping Apertures 34

REFLECTOR-SHAPING AND THE MULTIPLE-FEED PROBLEM 45

Artificial Tapering of Illumination 45
Alteration of the Reflector Contour 52
Deformation of the Phase Front 52

PRELIMINARY X-BAND DESIGN OF THE AN/SPS-2 ANTENNA 53

Method of Pattern Calculation 54
Method of Gain Calculation 60
Pattern Calculation for Final Model 61

CONTENTS (Cont.)

Experimental Patterns 66
Gain Calculations 66
Impedance Match of Horn Feed 69

PRELIMINARY L-BAND DESIGN OF THE AN/SPS-2 ANTENNA 78

ACKNOWLEDGMENT 81

APPENDIX I 83

APPENDIX II 85

APPENDIX III 89

ABSTRACT

The first model of an antenna for the AN/SPS-2 long-range search and height-finding radar set has been developed.

The system utilizes seven beams stacked in the vertical plane at such close spacing that the aperture dimensions of the horns in the feed array are severely restricted. The resulting over-illumination of the reflector reduces the gain and leads to excessively high side lobes. An effort has been made to avoid this difficulty by improving the feed horn directivity or by deforming the reflector in such a way as to broaden the secondary beam, but none of these measures has proved completely successful.

The antenna described in this report consists of a symmetrically-cut paraboloidal reflector of elliptical contour, fed by an array of ordinary horns of limited aperture. An f/D ratio of 0.88 has been chosen to provide the best compromise between illumination tapering and coupling between channels. The reflector dimensions of an X-band model are 60-3/4 x 24 x f = 21.1 inches, while the horns measure 0.8 x 1.05 inches in the E- and H-planes. The illumination taper averages 4 db in the vertical plane, 14 db in the horizontal.

The vertical patterns, which cross over at the 2-db level, have on the average a beam width of 3.15 degrees and a maximum side lobe of 18 db. In the azimuth plane the beam widths are 1.55 degrees, while the side lobes are nearly 30 db down. The gain of the lowest beam is 36.5 db, corresponding to an aperture efficiency of 49 percent.

These results are in good agreement with values given by formulas for the pattern and gain of antennas of elliptical aperture.

The Raytheon Manufacturing Company is constructing an L-band model of the antenna, of dimensions 36′ 6″ x 14′ 5″ x f = 12′ 8″, and will conduct flight tests to determine the effectiveness of the stacked-beam system as a height finder.

PROBLEM STATUS

This is an interim report; work is continuing.

AUTHORIZATION

NRL Problem No. R02-22R.

PRELIMINARY DESIGN OF THE AN/SPS-2 (XDQ) ANTENNA

INTRODUCTION

Coverage

The AN/SPS-2 is a 1300-Mc radar set designed to provide reliable detection of targets of one square meter cross section out to a range of 300 nautical miles as well as height finding with an accuracy of at least $\pm$ 1/2 degree.[1] Two versions of this set have been considered. One has the triangular coverage diagram shown in Figure 1 and is intended for plotting the course of missiles such as the V-2. The other provides coverage to a uniform altitude of 90,000 feet, which is sufficient for the detection or interception control of aircraft. Triangular coverage may be realized from a single paraboloidal reflector by means of several closely stacked beams. Each feed horn is part of a separate radar system on a different frequency. The antenna for coverage to 90,000 feet is similar except that the transmitting power is derived from a single high-power magnetron and must be divided among the feed horns with careful attention to phase. In either system, height finding is accomplished by comparison of signals received on the two beams which bracket the target. This report describes the development of a seven-beam, multiple-frequency antenna designed for the first type of coverage. The single-frequency system is still in the preliminary stages and may be the subject of a later report.

Antenna Specifications

Present design of the multiple-frequency AN/SPS-2 system requires eight beams stacked in the vertical plane as follows:[2]

Beam Number	Elevation Angle	Beam Width
1	1.0°	2.4°
2	3.1	2.3
3	5.2	2.5
4	7.5	2.8
5	10.0	2.9
6	12.5	2.9
7	15.0	3.0
8	17.7	3.2

[1] A. A. Varela, "Proposed Very Long Range Radar with Height Finding," NRL Report R-2759, 18 February 1946, Confidential.

[2] A. A. Varela, "Interim Report on the AN/SPS-2 (XDQ) Radar System," NRL Report R-3313, 14 July 1948, Confidential.

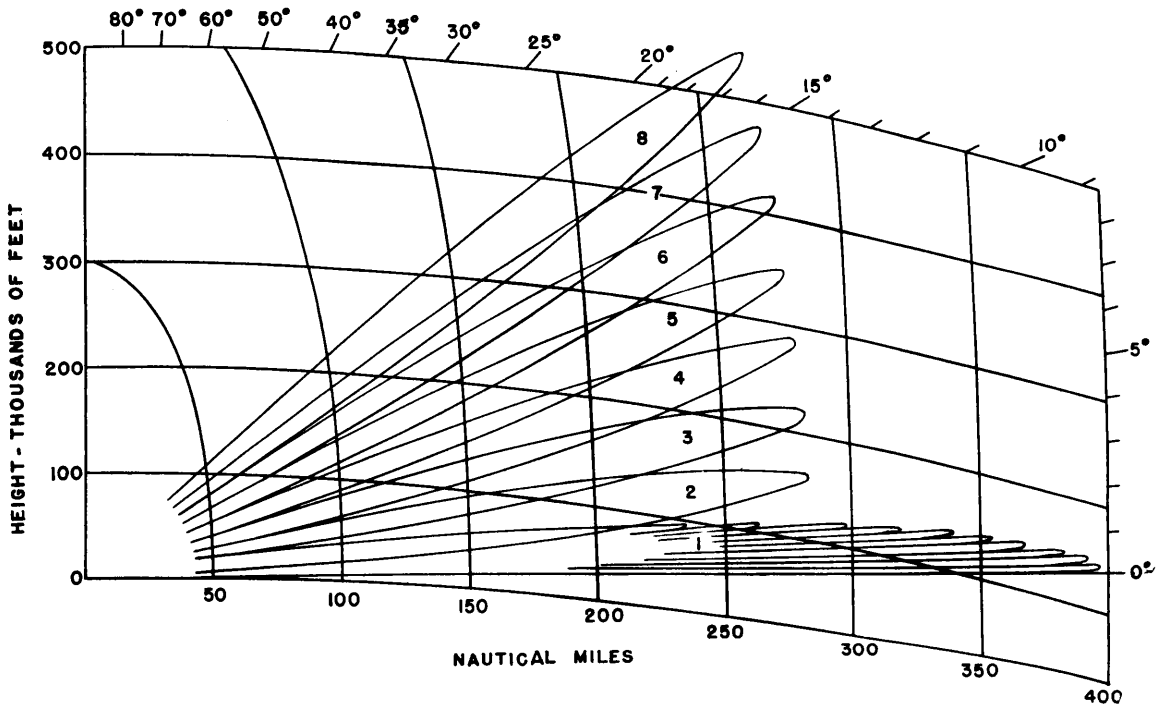

Fig. 1 - Proposed coverage diagram for the AN/SPS-2 radar

This arrangement, shown graphically in Figure 1, provides coverage to nearly 20 degrees with a 2-db crossover level between adjacent beams. The horizontal beam widths are all 1.5 degrees, so that the gain of the on-axis beam is 39 db. At 1300 Mc, a reflector approximately 36 feet wide by 21 feet high is required.

Modified Specifications

Preliminary antenna work showed that it would be very difficult to broaden successive beams as indicated above, since the 2-db crossover requirement limits the horn aperture in the vertical plane, which in turn prevents the illumination grading essential in beam broadening. Accordingly a single compromise beam width of 3.2 degrees has been chosen. This reduces the necessary antenna height to 15 feet and the gain to 37.7 db but ensures coverage to more than 20 degrees with only seven beams.

REFLECTOR VERSUS LENS ANTENNA

Electrical Considerations

Two general types of focusing devices are in current use for radar antennas, reflectors and lenses. From the standpoint of pattern quality it is advantageous to use a lens because (1) the tolerances on lens dimensions are much less critical[3], (2) the feed structure does not block the aperture, and (3) excellent off-axis correction can be achieved by shaping

---

[3] Winston E. Kock, Proc. IRE, 34, 828-836, November 1946.

both surfaces of the lens. While recognizing these usual advantages, it was felt that in this particular case they were not essential since the required pattern quality was attainable with a reflector. Moreover, the lens possesses certain mechanical disadvantages which will be discussed in the next section.

In considering the first factor effecting pattern quality, it may be noted that at this frequency the tolerances on plate contour and lens warpage are easily met. The plate spacing should be held to $\pm 1/4$ inch (in 5-1/2 inches) in order to keep path length variations within an eighth wavelength. By comparison, the tolerance on a reflector surface must be 1/2 inch in order to maintain an equal uniformity of the phase front. It is evident then that in regard to tolerances, careful mechanical design would permit the use of either a reflector or a lens for the AN/SPS-2 system.

Although it is a definite advantage to have the aperture clear of feed structure, the pattern of a large reflector is modified only slightly by the presence of the feed horn.

Finally, in regard to off-axis correction, it is realized that the binormal lens developed at the AMC Electronics Research Laboratory, Cambridge Field Station, maintains pattern quality out to the order of 25 beam widths. For present purposes, however, a range of 5 beam widths is adequate, and this can be obtained with a reflector of reasonable f/D ratio. Further, in the type of antenna to be described in this report, the off-axis patterns are limited by insufficiently tapered illumination rather than by phase errors. This point was not well understood when the project was undertaken, and it seemed desirable to compare the patterns of a metal-plate lens with those of a paraboloidal reflector of approximately the same f/D ratio to determine whether there was any significant difference in the off-axis performance. The results have no direct application to the problem at this stage but are included here as a matter of interest.

The lens shown in Figure 2 was loaned for this study by H. L. Gerwin of Radio Division III. Designed for a wavelength of 3.4 cm, this lens has a square aperture 48 inches on a side, with four steps along the axes, and a 48-inch focal length. Two feed horns were made up to give, respectively, an illumination taper of 10 and 20 db to the edges of the lens. For each horn, a sequence of patterns was run with the feed set at various angles to the axis in the plane of the pattern. The results are shown in Figures 3 through 6. The patterns are best for the more extreme taper, as would be expected, and for beam deflection in the H-plane. The reflector used for comparison, shown in Figure 7, has a 40-inch diameter and 30-inch focal length and was fed by a horn providing 15-db taper. Figure 8 is a set of H-plane patterns from this reflector. Taking into account the difference in f/D ratio and in illumination taper, it appears that a reflector and a conventional metal-plate lens give approximately equal performance under the same conditions.

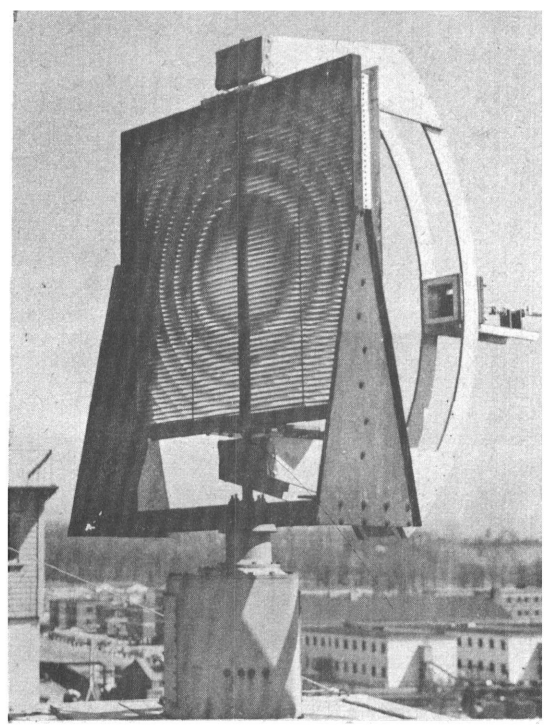

Fig. 2 - Arrangement for testing off-axis patterns of metal-plate lens

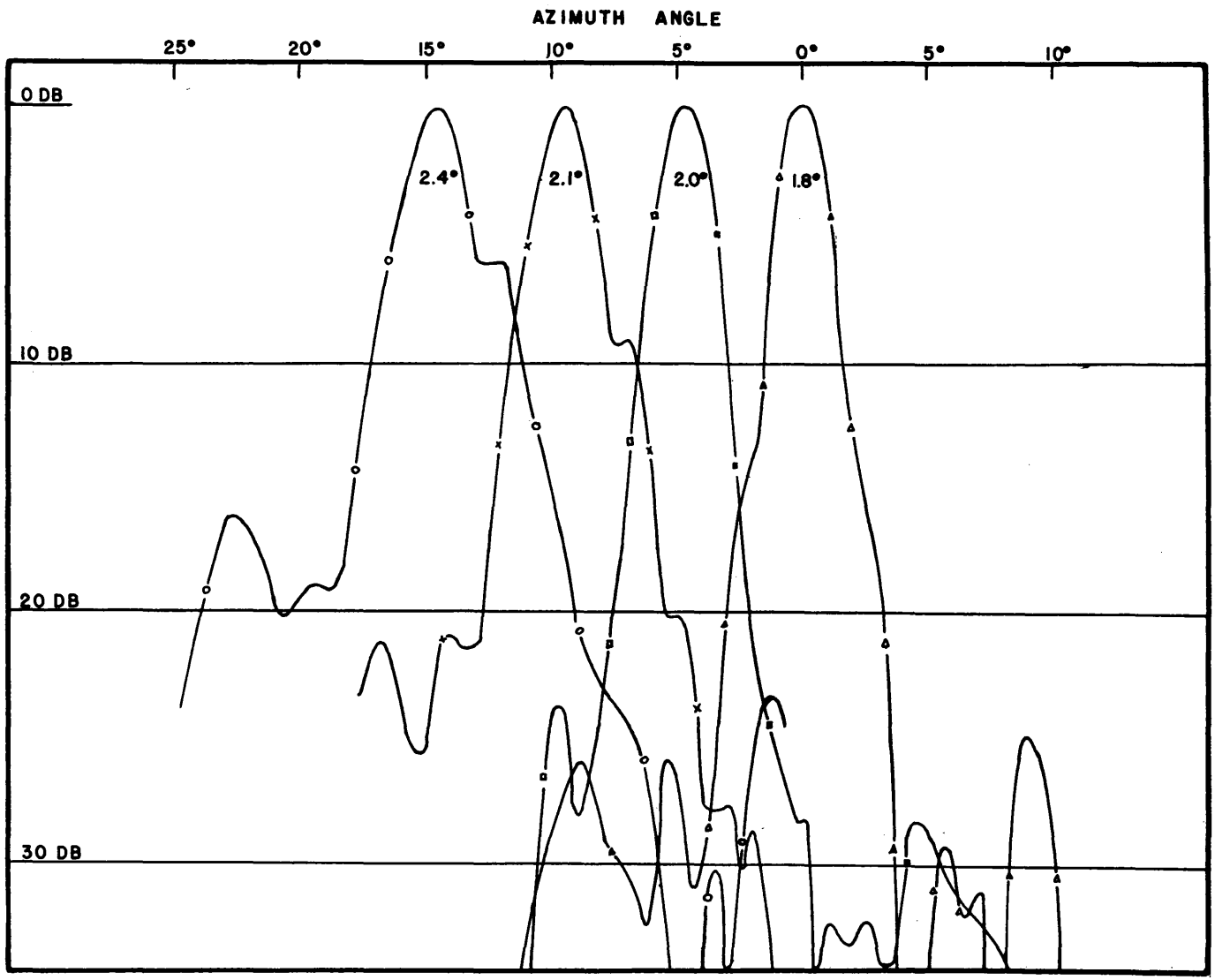

Fig. 3 - E-plane patterns of metal-plate lens with 10-db illumination taper

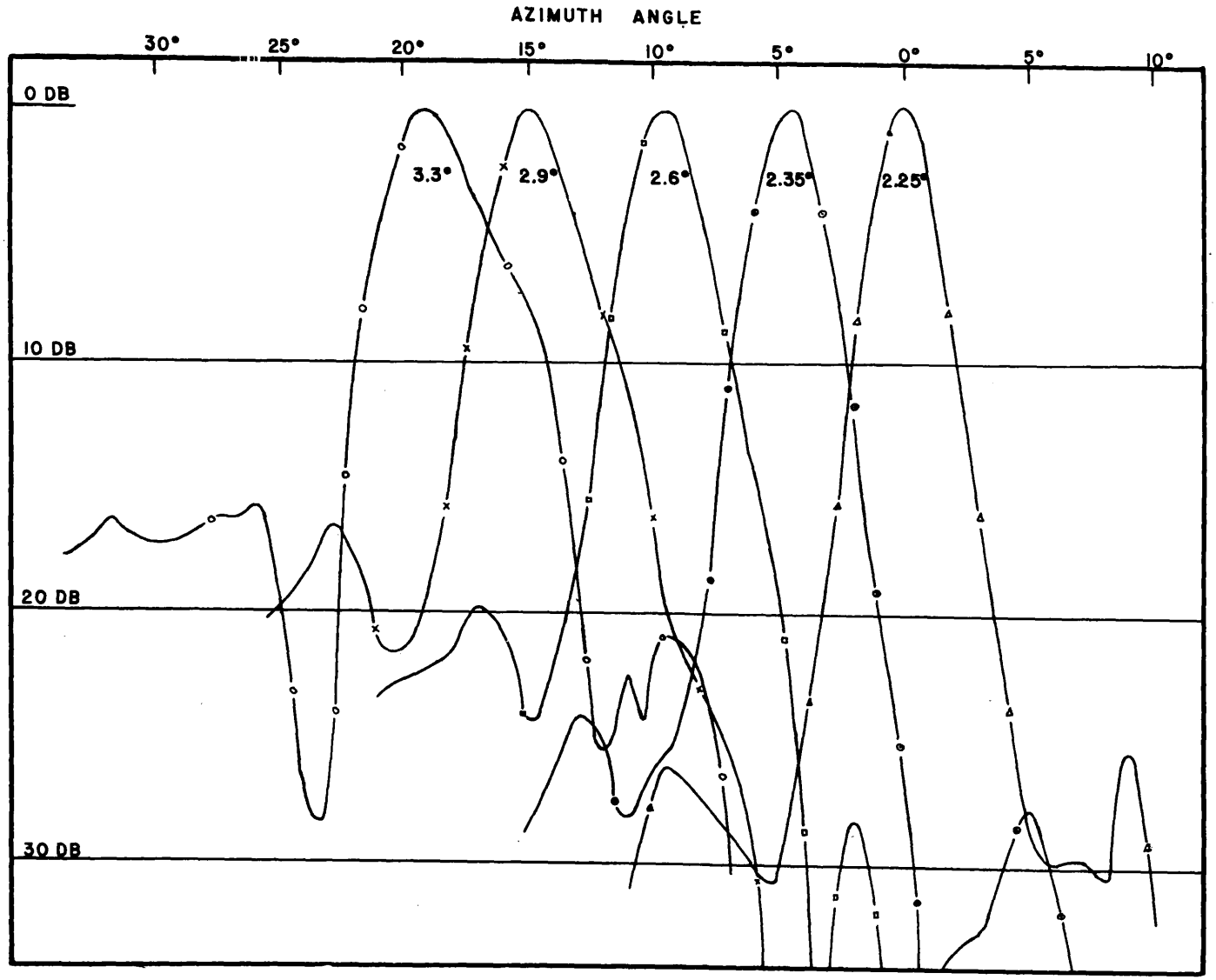

Fig. 4 - E-plane patterns of metal-plate lens with 20-db illumination taper

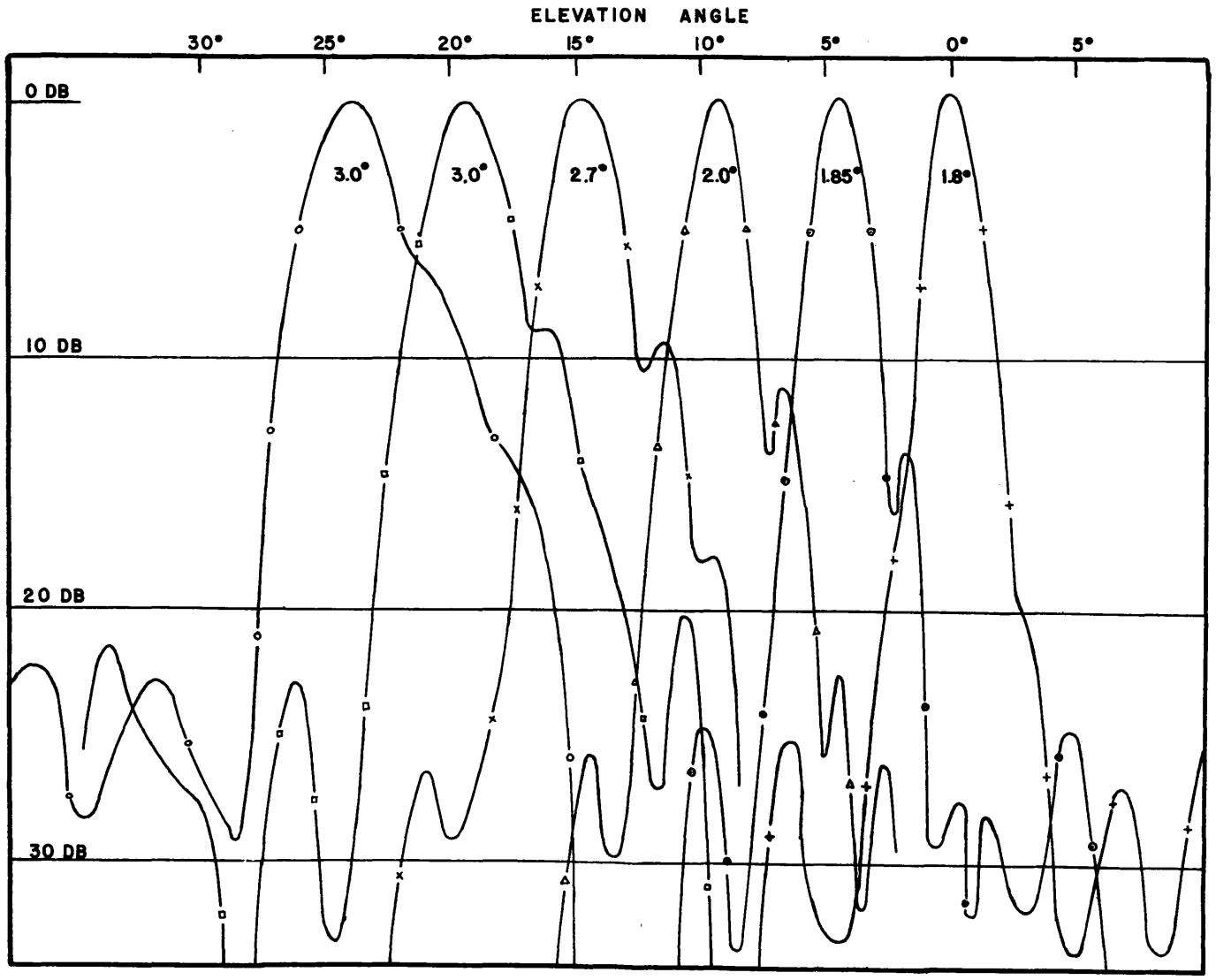

Fig. 5 - H-plane patterns of metal-plate lens with 10-db illumination taper

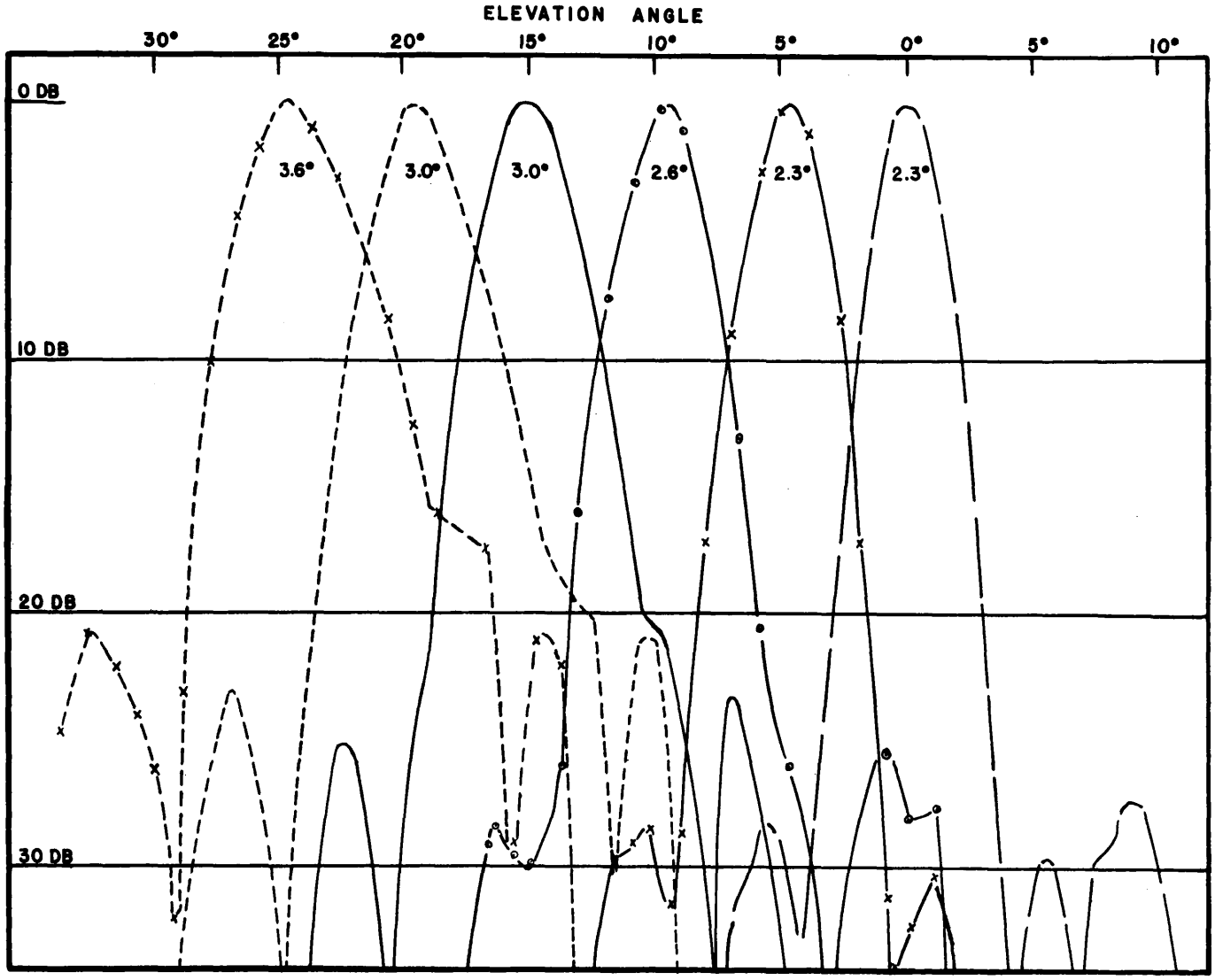

Fig. 6 - H-plane patterns of metal-plate lens with 20-db illumination taper

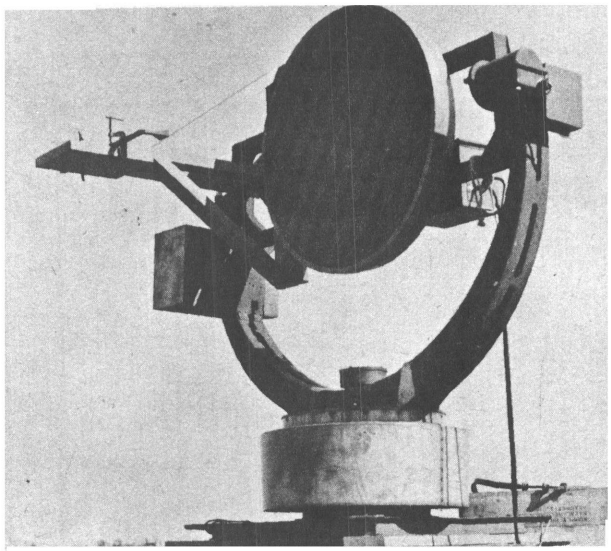

Fig. 7 - Arrangement for testing off-axis patterns of circular paraboloid: diameter, 40 in., focal length, 30 in.

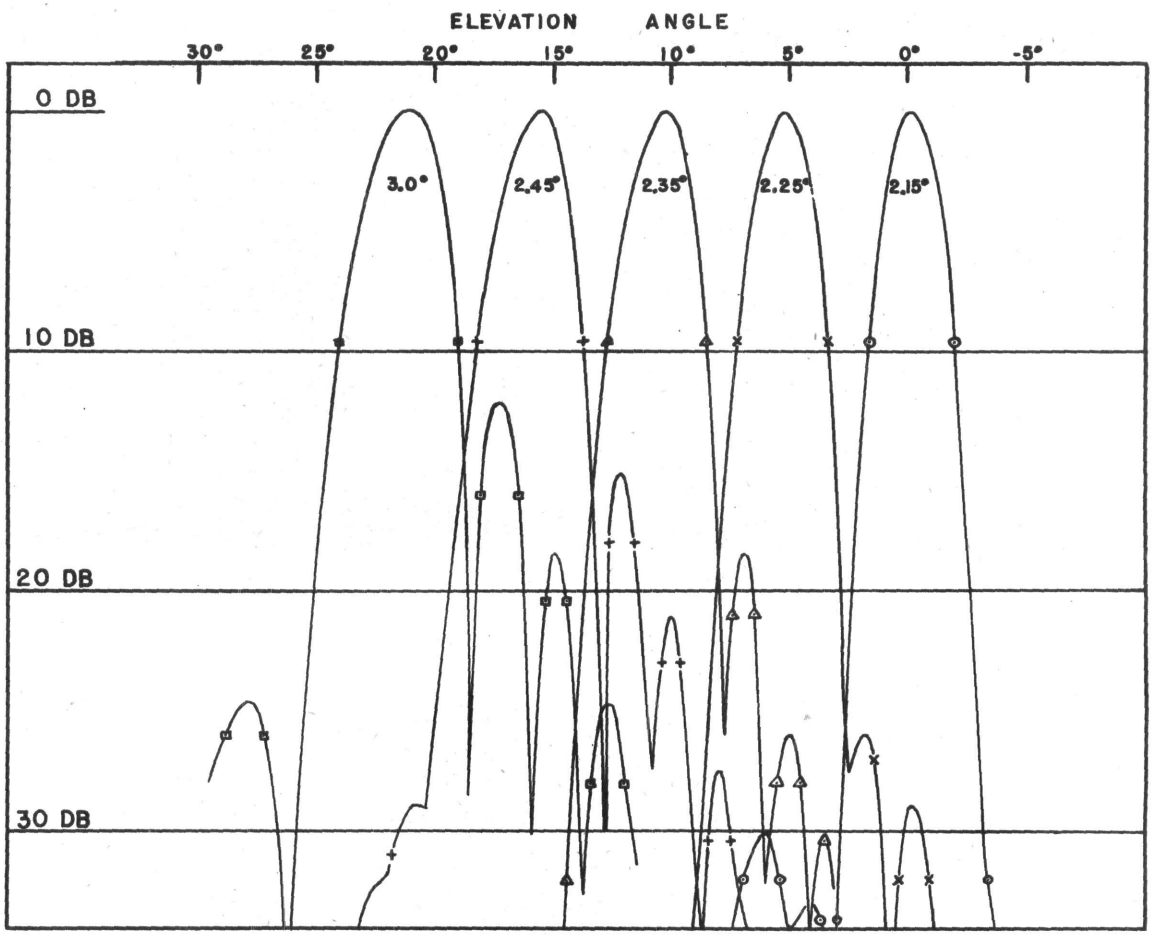

Fig. 8 - H-plane patterns of circular paraboloid with 15-db illumination taper

Mechanical Considerations

A choice for the AN/SPS-2 must be based on mechanical as well as electrical design. In view of its unprecedented size for a shipboard antenna, a reflector is preferred because it (1) may have a smaller focal length, (2) has better structural rigidity, (3) weighs less, and (4) can be expected to perform better under icing conditions.

Focal Length. The focal length of a wide-aperture metal lens is generally made at least as great as the largest dimension of the aperture. This arises from the fact that the number of steps, given approximately by

$$m \approx \frac{1}{8} \frac{D/\lambda}{f/D} \text{ , (Appendix I)}$$

must be kept small. Otherwise the pattern bandwidth may not be adequate and excessive loss of gain may result from shading at the boundaries of the steps. This antenna must operate on seven 10-Mc-wide bands at 1300 Mc, i.e., over a six-percent band. For this reason no more than six steps may be used if the usual value for the index of refraction, 0.6, is chosen.[4] Since a 36-foot aperture is 48 wavelengths at midband, the above relation leads to an f/D ratio of 1.0 and a focal length of 36 feet. The problem of supporting feed horns at this distance from the pedestal is considerable. On the other hand, a 12-1/2-foot focal length is adequate for a 36-foot reflector. This reduces the radius of the turning circle and saves weight in the feed horns since their size increases with the focal length.

Rigidity. Since the aperture of a lens must be kept free of braces that would intercept the beam, most of the stiffening must be accomplished by means of a rigid framework around the edge. Thus the structure is largely confined to a plane and offers little resistance to twisting moments. A further consequence of this type of construction is that the center portion of the lens is at great distance from any fixed support and may resonate at the low vibrational frequencies that are easily excited aboard ship. On the other hand, the back side of a reflector is available for mounting to the pedestal and for effective bracing. At the same time this type of mounting reduces the overturning moment due to the wind, though vanes may be required to compensate unbalanced moments about the vertical axis.

Weight. Appendix II contains calculations of the weight of a metal-plate lens and two types of reflectors of the size required for the AN/SPS-2. The height and width were taken as 14-1/2 and 36-1/2 feet, to agree with dimensions scaled from an X-band model antenna described in a later section. Welded construction of 61ST aluminum alloy was assumed; there was no allowance for the feed system and its braces or for the pedestal. One of the two reflector designs uses 1-inch-mesh screen wire while the other has 4-inch slats at 3-inch spacing. The lens plates have a maximum depth of 31 inches with 23-inch break between steps and are spaced 5-1/2 inches apart. Calculated weights are:

Reflectors:	
Screen wire	1950 lbs.
Slats	2650
Lens:	5550

[4] This is based on Reference (3), Equation (14). The bandwidth curve for a stepped lens shown in Kock's Figure 13 does not seem to agree with this equation.

While these actual weights may not be realistic, it seems definite that the lens would weigh twice as much as a reflector of comparable size.

Icing. Since the plate area of a metal lens is roughly three times as great as the aperture area, a lens may be expected to accumulate a great deal more ice than a screen-type reflector under the same conditions. Furthermore, a lens may be seriously defocussed by ice, which has a dielectric constant of about 3 at 1300 Mc. It is probably impractical to prevent icing by enclosing the lens in a dielectric sheath, since on so doing the wind-resistance may increase by a factor of two. In a reflector, no more than 8 percent of the energy should be reflected from the front surface of ice. Energy loss within the ice can be neglected since the loss tangent is of the order of 0.001 at L-band.

SYMMETRICAL VERSUS ASYMMETRICAL REFLECTOR

It is common practice to cut the contour of a paraboloidal reflector unsymmetrically with respect to one of the principal planes. As compared with the symmetrical design, the asymmetrical reflector has certain advantages which have been considered carefully for possible application to the problem of a multiple-beam antenna.

Effect of Feed Obstruction on Pattern

In a symmetrical dish the feeds obstruct the reflected wavefront, increasing the beam width slightly and raising the horizontal side-lobe level according to the formula[5]

$$p' = \frac{p + q}{1 - q}$$

where p′ and p are respectively the new and original side-lobe ratios to the main beam in field strength, and q is the fraction, weighted according to illumination, of the aperture obstructed by the feed. From the established requirements, it appears that the aperture area should be about 700 square wavelengths. A typical value for the average illumination, one-half of the maximum, reduces this figure to 350. The seven-horn feed assembly and the part of the wave guide obstructing the reflector have a combined area of about 7 square wavelengths, so that q is approximately 0.02. From the formula it appears that a 33-db side lobe in the horizontal plane would be brought up to 27.5 db by this effect.

Effect of Reflector on Mismatch

The horn tilt associated with an asymmetrical reflector reduces the mismatch in the feed line arising from dish reflections,[6]

$$|\Gamma| = \frac{\lambda g}{4\pi f} ,$$

by reducing the gain, g, of the feed horn in the direction of the vertex. However, if the dish is large enough that f/λ exceeds 15, and if the horn is small with a gain of the order of 8 db, the reflection coefficient is less than 0.033 in any case. This is not considered to be prohibitive.

---

[5] S. Silver, "Microwave Antenna Theory and Design," Radiation Laboratory Series Vol. 12, McGraw-Hill, 1949.

[6] T. J. Keary and J. I. Bohnert, "SU-2 Antenna, Shipborne Stabilized Radar Antenna for Sea Search," MIT Radiation Laboratory Report 659, 7 March 1945.

Disadvantages of Asymmetrical Reflector

It is evident that under ordinary circumstances an asymmetrical reflector is to be preferred, but in a multiple-feed antenna two difficulties arise which may outweight the advantages. First, the locus of off-axis feed positions for best horizontal patterns does not coincide with that for best vertical patterns, as in the case of a symmetrical reflector. The required 2-db crossover presents a second problem, namely, that the tilted horns, feeding an asymmetrical reflector, cannot be closely positioned without affecting their primary patterns. Experimental investigations were undertaken to clarify these matters.

Pattern Evaluation

Pattern measurements were made with two reflectors, a symmetrical paraboloid 40 inches in diameter with a focal length of 30 inches (Figure 7), and an asymmetrically cut dish, 21.1 inches focal length, 60-3/4 inches wide, and 35-1/2 inches high with the vertex 10 inches above the lower edge (Figure 9). The feed horns were designed to give an illumination taper of 15 and 20 db in the two cases. In the first antenna the horn axis was kept parallel to the axis of the reflector, but in the second it was aimed toward the center of height, a point 7-1/2 inches above the vertex. Horizontal and vertical patterns of the two antennas are plotted in Figures 10 and 11 as a function of feed position in the vertical plane of symmetry. The vertical pattern is plotted on the left in each case, the 3-db beam width is given above each pattern, and the gain in db, where available, is at the center of the block. For each distance off axis, the best horizontal and vertical pattern was chosen on the basis of low side lobes and narrow beam and is indicated by a round or rectangular dot. Best patterns and highest gain are obtained from the symmetrical reflector when the feed is displaced along a line through the focus and perpendicular to the axis. In the other antenna, the horizontal patterns are best along such a line, but the vertical patterns below the axis improve as the feed is brought closer to the reflector.

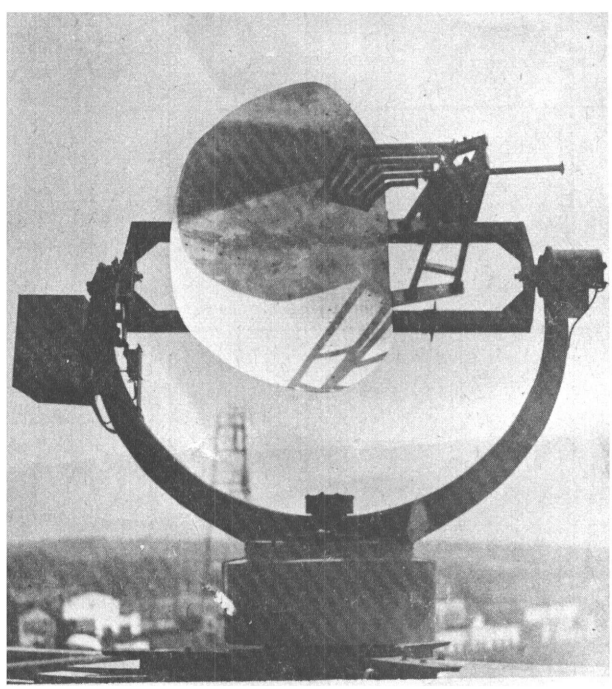

Fig. 9 - Asymmetrically cut paraboloidal reflector used to study off-axis patterns: dimensions 60-3/4 x 35-1/2 x f = 21.1 inches

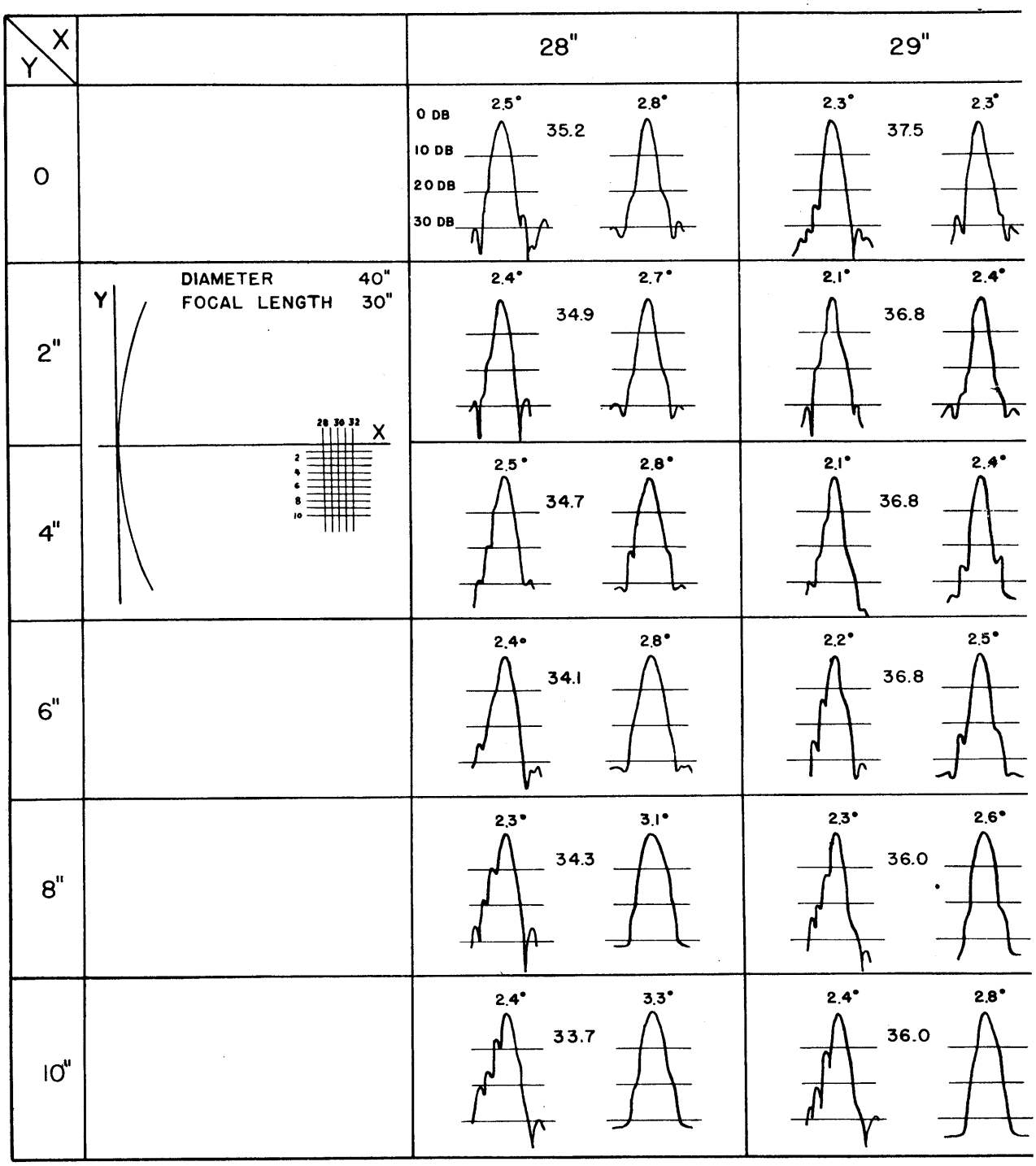

Fig. 10 - E- and H-plane patterns of symmetrical reflector for various feed positions. Illumination taper 15 db

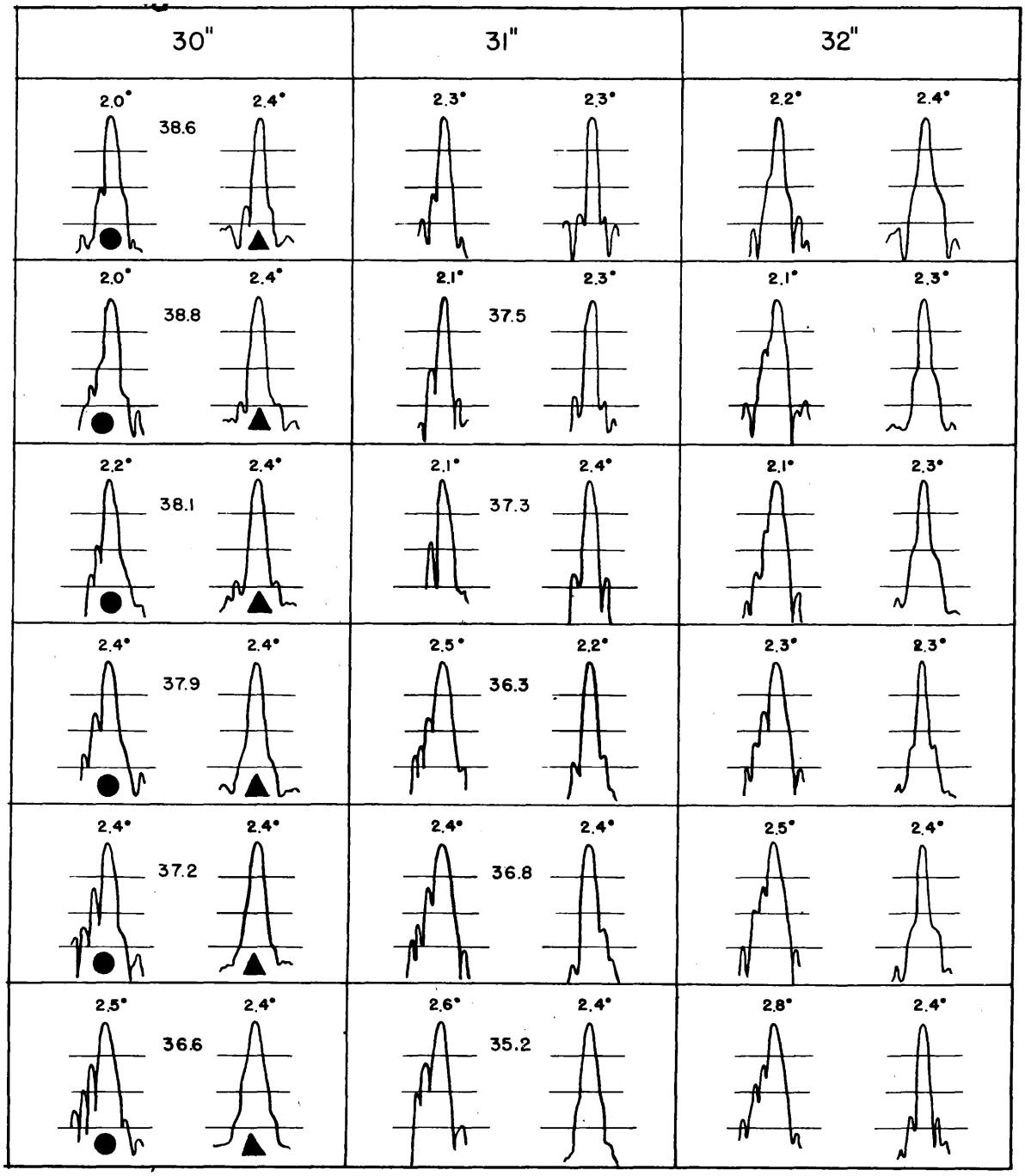

Fig. 10 - Continued

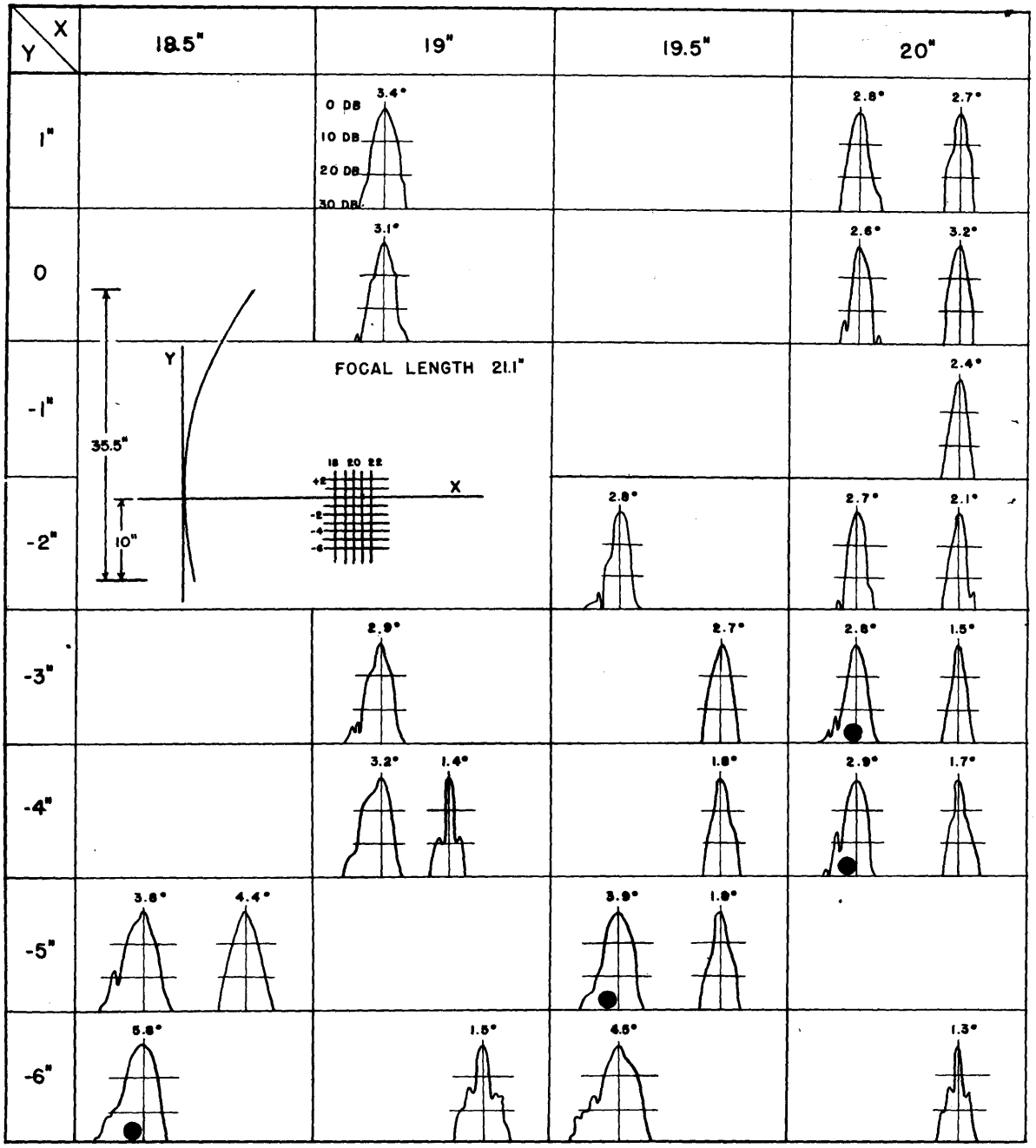

Fig. 11 - E- and H-plane patterns of asymmetrical reflector for various feed positions. Illumination taper 20 db

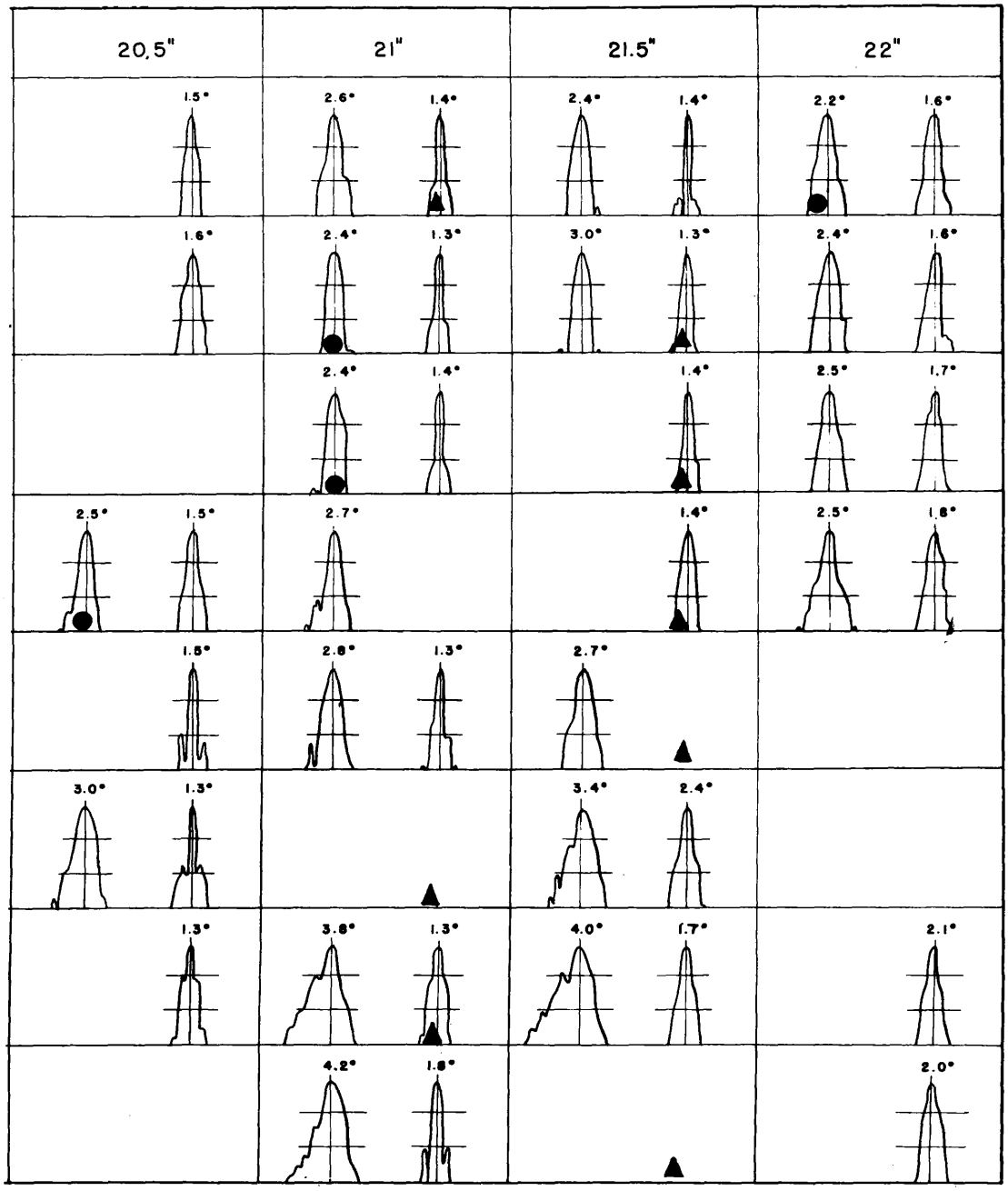

Fig. 11 - Continued

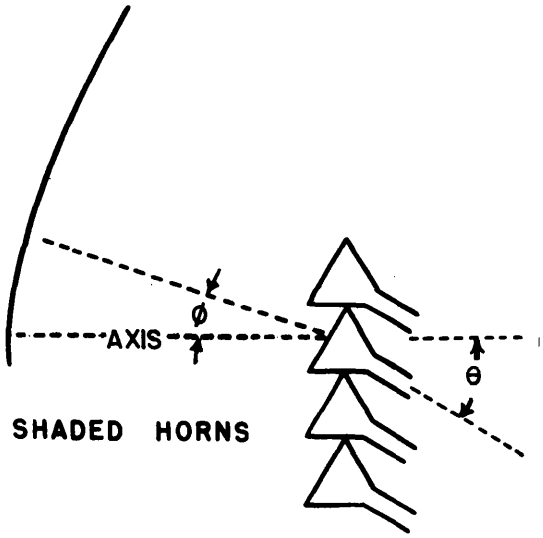

Fig. 12 - Mutual shading by horns in an asymmetrical reflector

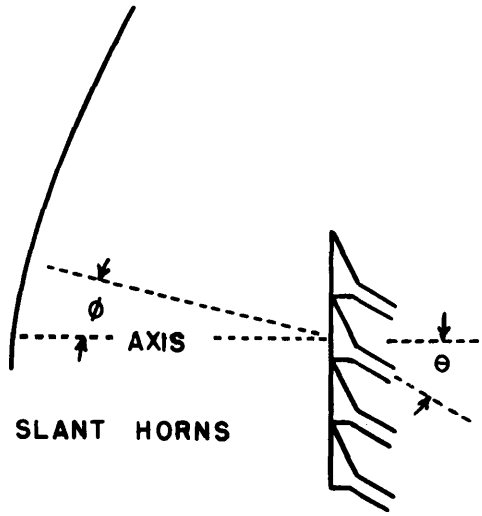

Fig. 13 - Modification of horns to eliminate shading

Feed Problem

If an asymmetrical reflector were used for the AN/SPS-2, it would be necessary to incline the horns at an angle somewhere between 20 and 40 degrees to the axis, depending on the way the dish is cut with respect to the vertex, in order to provide balanced illumination in the vertical plane. At the same time the horns must be stacked along a line approximately perpendicular to the axis at the smallest possible spacing. Under these circumstances, symmetrically cut feed horns shade one another, as shown in Figure 12. Slant horns (Figure 13) have been proposed.[7] The primary patterns of Figures 14 and 15 show, however, that neither arrangement is entirely satisfactory. These patterns were taken feeding the center horn of 3-element arrays of the type indicated in Figures 12 and 13. The angle θ measures the horn tilt, and ϕ is a variable angle away from the reflector axis. It is apparent that in all cases the pattern is shifted from the horn axis toward the reflector axis. Thus, to center the illumination on the reflector, a tilt angle is required considerably greater than would be anticipated. The direction of the primary beam, based on the 6-db level, is given in the following table:

	Beam Direction	
θ	Shaded Horns	Slant Horns
20^0	$14\frac{1}{2}^0$	$14\frac{1}{2}^0$
30	23	$13\frac{1}{2}$
40	33	23

[7] S. J. Mason, "Horn Feeds for Parabolic Antennas," MIT Radiation Laboratory Report 690, 22 Jan. 1946.

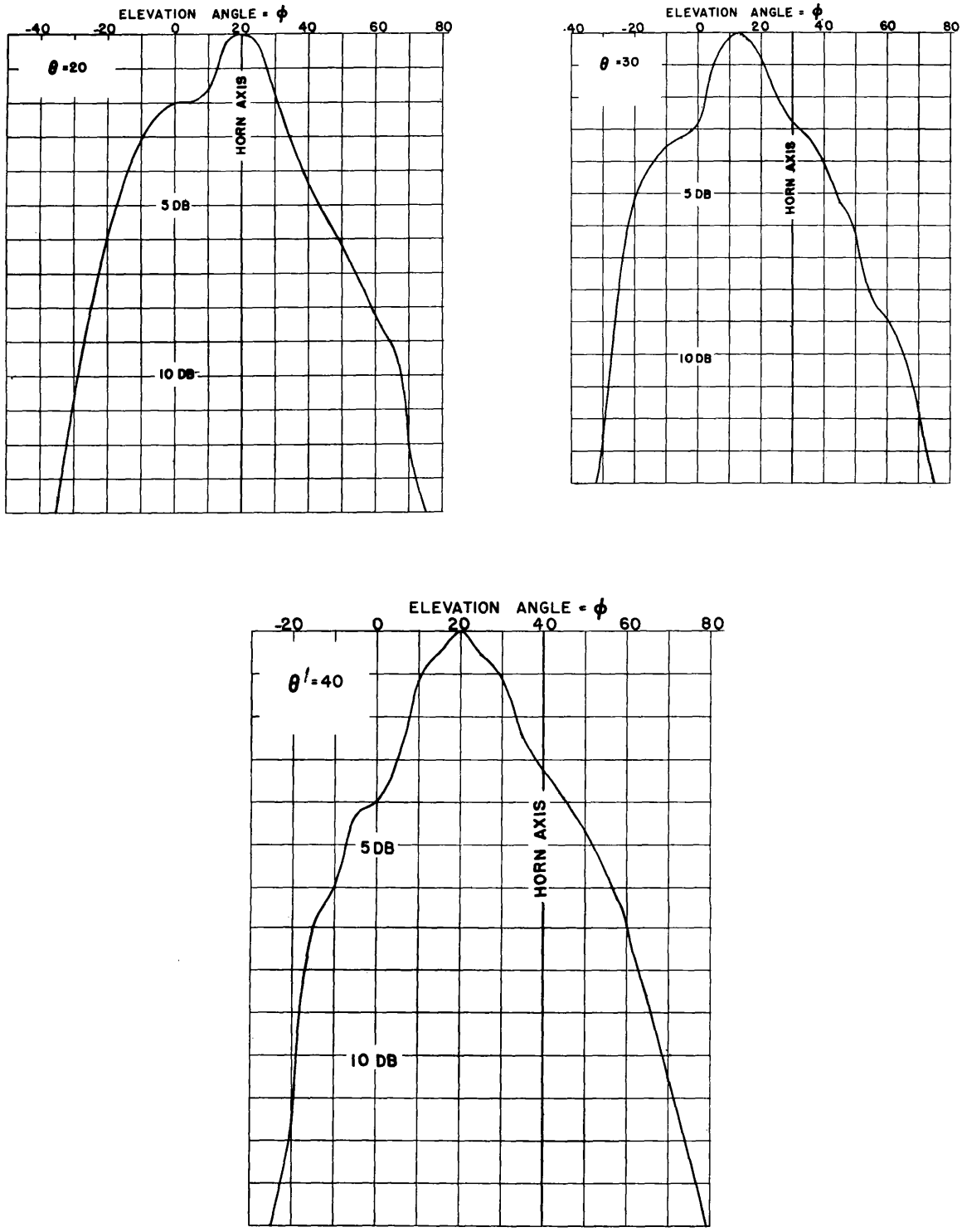

Fig. 14 - H-plane primary patterns of on-axis horn of Figure 12

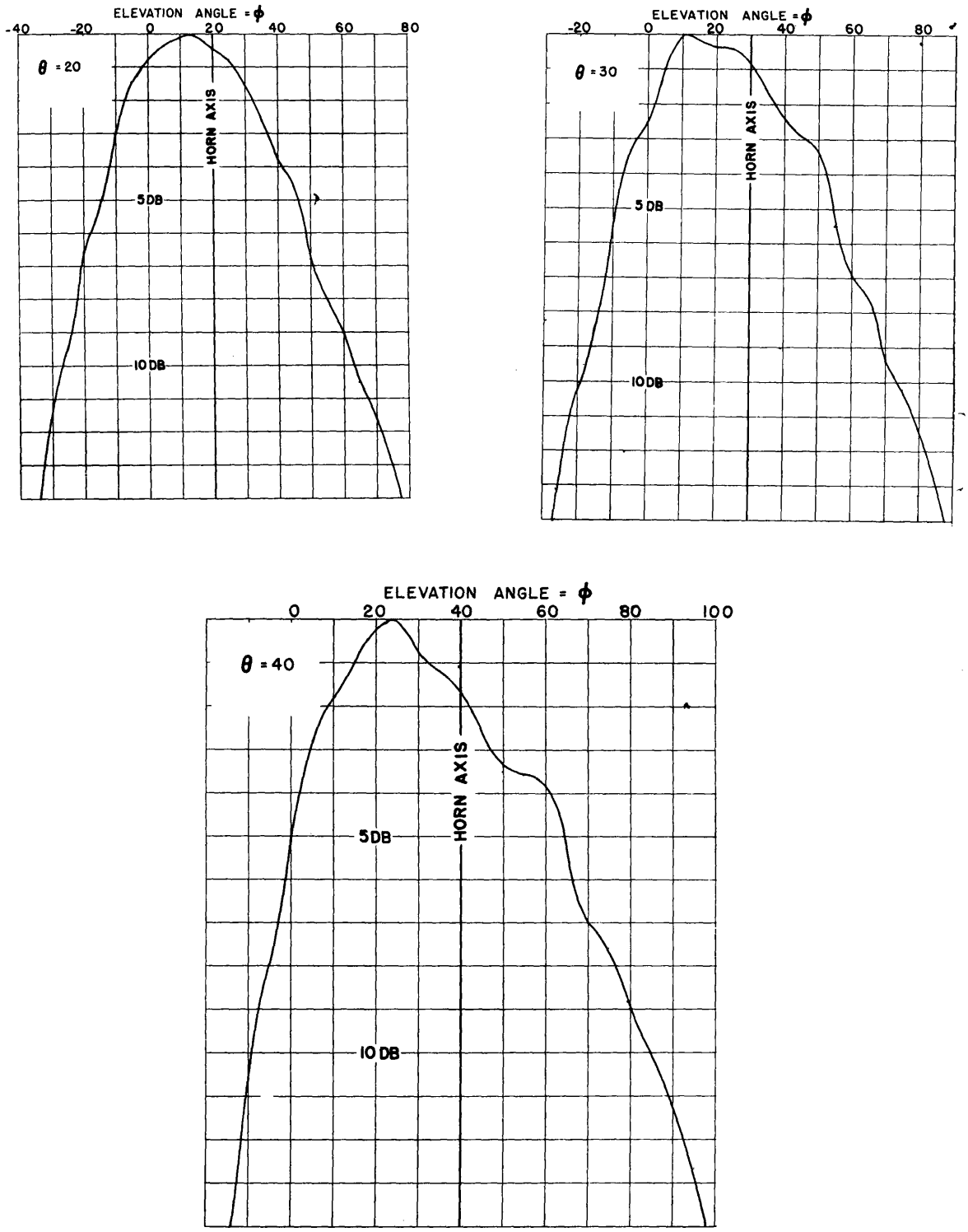

Fig. 15 - H-plane primary patterns of on-axis horn of Figure 13

It is felt that the superior vertical patterns and simpler feed arrangement of the symmetrical reflector are more important than the well known advantages of an off-center dish. Accordingly the former has been adopted for the AN/SPS-2.

MULTIPLE-FEED PROBLEM

Illumination-Taper Problem

The gain of a conventional single-beam antenna is a maximum when the illumination at the edges of the reflector is approximately 10 db down from that at the center. More gradual taper reduces the gain through spillover, while more extreme tapering results in inefficient use of the reflector area. On the other hand, the side-lobe ratio improves steadily as the edge illumination is decreased. For this reason a 14-db taper is ordinarily used, and this determines the aperture dimensions of the feed horn once the f/D ratio of the reflector has been chosen.

In the AN/SPS-2 antenna, the requirement that adjacent secondary beams cross over at the 2-db level fixes the vertical aperture of the horns at a value too small to satisfy the 14-db criterion. In fact, it can be shown that the illumination taper lies in the range of 2 to 5 db, depending on the f/D ratio. Consider, for example, the following four sections.

Space Attenuation

The illumination taper is the sum of the space attenuation, A_S, and of the attenuation of the primary pattern at the edges of the reflector, A_p. The first factor may be expressed (Figure 16) as

$$A_S = 20 \log \frac{\rho}{f} = 20 \log \left[1 + \left(\frac{1}{4}\frac{1}{f/D}\right)^2\right] \qquad (1)$$

and is plotted in Figure 17.

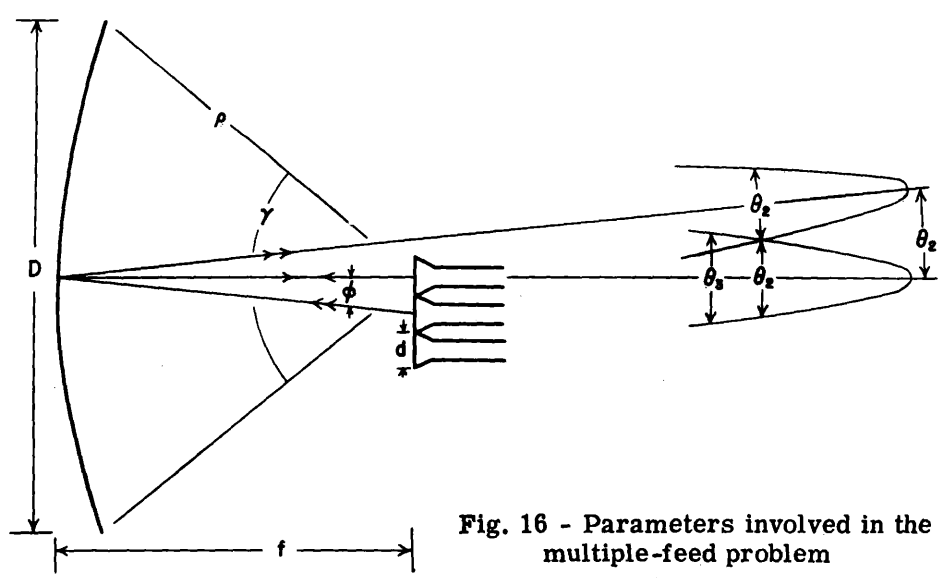

Fig. 16 - Parameters involved in the multiple-feed problem

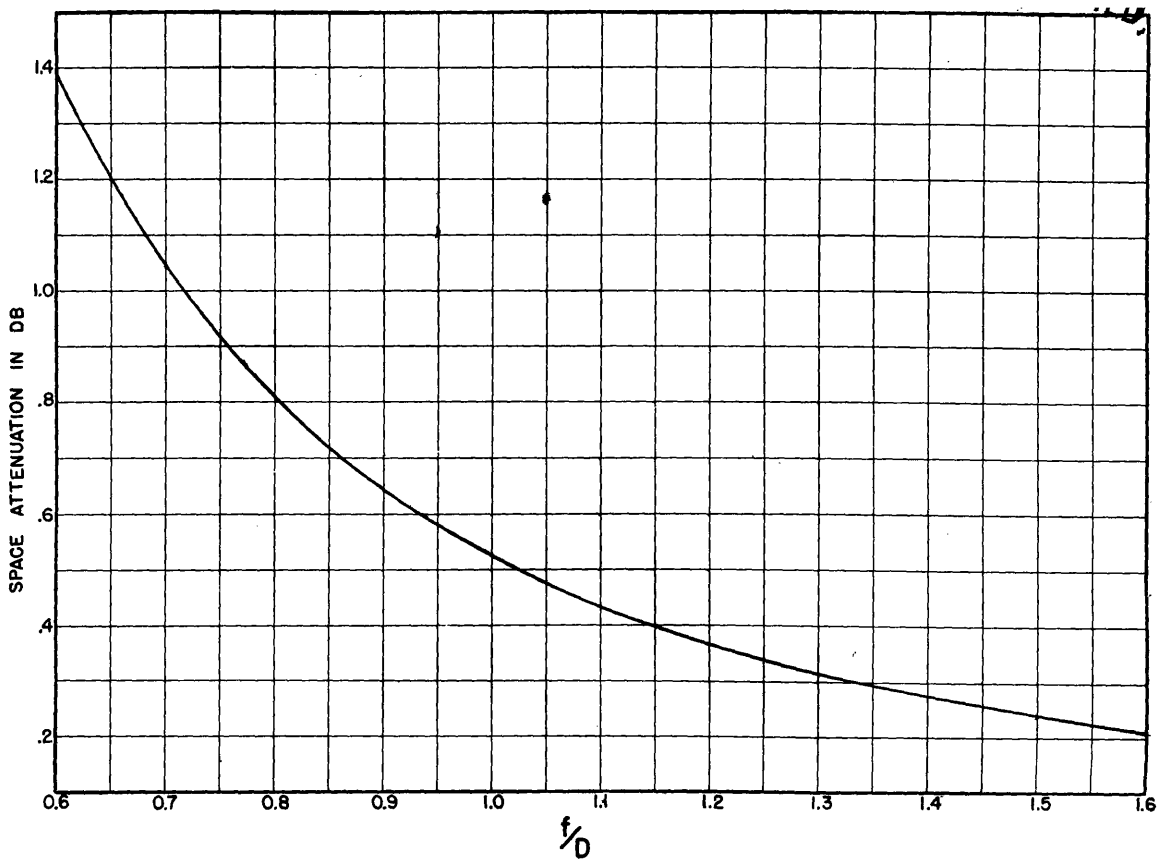

Fig. 17 - Space attenuation as a function of f/D ratio

Dependence of Horn Size on f/D Ratio

The primary patterns depend on the horn aperture, d/λ . It is therefore necessary to determine what value of d/λ will produce a 2-db crossover in the patterns from a reflector of any given f/D ratio. In order to do this, a number of empirical and theoretical relations among the parameters of Figure 16 are used. In the first place, the vertical beam width of a reflector of elliptical outline and height D is approximately

$$\theta_3 = 60^0 \frac{\lambda}{D} = 1.047 \frac{\lambda}{D} \text{ radians},$$

if the illumination taper in the vertical plane lies between 3 and 5 db. Of course the exact beam width depends on the actual illumination, but this formula avoids the necessity of repeated approximations.

The ratio of the beam widths at 2 db and 3 db of a typical antenna pattern may be read from Figure 18, where the average of a large number of secondary patterns is plotted:

$$\theta_2 = 0.841 \ \theta_3 .$$

Combining these relations,

$$\theta_2 = 0.881 \frac{\lambda}{D} , \qquad (2)$$

and this is the angle between beams of the AN/SPS-2 antenna.

But θ_2 is connected to ϕ, the angle between horns, through the relation

$$\theta_2 = B\,\phi \simeq B\,\frac{d}{f}\,. \qquad (3)$$

For moderate values of ϕ, B is a function only of the f/D ratio; a theoretical curve of this function is plotted in Figure 19.[8] Equating the two expressions for θ_2 there results (Figure 20),

$$\frac{d}{\lambda} = 0.881\,\frac{1}{B}\,\frac{f}{D}\,, \qquad (4)$$

which is the required relation between d/λ and f/D.

Primary Patterns Versus Horn Aperture

It has been observed that the H-plane pattern of a small horn is affected by the presence of close neighbors in that plane and by the termination of their waveguides. These effects were studied by feeding the center horn of a three-element array (Figure 21), the outer waveguides of which were terminated by adjustable shorting plungers. Figure 22 shows the envelope of patterns obtained in this way for a number of horn apertures. The pattern attenuation, A_p, may be read at the angles $\pm\,\gamma/2$ marking the edges

[8] K. S. Kelleher, "Analysis of Antenna Wavefronts," NRL Report R-3329, July 29, 1948.

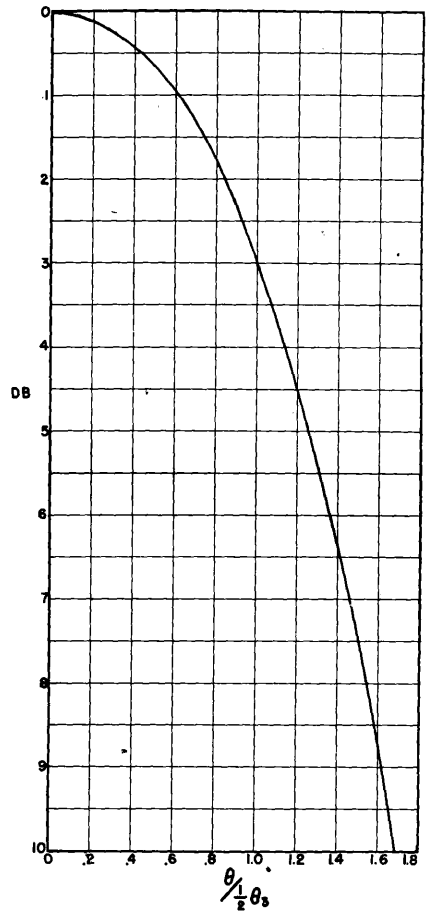

Fig. 18 - Universal secondary pattern

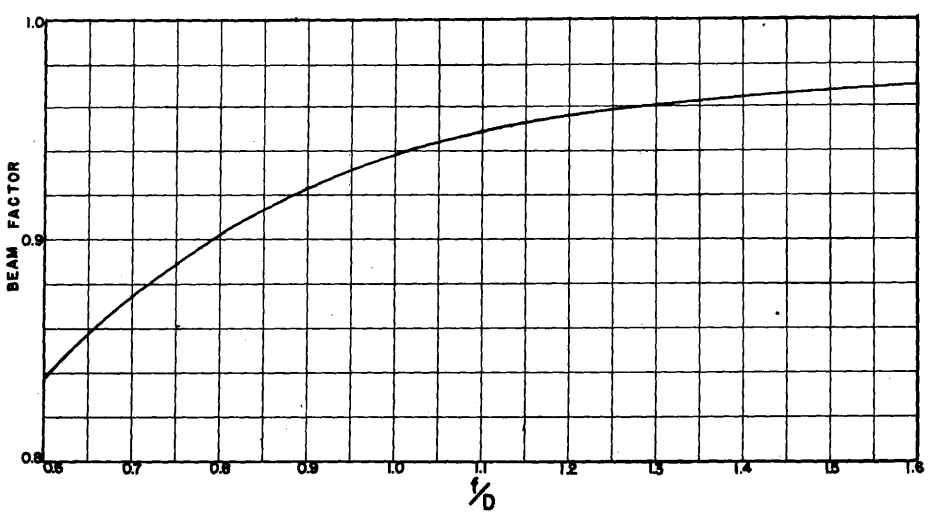

Fig. 19 - Beam factor as a function of f/D ratio

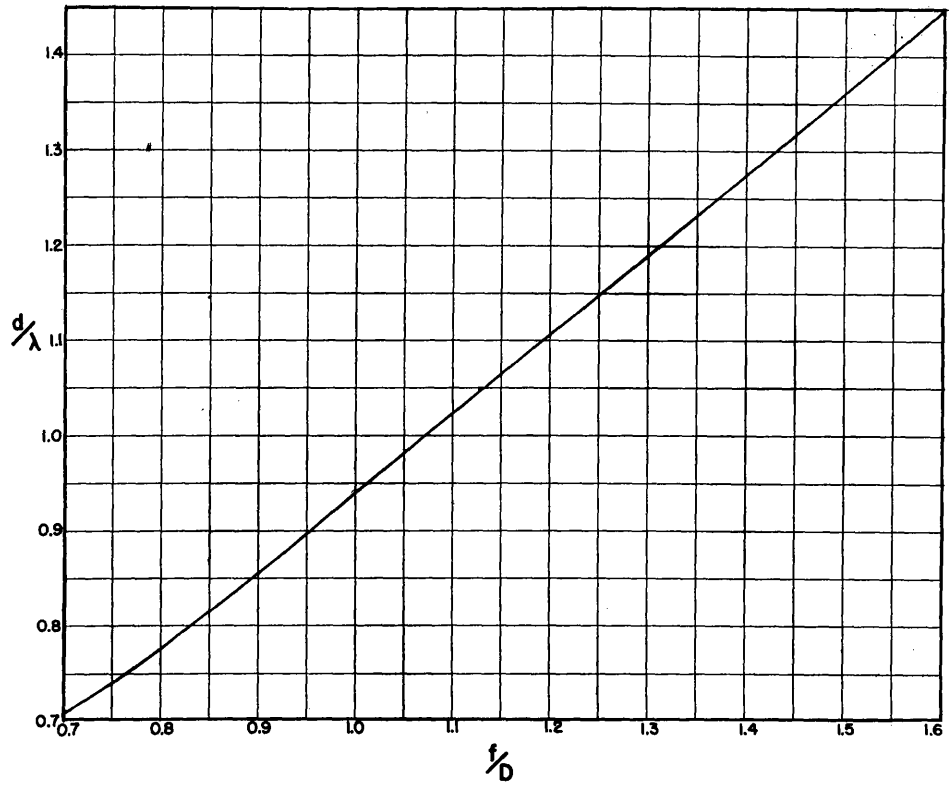

Fig. 20 - Relation of horn aperture to f/D ratio for 2-db crossover

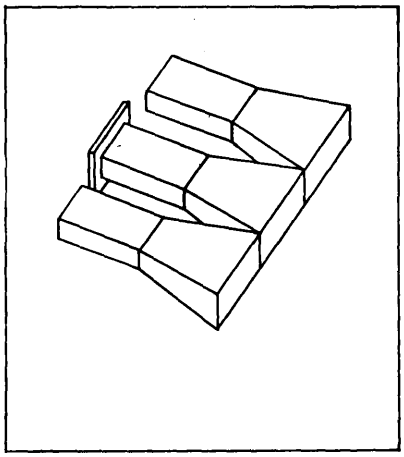

Fig. 21 - Arrangement used to study characteristics of horn in an array

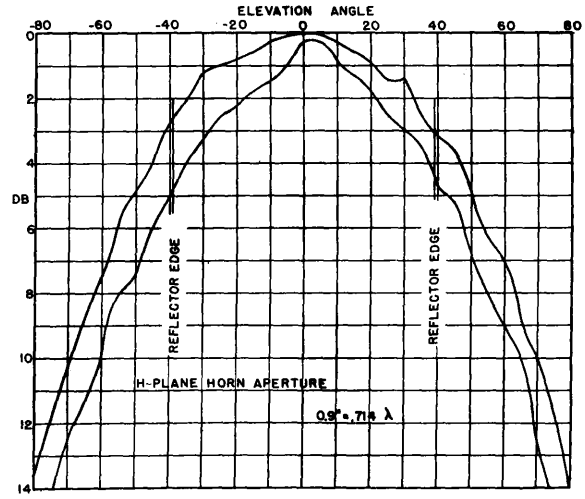

Fig. 22 - H-plane patterns of horns in an array

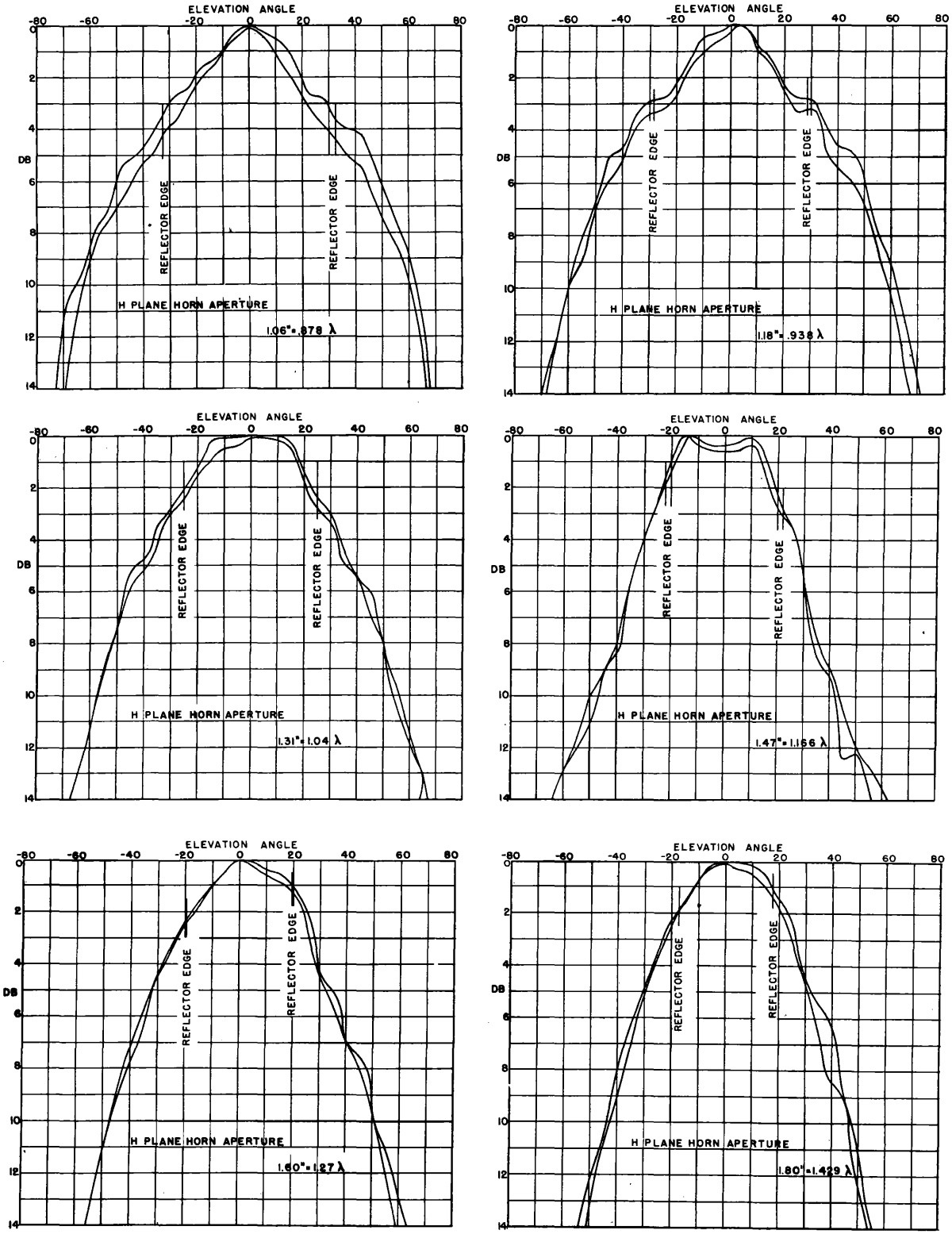

Fig. 22 - Continued

of the reflector, as determined from the relation (Figure 23)

$$\tan\frac{\gamma}{4} = 1/4 \ \frac{1}{f/D} \quad . \tag{5}$$

As a matter of interest, the 10-db beam widths are plotted as a function of d/λ in Figure 24.

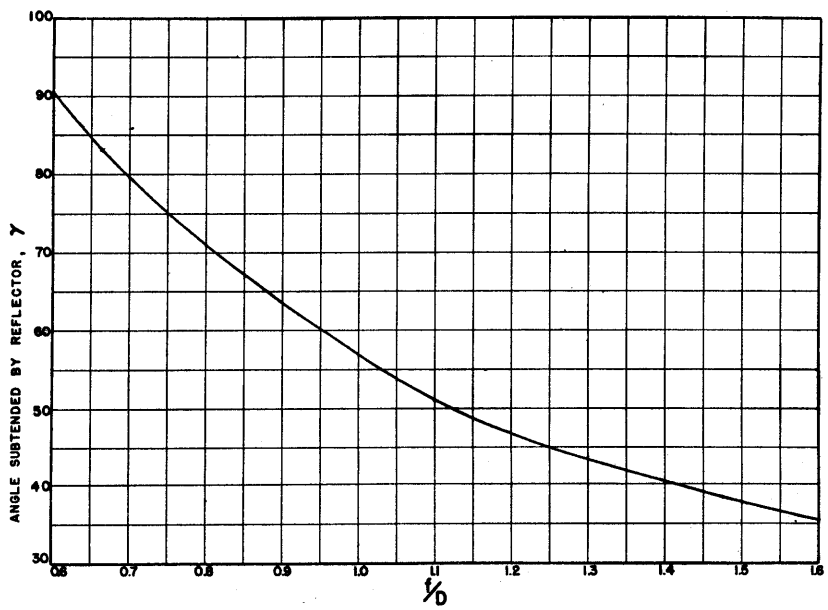

Fig. 23 - Reflector angle as a function of f/D ratio

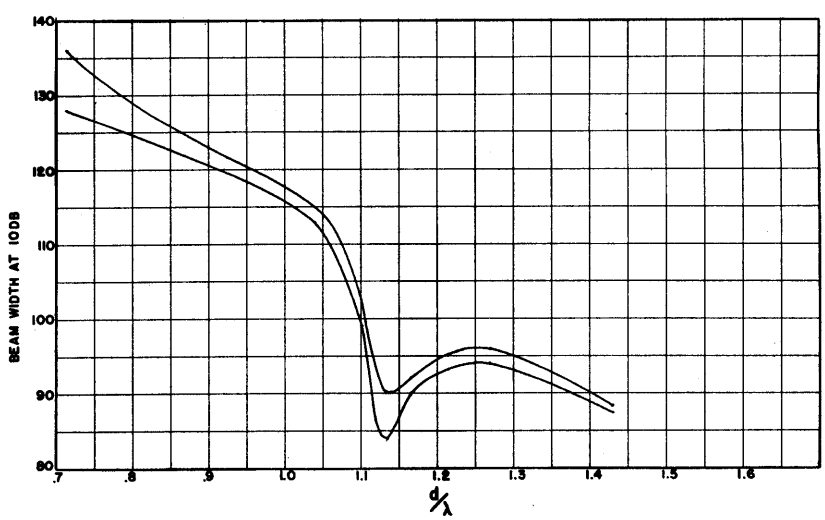

Fig. 24 - Ten-db beam widths of horns in an array for various apertures

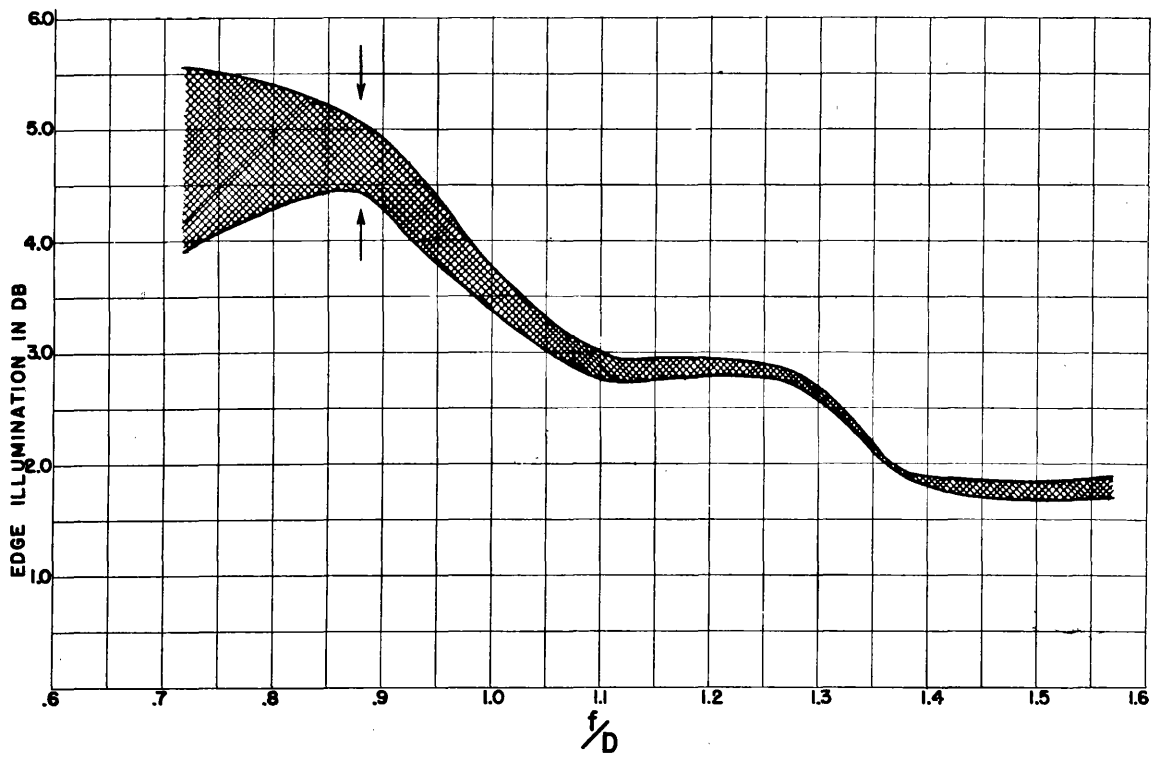

Fig. 25 - Illumination taper as a function of f/D ratio for 2-db crossover

Illumination Taper as a Function of f/D Ratio

The resultant illumination taper, $A_s + A_p$, is given in Figure 25, where the extent of the crosshatched section indicates the uncertainty resulting from variations in the primary patterns. The curve reaches a maximum of approximately 5 db for an f/D ratio of 0.72, corresponding to horns of waveguide size, but the illumination is quite unpredictable in this region. At larger values of f/D, the curve is better defined but falls off rapidly after a certain point. The arrows at f/D = 0.88 indicate a desirable compromise.

HORN DESIGN AND THE MULTIPLE-FEED PROBLEM

Horn Designs for Improved Directivity

It is natural to attempt improvement in the illumination taper in a multiple-beam antenna by the substitution of some more directional type of feed for the conventional H-flared horns just considered. The schemes which have been investigated fall into two categories: (1) the horn patterns may be sharpened by the use of pins, obstacles, dipoles, or polyrods, or (2) the horn apertures may be increased but overlapped in some way so that the same space is used for two or more horns. None of the feeds of the first type was found to effect any pronounced improvement, and the only schemes in the second

group which showed promise were those in which signals from adjacent horns were separated by differences in polarization or frequency. Unfortunately, these schemes are ruled out by the fact that target cross section of an airplane at any particular instant is quite sensitive to polarization and frequency, so that height finding with such an antenna would be subject to unpredictable errors.

While the study of beam sharpening and horn overlapping failed to yield a design suitable for the AN/SPS-2 antenna, the results may be of interest in other applications.

Methods of Improving Aperture Efficiency

Obstacles in E-Flared Horns. Early attempts at beam sharpening followed methods investigated at the Radiation Laboratory during the war.[9] One of these consisted of placing a rectangular obstacle in the aperture of E-flared horns. Figure 26 is a photograph of two experimental horns; their E-plane apertures, d, are 1.28 and 0.85 inches or 0.99 and 0.65 wavelengths at 3.3 cm. Curve A of Figure 27 shows the 10-db beam widths obtained from the smaller horn as the width of the obstacle, w, was varied. Curve B was obtained from the formula,

$$F(\theta) = 20 \log \left\{ \cos u \; \frac{1 + \lambda/\lambda g \; \cos\theta}{1 + \lambda/\lambda g} \; \frac{\sin u'}{u'} \right\}, \qquad (6)$$

where

$$u = \frac{d + w}{\lambda} \; \frac{\pi}{2} \; \sin\theta \; ,$$

$$u' = \frac{d - w}{\lambda} \; \frac{\pi}{2} \; \sin\theta \; ,$$

and $\frac{\lambda}{\lambda g} = 0.629$.

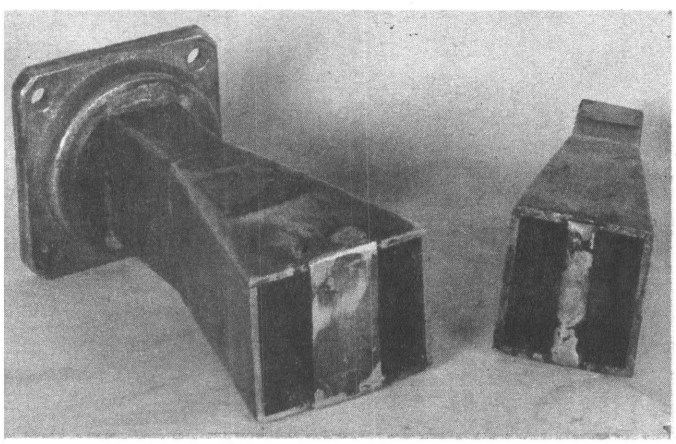

Fig. 26 - E-flared horns used for testing the effect of obstacles

In this expression, cos u is an array factor for the two openings, and the other factor is the pattern of either one alone.[10] It is evident from Curve A that a wide obstacle is required to produce a narrow beam, but Curve C shows that this leads to a very high standing wave ratio, which can be predicted (Curve D) by the formula

$$SWR = 20 \log \frac{1 + w/d}{1 - w/d} \; . \qquad (7)$$

In Figure 28, the circles indicate the beam sharpening obtained with the larger horn and Curve A is obtained from Equation (6). However, in this case the two

[9] C. S. Pao, "Shaping the Primary Pattern of a Horn Feed," MIT Radiation Laboratory Report 655, 22 January 1945.

[10] J. R. Riser, "Characteristics of Horn Feeds on Rectangular Waveguides," MIT Radiation Laboratory Report 656, December 28, 1945.

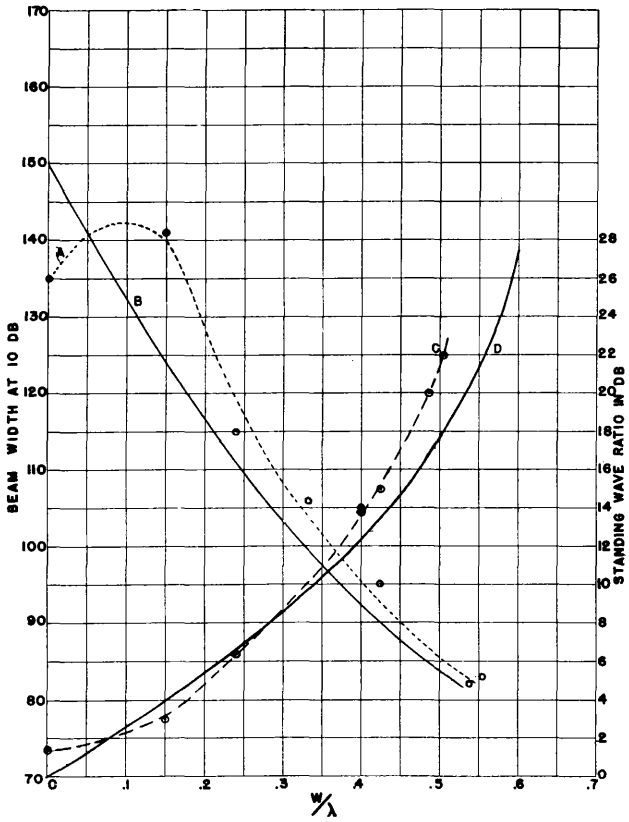

Fig. 27 - Characteristics of the smaller horn of Figure 26: A - measured beam width, B - calculated beam width, C - measured SWR, D - calculated SWR

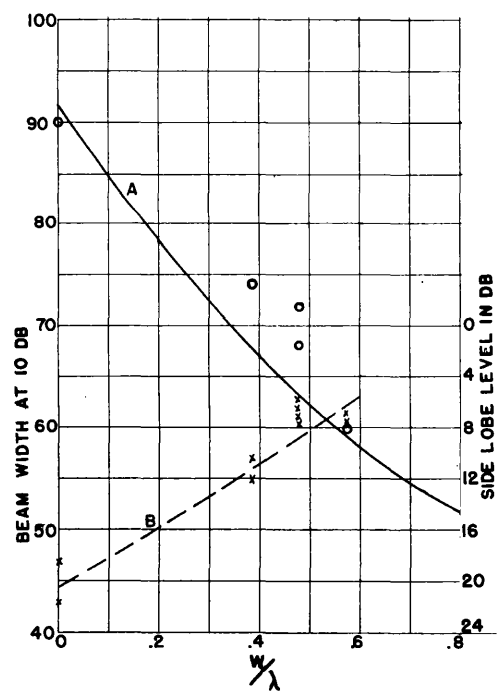

Fig. 28 - Characteristics of the larger horn of Figure 26: A - beam width, B - side lobe level

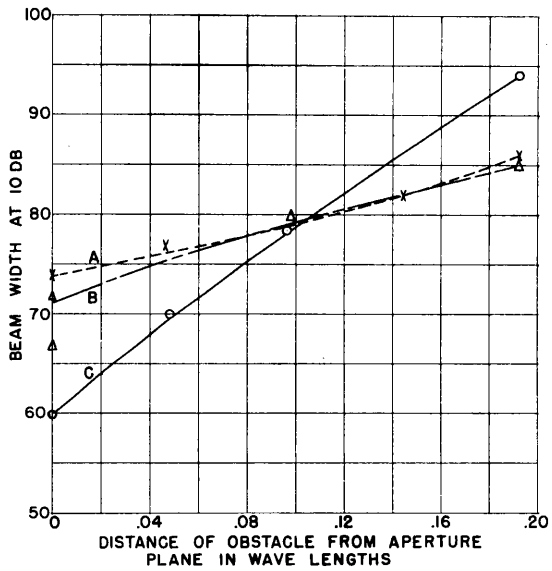

Fig. 29 - Effect of obstacle position on beam width in the larger horn

openings are separated by nearly 1 wave length, and high side lobes (Curve B) result. The effectiveness of this method decreases as the obstacle is moved back into the horn. This is demonstrated for the larger horn by the curves of Figure 29, where A, B, and C apply to obstacle widths of 0.385, 0.481 and 0.577 wavelengths respectively.

To summarize, beam sharpening by obstacles in E-flared horns is limited by mismatch and high side-lobe ratios and unfortunately leads to the wrong polarization for the AN/SPS-2 antenna.

Pins in H-Flared Horns. The H-plane pattern of a horn can be sharpened by placing pins across the mouth parallel to the electrical vector (Figure 30). This undoubtedly has the effect of making the field distribution more nearly uniform. Pao[11] was able to reduce the 10-db beam width of a 2-1/2-inch horn at 3.2 cm from 78° to 46-1/2° by the use of pins. Since an optimum horn of this aperture gives a beam width of 60°,[12] the sharpening may be reckoned as 23 percent.

This method has been applied to a number of horns of different aperture dimensions with the results shown in Table I. The wavelength is 3.2 cm.

TABLE I

Horn Dimensions (Inches)			H-Plane Beam Width at 10 db			
E	H	Taper	Optimum Horn[13]	Without Pins	With Pins	Beam Sharpening
0.7	2.35	2.0	65-1/2°	66°	43-1/2°	33%
0.75	1.62	2.0	93	92	66	29
0.8	1.30	2.0*	111	114-1/2	94	17
0.8	1.18	2.0*	119	120	91	24
0.7	0.90	2.0*	143	127	116	9

*Center horn in an array of three.

---

[11] Pao, op. cit.

[12] Risser, op. cit.

[13] Risser, op. cit.

Because of the necessity of keeping the f/D ratio of the antenna at a reasonable value (Figure 20), the three smaller horns were the only ones seriously considered, and their patterns were taken under conditions simulating the actual case of feeds in a close-spaced array.

Secondary patterns of a reflector 60-3/4 x 28 x f = 21.1 inches were taken using a set of feed horns 0.8 x 1.18 inches, with and without pins. Table I indicates that beam sharpening is most effective for horns of about this size. The results are summarized in Table II.

TABLE II

Horn Number	Without Pins			With Pins		
	Beam Width	Side Lobes Left	Side Lobes Right	Beam Width	Side Lobes Left	Side Lobes Right
1	--	--	--	2.6°	20.5	20.0 db
2 (On Axis)	2.8°	21.0	21.0 db	2.9	24.0	21.0
3	2.8	18.0	21.0	2.9	22.0	21.5
4	2.8	21.5	21.0	2.8	19.0	19.0
5	2.9	21.0	21.0	2.7	23.0	23.0
6	2.8	22.5	20.0	2.9	20.0	24.0

It should be pointed out that these patterns have a crossover between 3 and 4 db, so that their sidelobe level is lower than can be expected in the actual system. The table is intended only to indicate the degree of improvement possible with pins, and this was considered insufficient to outweigh such disadvantages as mismatch and possible voltage breakdown.

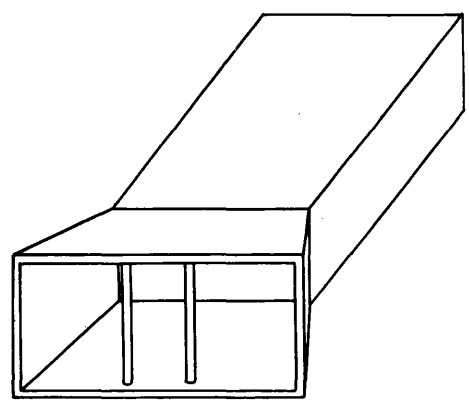

Fig. 30 - Arrangement of pins in H-flared horn

Array of Pins. In order to obtain greater beam sharpening, an extension of the previous method was studied. Figure 31 shows how the effective aperture of a horn can be increased by permitting it to energize an array of pins. The pattern for a single channel then is a combination of the horn pattern and that of the pin array, with the result that sharpening of better than 40 percent may be obtained. However, it was found that the pattern of any horn was sensitive to the termination of the guides connected to its neighbors. In practice these feed lines lead to magnetrons that are tuned to a number of frequencies, all different from that of the one feeding the original horn. Therefore, any power coupled into adjacent channels will be completely reflected, even if the magnetrons are firing; the phase of the reflected wave must be considered arbitrary, as it depends on the exact length of the lines. This condition may be simulated by the use of shorting plungers adjustable through a range of a half wavelength.

The array of pins was tested by feeding the second horn from the right in Figure 31 and inserting shorts in the adjacent waveguides. Figure 32 shows that the variations produced in the secondary patterns are so great as to prevent accurate height finding.

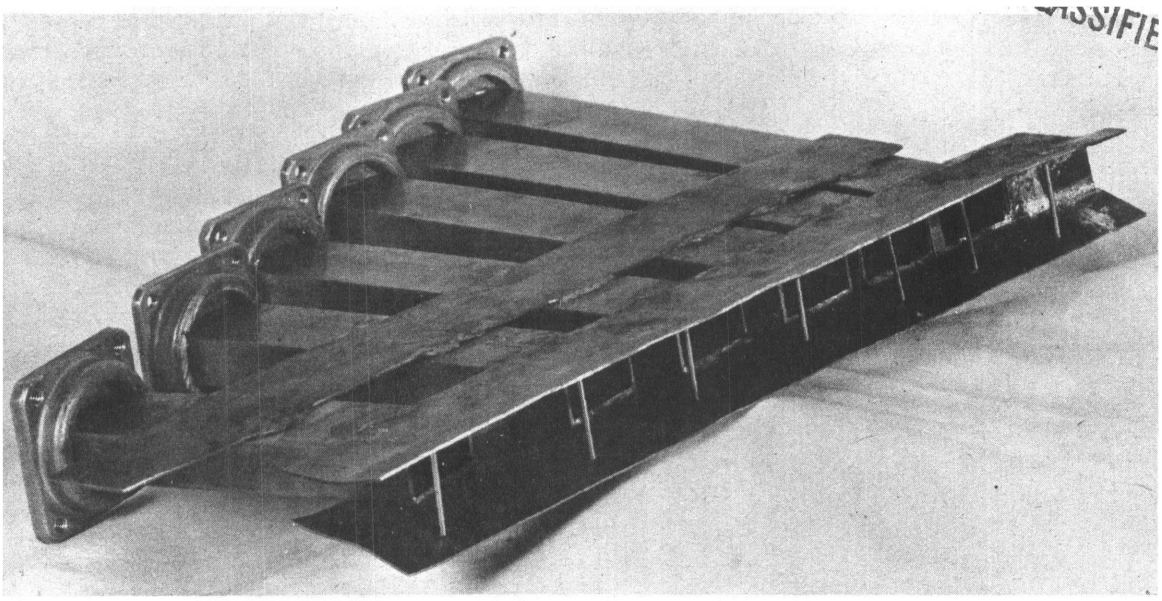

Fig. 31 - Waveguides exciting an array of pins

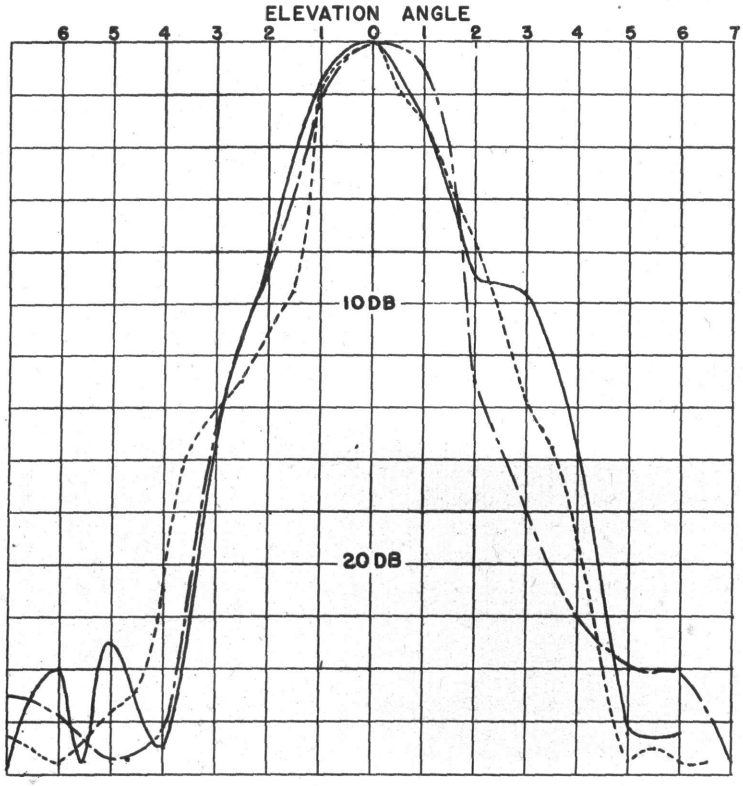

Fig. 32 - Secondary H-plane patterns obtained using the feed of Figure 31

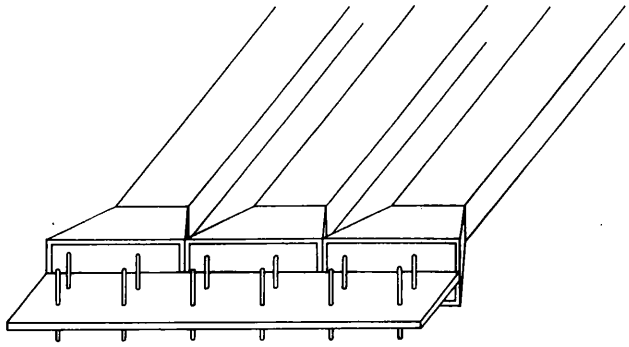

Fig. 33 - Dipole array for sharpening the patterns of H-flared horns

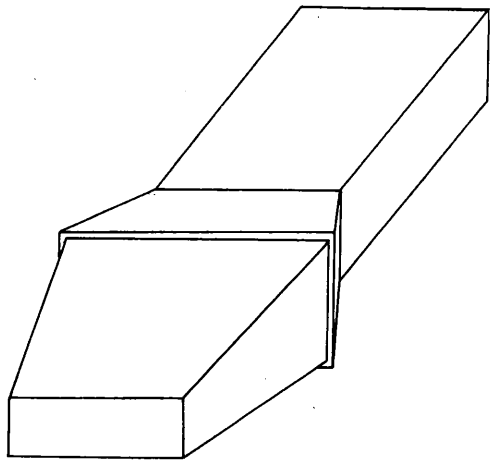

Fig. 34 - Polyrod radiator

The coupling between horns was also measured directly by comparing the power level in the fed horn to that of the other channels:

Horn Number	1	2	3	4	5	6
Power Level, (db below fed horn)	33.0	0	21.5	30.0	39.0	43.5

Evidently, coupling of the order of 21 db is sufficient to cause instability in the secondary patterns.

Array of Dipoles. When the pins were replaced by dipoles as shown in Figure 33, a sharpening of 25 percent was obtained and the coupling was somewhat less. However, because of the voltage breakdown possibilities of such an array, no further work was done in this direction.

Polyrods. Another obvious method of sharpening the primary pattern of a horn is by the use of dielectric rods, as indicated in Figure 34. Such a system is an end-fire radiator and obtains its directivity from a new dimension, length, which is not restricted by the crossover condition. As the length of the rod increases, the beam widths in the two principal planes tend to become equal, no matter what the ratio of the horn dimensions may be. However, the AN/SPS-2 system requires a ratio of the primary beam widths in the E- and H-planes of at least 2 to 1. A study has, therefore, been made of short dielectric rods in an attempt to find an arrangement which would maintain this ratio and at the same time produce some sharpening in the H-plane.

In the first experiment, a horn was chosen with E- and H-plane apertures of 0.32 and 1.11 wavelengths and 10-db beam widths of 206 and 103 degrees, a ratio of 2 to 1. By the use of the tapered polyrod shown in Figure 35, the patterns were narrowed to 117 and 80 degrees (Curves A and B). Thus the ratio of the two beam widths is reduced to approximately 1.5 to 1 in sharpening the H-plane pattern by 22 percent. This is a typical result.

When this horn was placed in an array of like radiators, the H-plane pattern broadened as shown in Curve C of Figure 35. The pattern was then very similar to

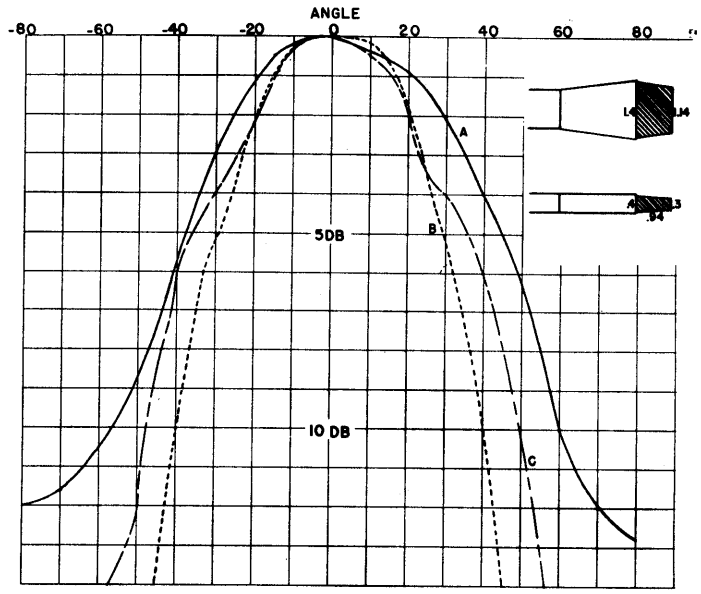

Fig. 35 - Characteristics of polyrod radiator: A - E-plane primary pattern, B - H-plane primary pattern, C - H-plane primary pattern in array

that which could be obtained in the array without the use of polyrods (Figure 36). A tentative conclusion, therefore, is that the different boundary conditions on a polyrod in a close-spaced array reduce its effectiveness in the plane of the array.

A further investigation was made using an array of horns of 0.56 x 0.71 wavelength aperture in the E- and H-planes and polyrods of square cross section 0.3 wavelength on a side. The primary beam widths at 10 db are given in Figure 37 as a function of the length of the polyrod. These curves indicate that the pattern widths change very rapidly in the E-plane and much more slowly in the plane of the array. In making a compromise between beam-width ratio and H-plane sharpening, a polyrod 0.6 wavelength long might

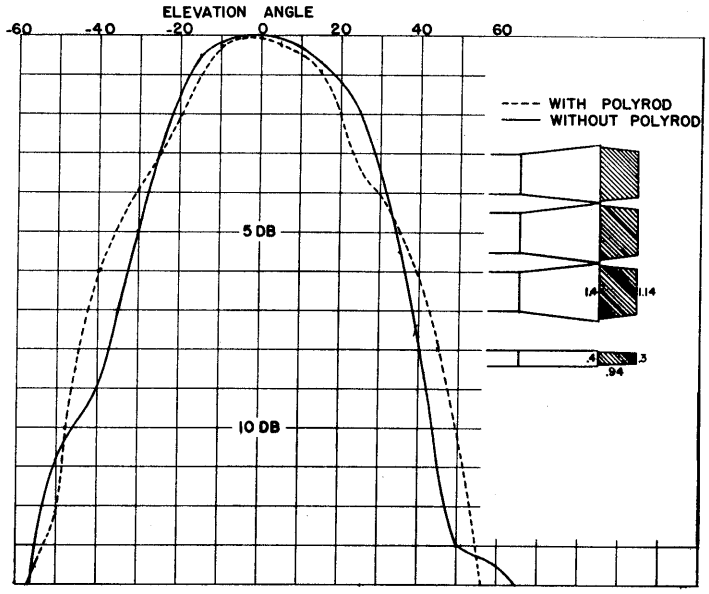

Fig. 36 - Effect of polyrods on H-plane patterns of horn in an array

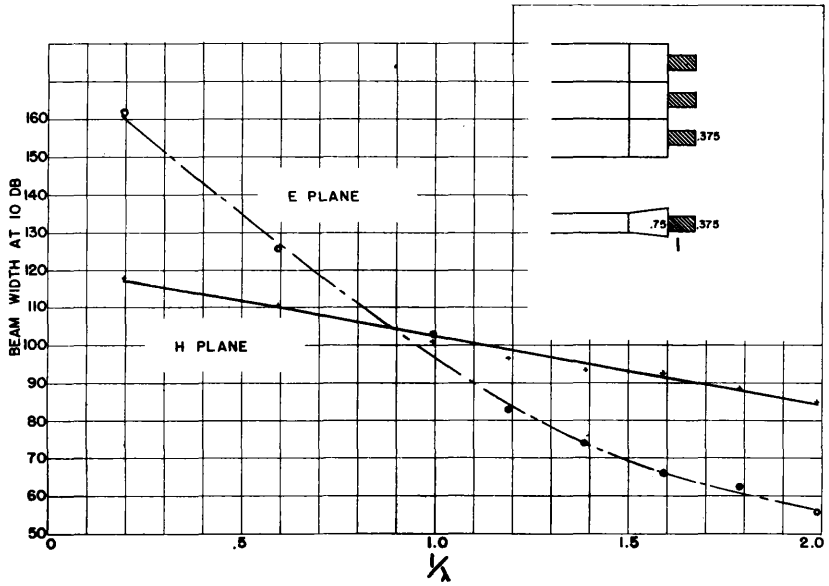

Fig. 37 - Effect of polyrod length on E- and H-plane beam widths

be chosen. Patterns for this case are shown in Figure 38. Since the horn aperture is 0.71 wavelength, a suitable reflector must, by Figure 20, have an f/D ratio of 0.70 and subtend an angle of 79 degrees (Figure 23) in the vertical plane. Figure 38 indicates that the pattern attenuation to the edges of the dish would be 4.4 db, and since the space attenuation is 1.1 db (Figure 17), the illumination taper is 5.5 db in this plane. In the horizontal plane the f/D ratio is 0.28, the subtended angle is 166 degrees, and the illumination taper exceeds 20 db.

This polyrod feed system shows some promise and may be compared with an ordinary horn array of optimum design, as indicated by the arrows in Figure 25.

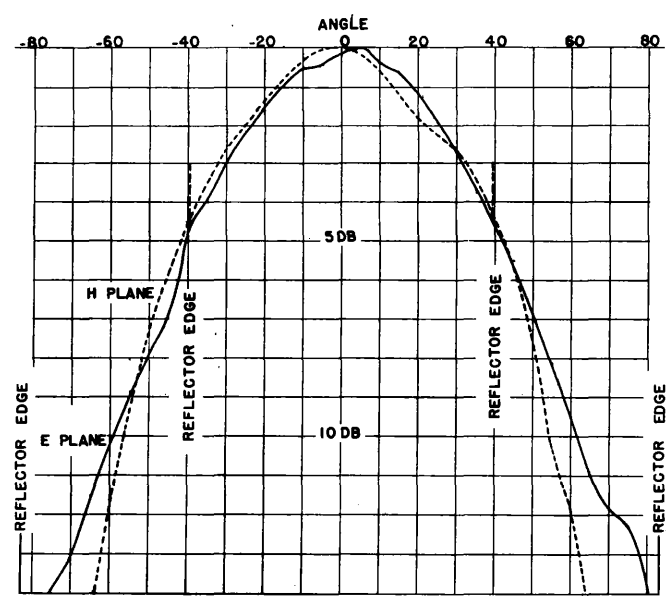

Fig. 38 - Primary patterns of the array of Figure 37. Polyrod length, 3/4 inch

Feed	Illumination Taper		Coupling
	Vertical	Horizontal	
Polyrod Array	5.5 db	20 db	32.5 db
Horn Array	4.7	Adjustable	30*

*Taken from Figure 91, page 76.

The slight improvement in the vertical illumination afforded by the polyrod array and its greater isolation between channels are offset by an excessive taper in the horizontal plane as well as by problems of matching and voltage breakdown.

It is concluded that this type of feed system is not well suited to the AN/SPS-2 antenna, but it may find application in low-power systems using a circular reflector.

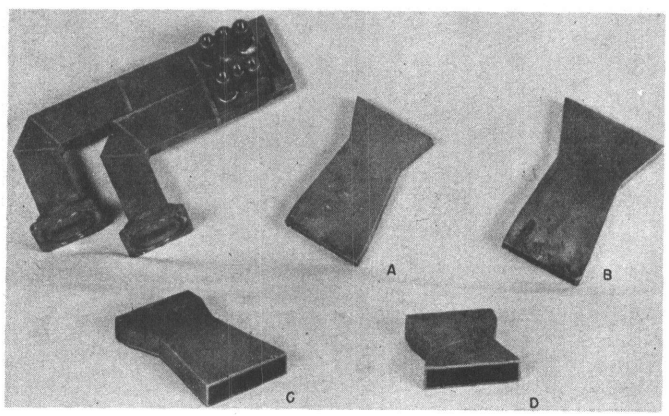

Fig. 39 - Double-horn components

Methods of Overlapping Apertures

Double Horn. The simplest scheme for overlapping a number of feeds is to bring their wave guides into a single large horn. It might be hoped that the primary pattern beam widths would correspond to the aperture dimension, while the phase centers would lie opposite the center lines of the various guides. This idea has been studied experimentally for the case of two feeds with the arrangement shown in Figure 39. Any one of the horns A, B, C, or D could be soldered to the output of the two-guide assembly at the left. Figure 40 is a typical set of primary patterns, obtained with horn C, in which the main lobe is beamed nearly 20 degrees away from the axis. The two phase centers are separated by approximately 1 inch, as expected. By lengthening the input and output tapers of the horn, and reducing the width at the point where they meet, it is possible to bring the patterns together as indicated by Figure 41. Unfortunately the phase centers are only 1/2 inch apart in this case.

As might be expected, the coupling between channels of a double horn is very great. Measured values for the ones shown in Figures 39 and 41 are:

Horn	Coupling
Figure 39, A	8.0 db
B	13.5
C	16.5
D	8.0
Figure 41	7.5

To summarize, the pattern and phase-center problems are overshadowed by such severe coupling that this type of arrangement holds little promise.

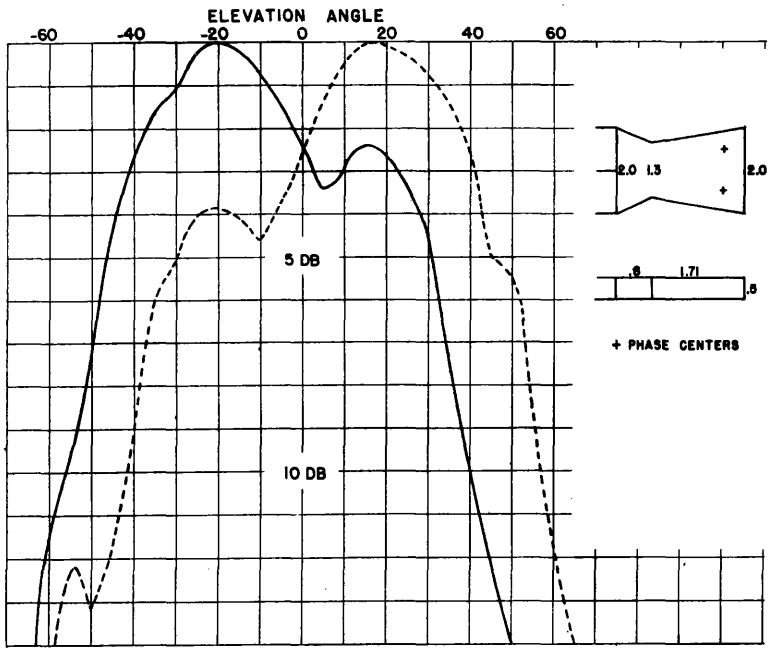

Fig. 40 - H-plane primary patterns obtained with horn C of Figure 39

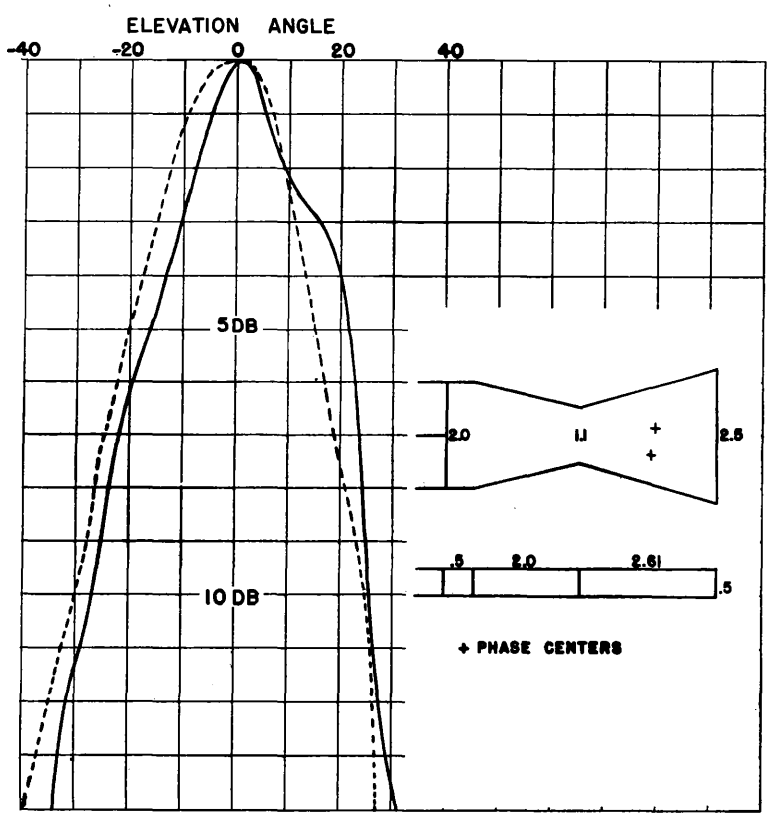

Fig. 41 - H-plane primary patterns of a double horn

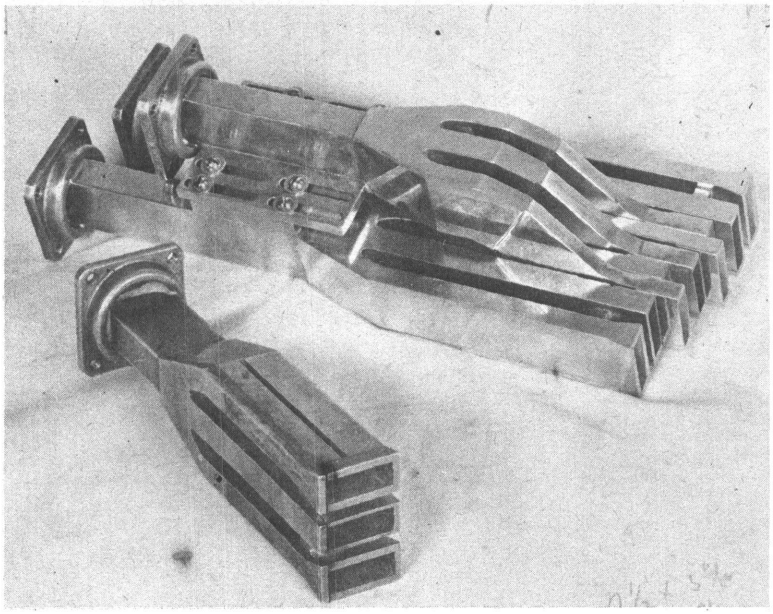

Fig. 42 - Three-element horns

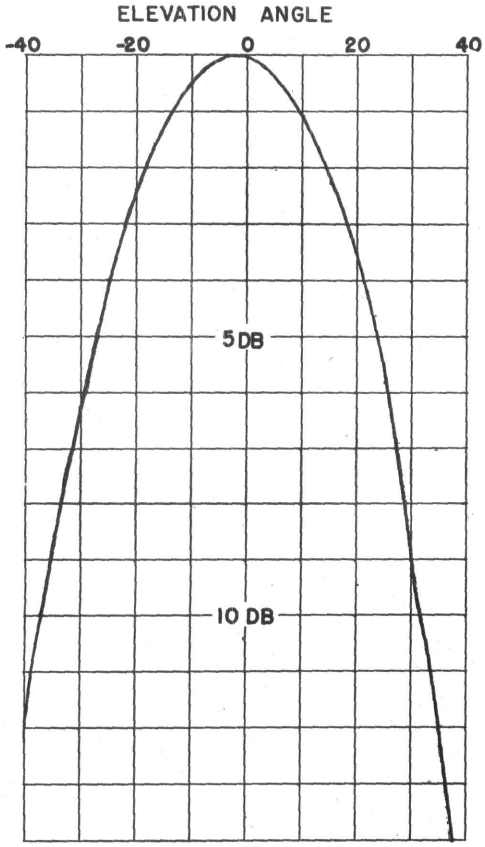

Fig. 43 - E-plane pattern of a single three-element horn

Three-Element Horn. The E-flared horn with obstacle, already described, suggested the development of a new type of horn that can be interlaced with its neighbors. The only purpose served by the obstacle is to separate the horn into two sections, and if this is done by splitting the wave guide into two or more thinner ones, the obstacle can be replaced by a section of the adjacent horn. Figure 42 shows a set of three triple horns constructed according to this principle. The phase centers are separated by only 60 percent of the aperture of each horn.

The three-element horn in the foreground has an excellent primary pattern (Figure 43) and the standing wave ratio (Figure 44) is such that a match should be possible, at least over a narrow band. However, when three of these horns were placed in the array, the effect of coupling was very noticeable. Figure 45 shows the variation in the pattern of the center horn with position of shorting plungers in the adjacent guides. The coupling measures 24 db between the two outer horns and 13 or 14 db between the center and either one of these; for this reason the device is considered unusable. Incidentally the polarization is wrong (vertical) for the AN/SPS-2 system.

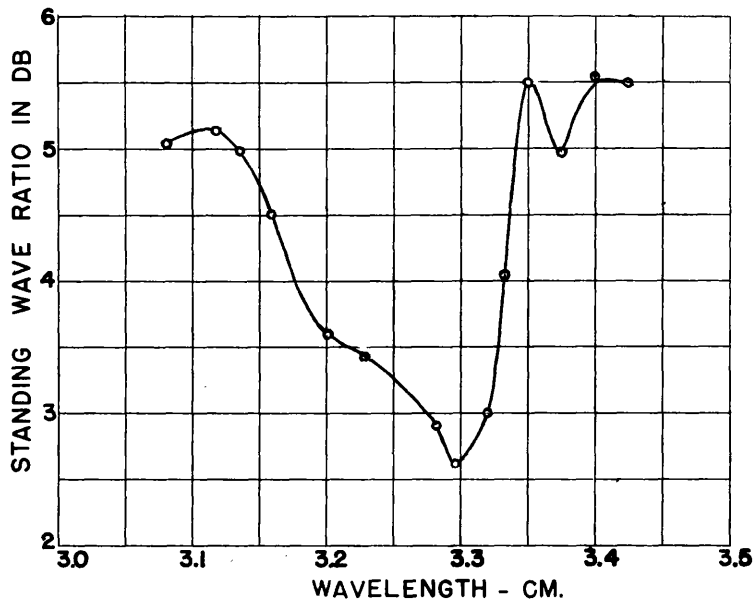

Fig. 44 - Standing wave ratio of three-element horn

Interlocking H-Flared Horns. A means for overlapping H-flared horns is shown in Figure 46. The phase centers of the pair at A are spaced one inch apart, or half the aperture dimension, and the patterns of either feed are excellent (Figure 47). Unfortunately the coupling is very strong. It has been measured for the two horns at B as a function of spacing with the following results:

Spacing	Coupling
0 (As at A)	13.0 db
0.25 in.	16.3
.50	20.6
.75	23.5
1.00	27.8
1.25	36.0

Thus if the horns are interlocked at all, the coupling is excessive.

In order to make certain that the method is unusable, a horn array with only a 1/4-inch overlap was made up and tested (Figure 48). When the second horn from the right (number 2) was fed, the signal level in the other guides had the following values:

Horn	Coupling
1	24 db
2	0
3	22
4	32
5	40

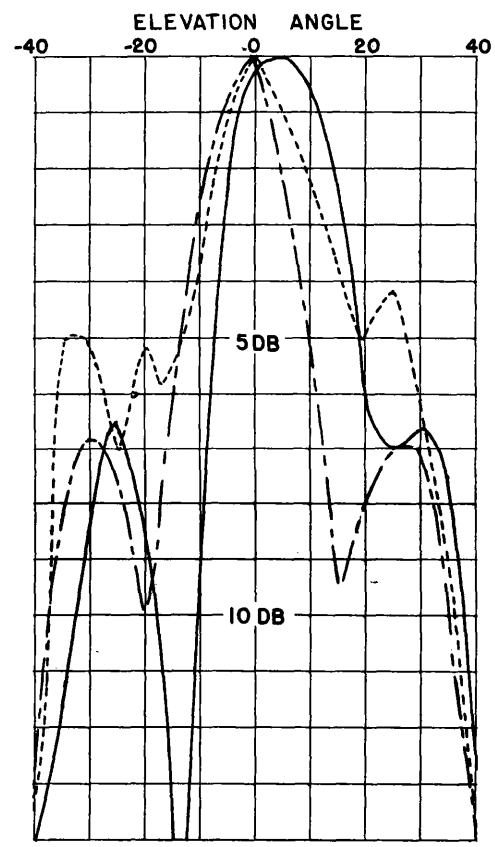

Fig. 45 - E-plane primary patterns of center channel of the array in Figure 43

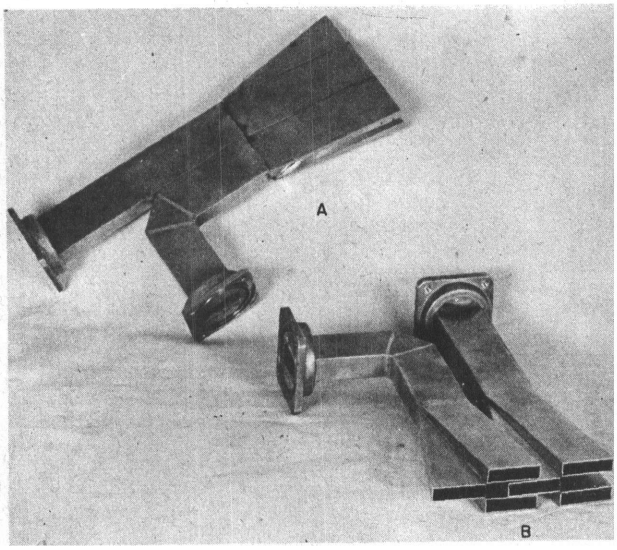

Fig. 46 - Interlocking H-flared horns

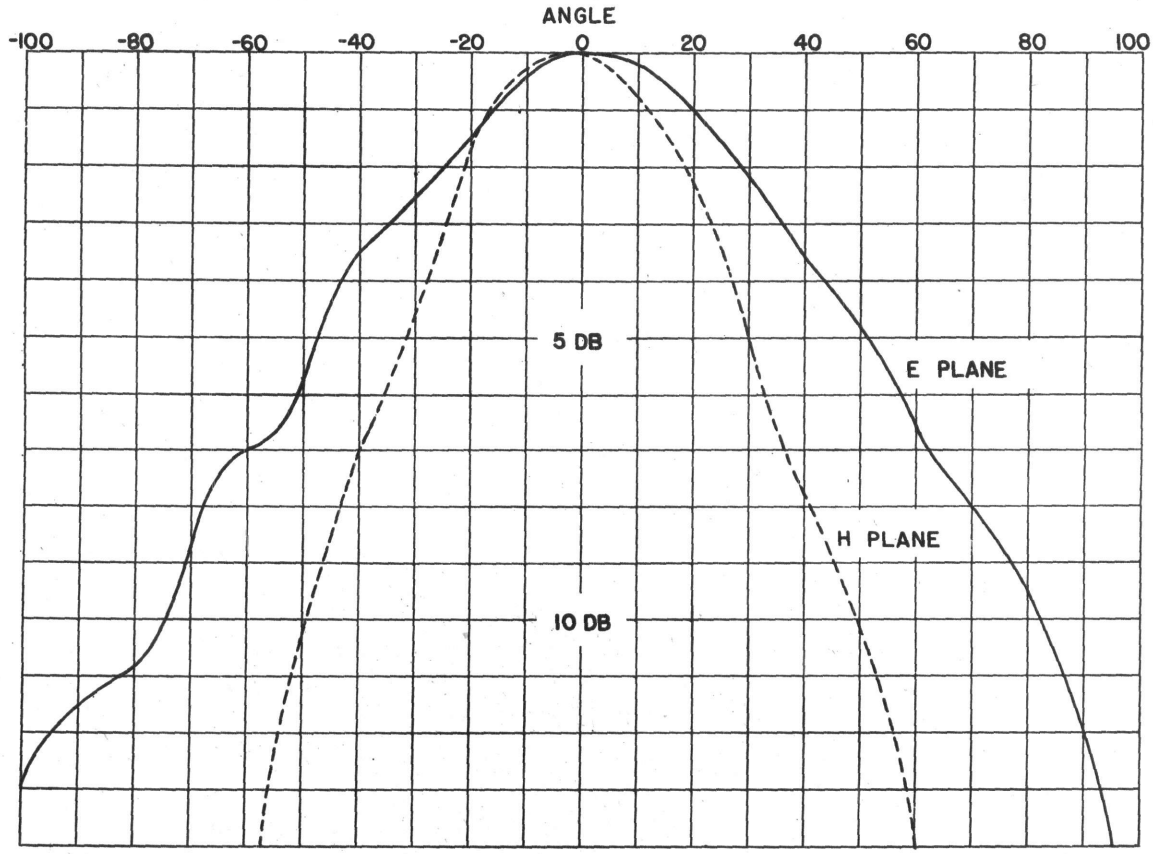

Fig. 47 - Primary patterns of a single interlocking horn

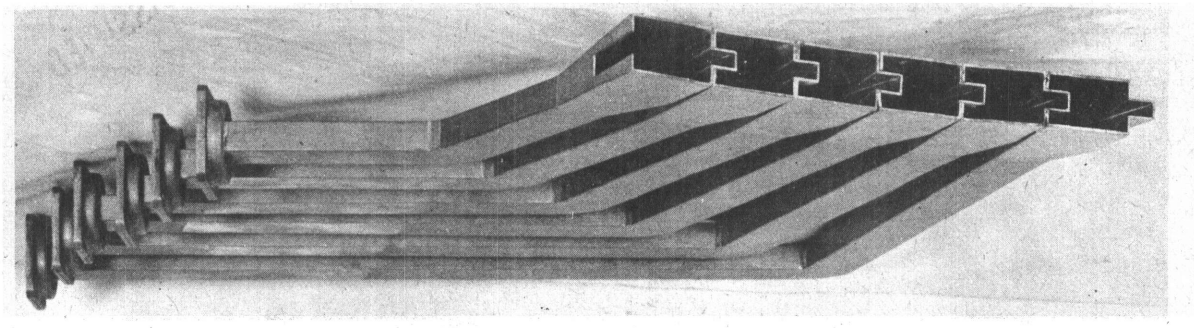

Fig. 48 - Array of interlocking horns

Then the feed assembly was mounted in the asymmetrically cut reflector shown in Figure 9 (60-3/4 x 35-1/2 x f = 21.1 inches). Figure 49 is a set of vertical patterns for horn number 2 taken to show the effect of shorting plungers in guides 1 and 3. The pattern variations are so great that this type of feed has little practical value.

Horns With Alternate Polarization. One method of reducing the coupling between overlapping horns is shown in Figure 50, where the outer two feeds are horizontally polarized and the center one is vertically polarized. In order to make it possible for

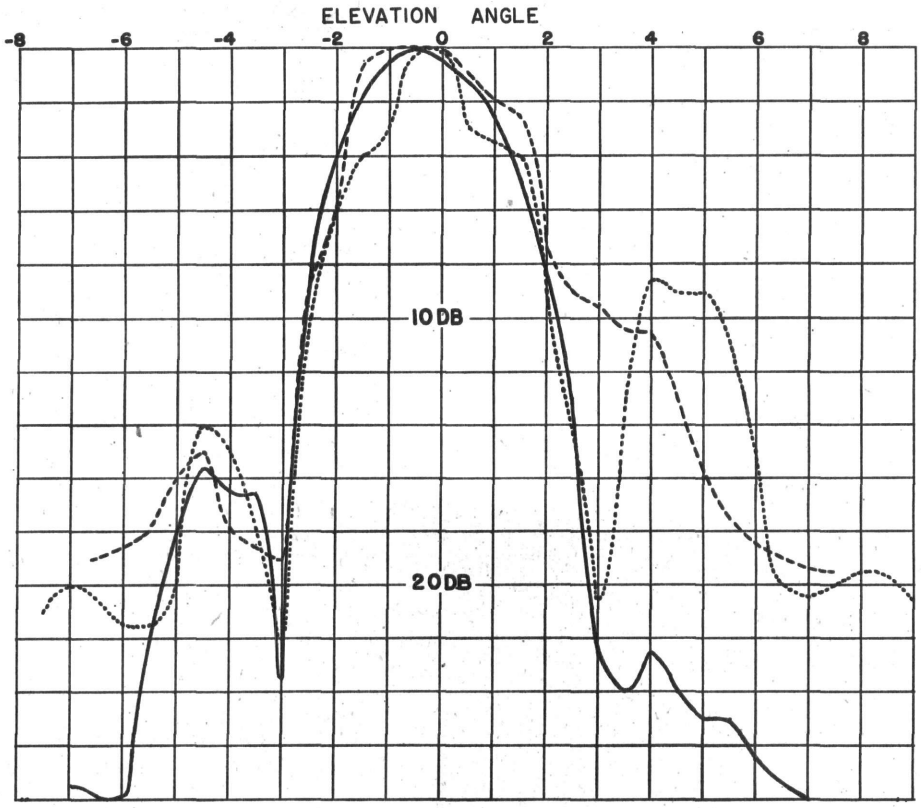

Fig. 49 - H-plane secondary patterns obtained with on-axis horn of Figure 9

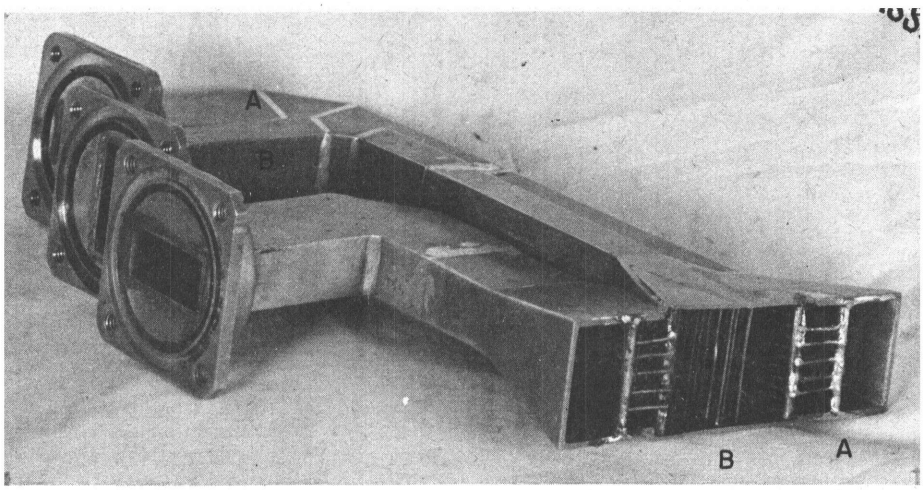

Fig. 50 - Set of three horns with alternating polarizations

two horns to occupy the same space, the inside walls of the outer horns have been replaced by vertical wires which support the essential transverse currents but do not interfere with the field of the center horn. On the other hand, the walls of the center horn have been replaced by longitudinal wires supported at the aperture by the pins used to produce beam sharpening in the H-flared horns. Since the currents in the broad face of a guide are not entirely longitudinal, it was expected that these walls might be somewhat leaky, and this turned out to be the case. The fine wires soldered across the front of the pins are not a part of the original scheme, but were added in an attempt to suppress some of the radiation leaking from the center horn.

The most promising characteristic of this feed is the very small coupling between channels: 39 db between the center and outside horns, and 45 db or more from one outer horn to the other. When it was installed in the reflector of Figure 9, the vertical patterns of two adjacent horns (Figure 51) were found to be quite stable. Unfortunately, the vertically polarized beam, Curve B, is much broader than the horizontally polarized one. This led to the discovery that the center horn excites the entire aperture by leakage through the horizontal wires.

In order to study this effect further, a second model was constructed containing two E-flared horns (Figure 52). If the horns in this figure are numbered from left to right, the coupling can be described as follows:

Feeding Horn 2		Feeding Horn 3	
Horn	Coupling	Horn	Coupling
1	28 db	1	27 db
2	0	2	28
3	27	3	0
4	37	4	30

The degree of isolation in this array was considered insufficient, and the work was discontinued in favor of another arrangement.

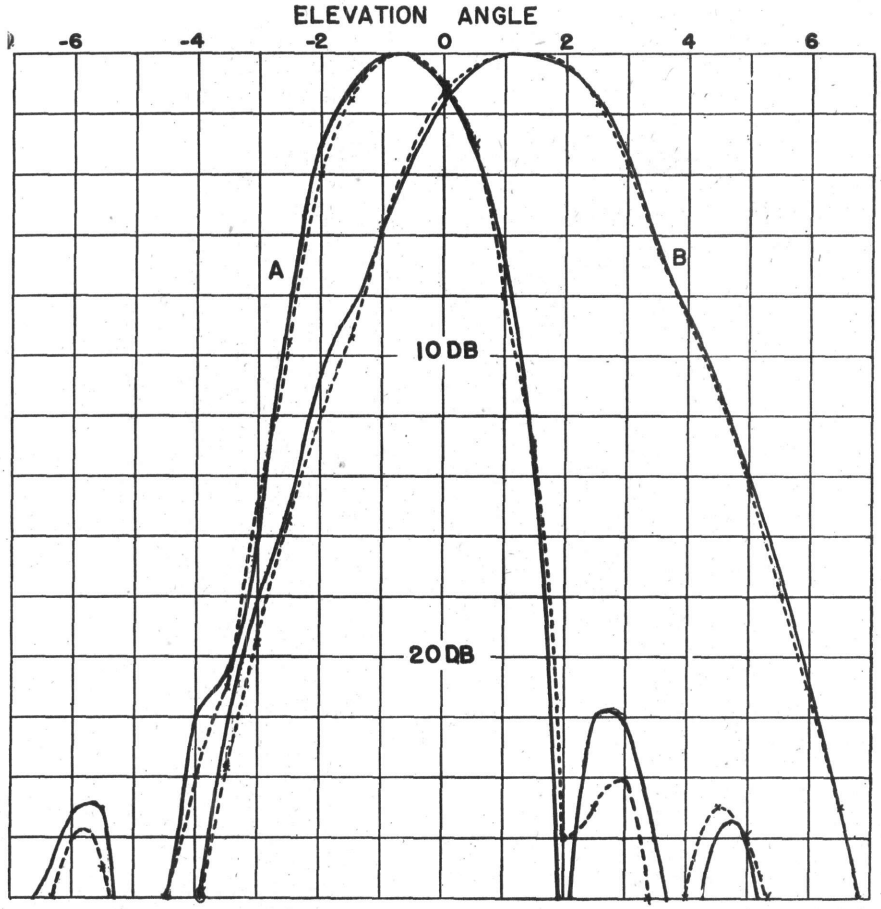

Fig. 51 - Vertical secondary patterns obtained with horns A and B of Figure 50

Fig. 52 - Set of four horns with alternating polarizations

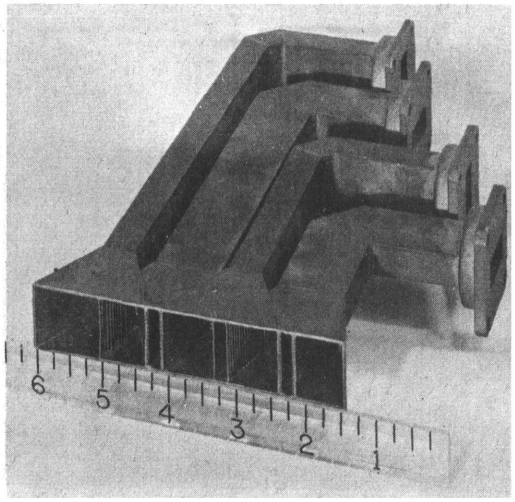

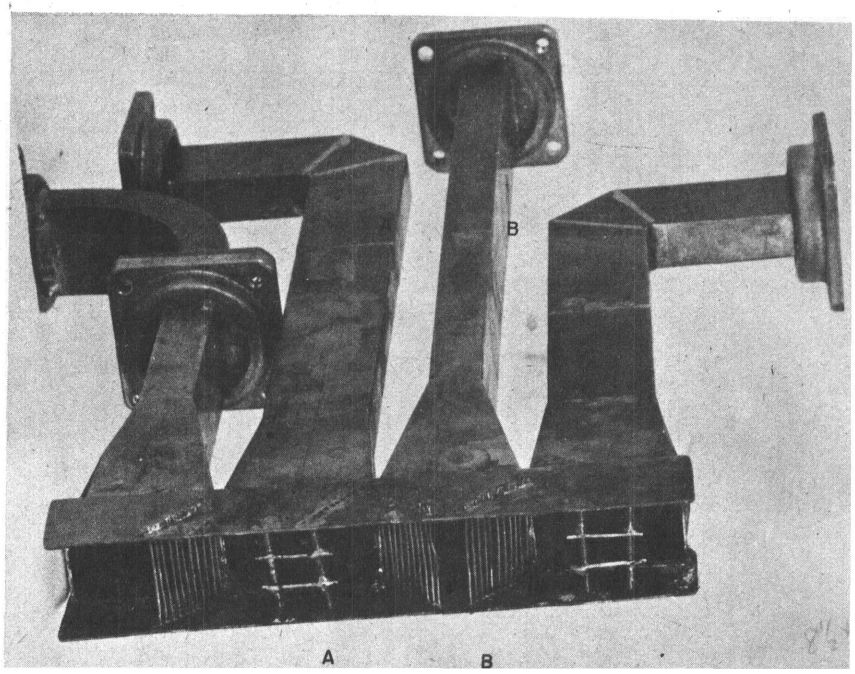

Fig. 53 - A second type of alternating polarization feed

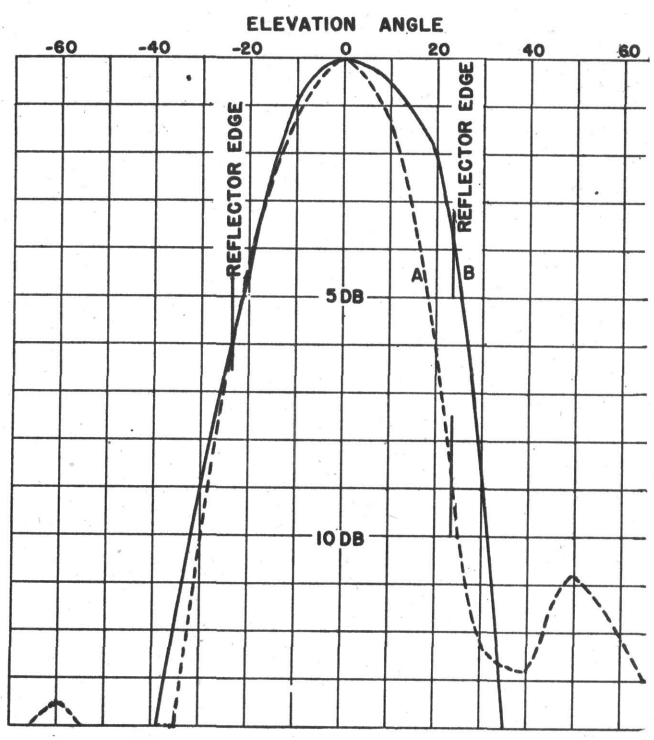

Fig. 54 - Vertical primary patterns of horns A and B of Figure 53

A second type of alternate-polarization horn is shown in Figure 53, where the E-flared horns are bounded by metal plates, mounted on pins in the aperture of the H-flared horns, rather than by longitudinal wires. These plates, 5/8 inch wide by 1/2 inch deep, are intended to function as wave guides operating below cut-off in isolating the E-horns. The coupling in this model is very small:

E to E	35 db
E to H	43
H to H	45

Figure 54 shows vertical patterns of the inner E- and H-horns and the angular limits of a reflector appropriate to a 2-db crossover level. The illumination taper is not much better than could be obtained with ordinary horns, but it is believed the situation could be improved by starting with smaller horns.

Other difficulties with this type of feed are high standing wave ratio (18 db in the H-horn), low power-handling capacity, and the uncertain dependence of target cross section on polarization.

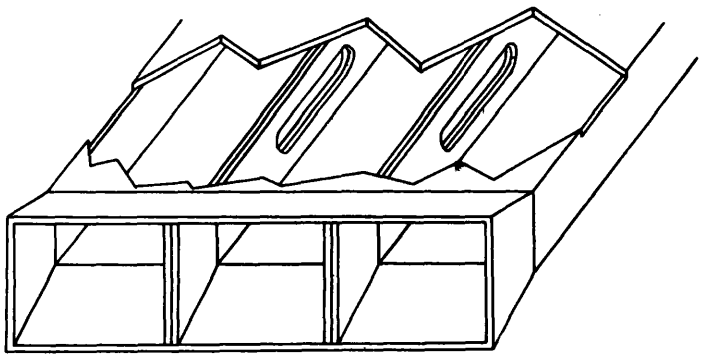

Fig. 55 - Feed system using directional couplers

Feeds Involving Directional Couplers. If the center wave guide in Figure 55 is fed, part of the energy is diverted into the horns on either side through directional couplers in the narrow walls, thus increasing the effective aperture. It should be possible to taper the illumination across the three horns and produce a sharp primary pattern free of side lobes. If these horns were part of a large array, a similar pattern could be obtained for each wave guide.

A set of three horns, 0.8 by 0.9 inches, was constructed with four-hole couplers between adjacent guides. Owing to the wall thickness, the horn spacing was one inch, which requires a reflector subtending an angle of 70 degrees. Curve A of Figure 56 is a typical H-plane pattern. The illumination taper across the dish is only 3.8 db (including 0.8-db space attenuation), so that the couplers are not particularly effective. This is explained by the fact that energy coupled through the narrow side of a guide is retarded 90 degrees in phase, producing a variation across the three-horn aperture. When a 3/4-inch slab of polystyrene was inserted in the center guide, the pattern was improved as shown in Curve B. Obviously the method cannot be applied to adjacent channels in an array.

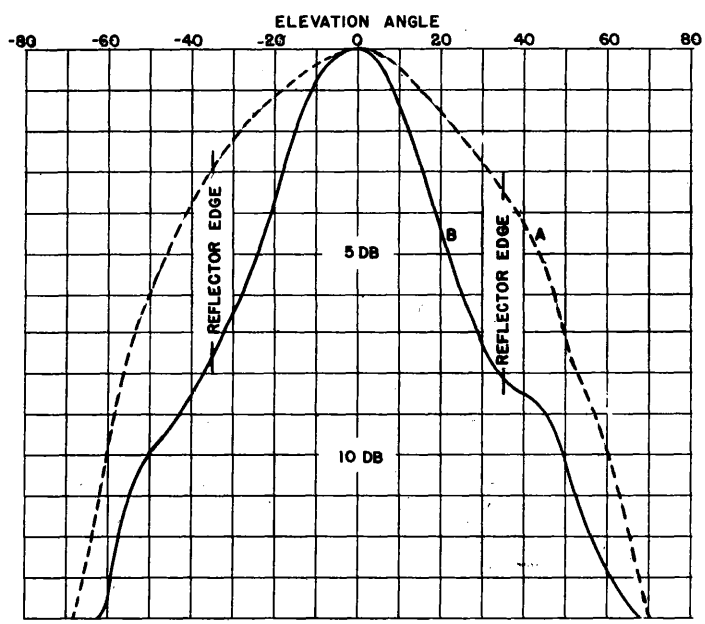

Fig. 56 - H-plane primary patterns of directional coupler feed with small coupling ratio: A - no phase correction, B - with phase correction

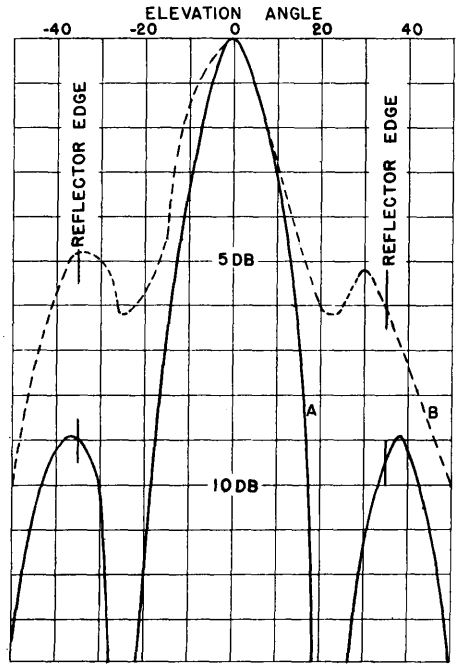

Fig. 57 - H-plane primary patterns of directional coupler feed: A - High coupling ratio, B - Moderate coupling ratio

The phase variation can be eliminated by coupling all of the power out of the wave guide being fed and dividing it equally between the neighboring guides. This may be accomplished by the use of long-slot couplers. The resulting primary pattern (Curve A of Figure 57), similar to that of two 0.9-inch horns separated 2 inches on centers, is so narrow that a reflector of f/D = 1.4 would be required for satisfactory illumination. But the spacing of the feed centers of adjacent channels is only 1 inch, and the crossover would be at the 3/4-db level. Such an antenna would be unsatisfactory for several reasons: The focal length is too great, the gain is reduced unnecessarily, and too many beams are required to cover a given angular sector.

Curve B of Figure 57 is typical of the patterns obtained with intermediate values of coupling. The side lobes are high and fall on the dish if it subtends the 70-degree angle required for a 2-db crossover.

It may therefore be concluded that directional coupler feeds will not be useful for a multiple-beam antenna until some means is devised for avoiding the adverse effect of the inherent phase shift.

Feeds Employing Band-Pass Filters. Figure 58 shows another scheme for overlapping the apertures of H-flared horns. Power from a magnetron on frequency f_2 is divided in a hybrid ring and fed into horns B and C in phase. In a similar manner, energy on frequencies f_1 and f_3 excites horn pairs A,B and C,D. Thus each channel uses an aperture twice as great as the spacing of the phase centers. The filters are required to prevent loss of power at the junctions T_1 and T_2.

A single channel of this feed system was made up using horns 0.8 x 0.9 inches, but omitting the filters. Figure 59 shows calculated and measured primary patterns for this arrangement. Since the phase centers are 1 inch apart, the reflector subtends 70 degrees, and the illumination taper is 13 db, a satisfactory figure.

The insertion loss of the filters depends on the Q required, and this in turn depends on the permissible

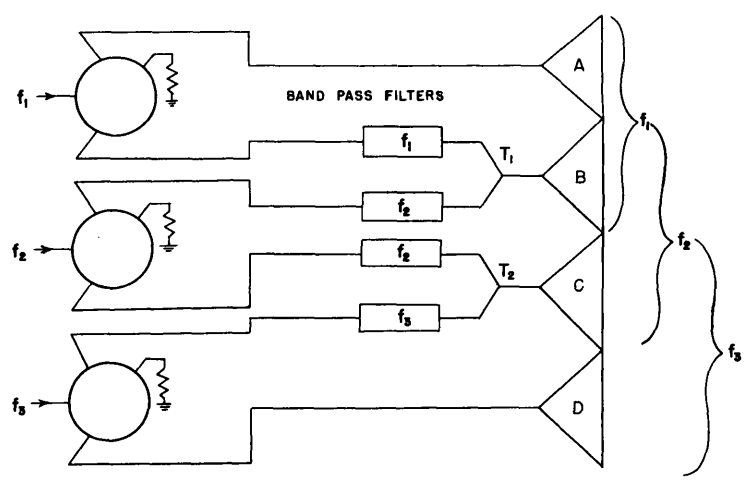

Fig. 58 - Feed system employing band-pass filters

frequency difference between adjacent channels, as determined by the variation of target cross section with frequency. Mumford[14] has described a filter with 0.3-db insertion loss that would permit operation 20 Mc apart at 1300 Mc. This might be a reasonable compromise. Loss in the filter would be more than compensated by the elimination of spillover, and the side lobes in the vertical pattern should be greatly reduced. On the other hand, the feed system is complicated by the use of hybrid rings and filters. It is anticipated that this idea will be investigated more thoroughly when time permits.

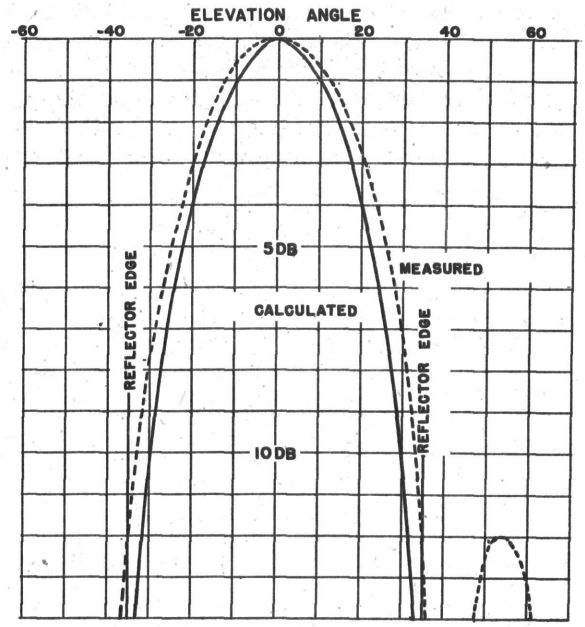

Fig. 59 - H-plane primary patterns of a feed simulating one channel of Figure 58

REFLECTOR-SHAPING AND THE MULTIPLE-FEED PROBLEM

Artificial Tapering of Illumination

Since no satisfactory improvement in the illumination taper could be effected by changes in the feed arrangement, methods involving alteration of the reflector were studied. Ordinary horns, flared to 0.8 x 1.18 inches, were used to feed reflectors of the type shown in Figures 60 and 61 where part of the metal was cut away or covered with harp material. This was done in an attempt to

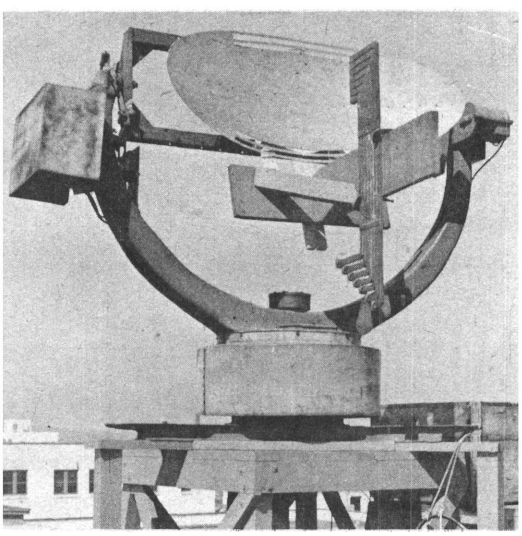

Fig. 60 - Reflector with longitudinal slots

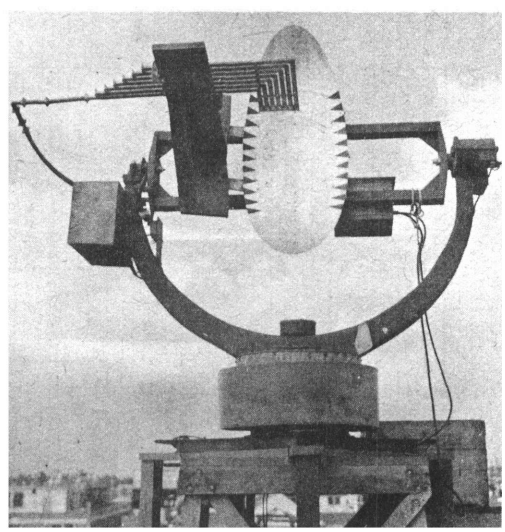

Fig. 61 - Reflector serrated with harp material

[14] W. W. Mumford, Bell System Tech. J., XXVII, 684-713, October 1948.

reduce the illumination at the edges of the dish artificially and thus to lower the side-lobe level. Figures 62 and 63 are the vertical and horizontal patterns of the complete paraboloid (60-3/4 x 24 x f = 21.1 inches), while Figures 64, 65, 66, and 67 were obtained with the cut reflectors. It is evident that these modifications broaden the secondary beam and raise the crossover, but they leave the side-lobe level essentially unchanged and therefore offer no great advantage over merely decreasing the height of the dish.

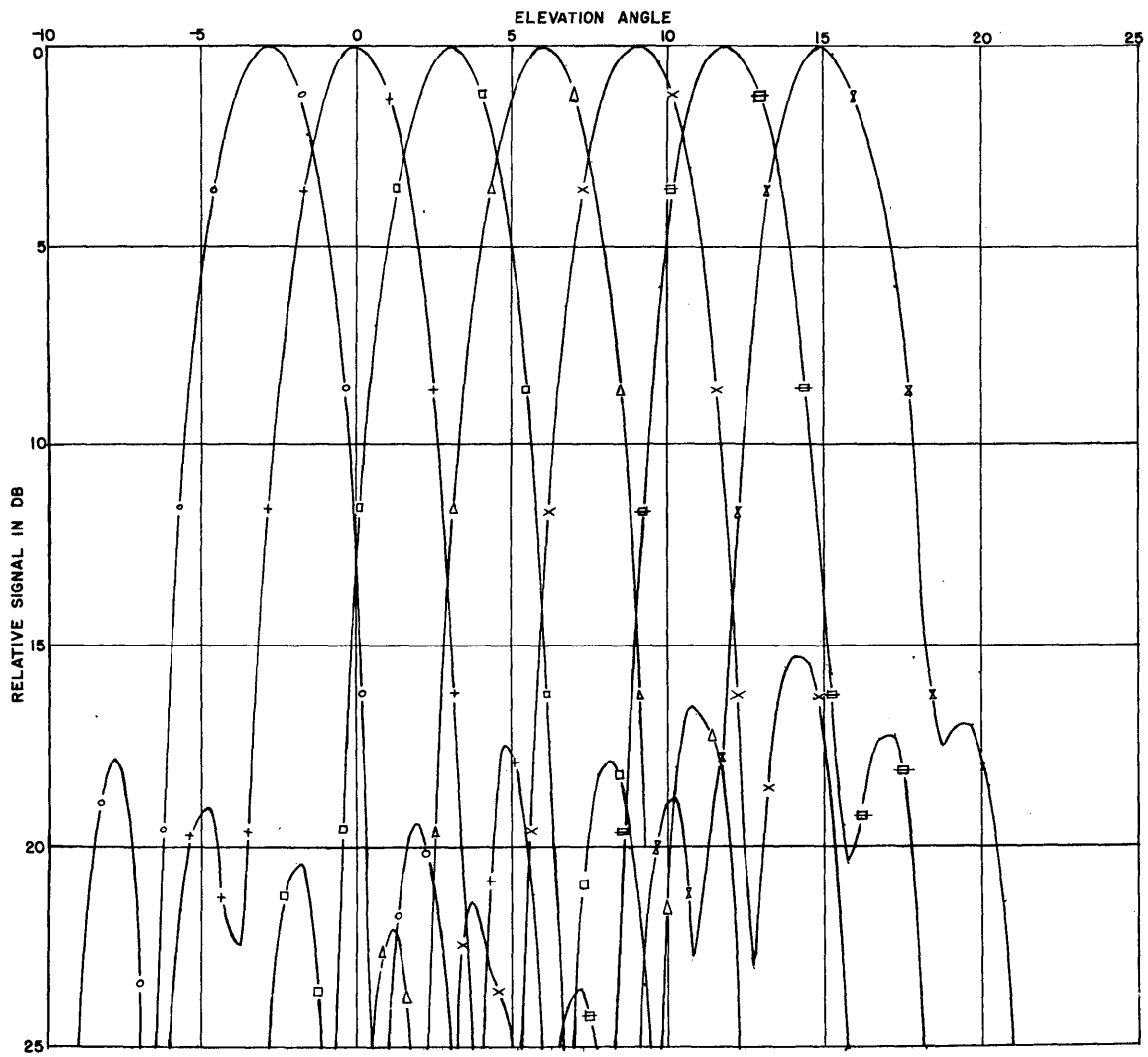

Fig. 62 - Vertical patterns of antenna of Figure 61, harp material removed

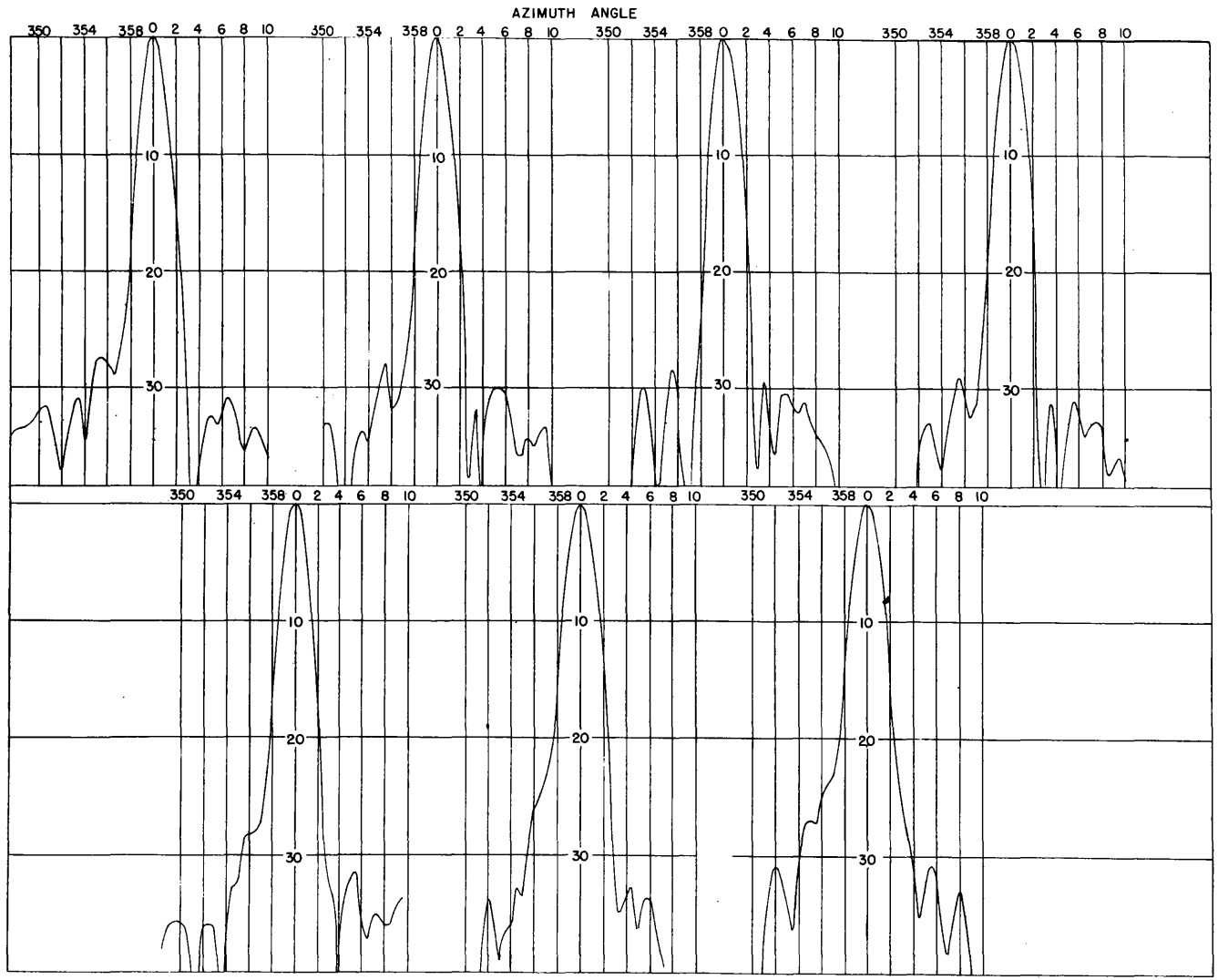

Fig. 63 - Horizontal patterns of antenna of Figure 61, harp material removed

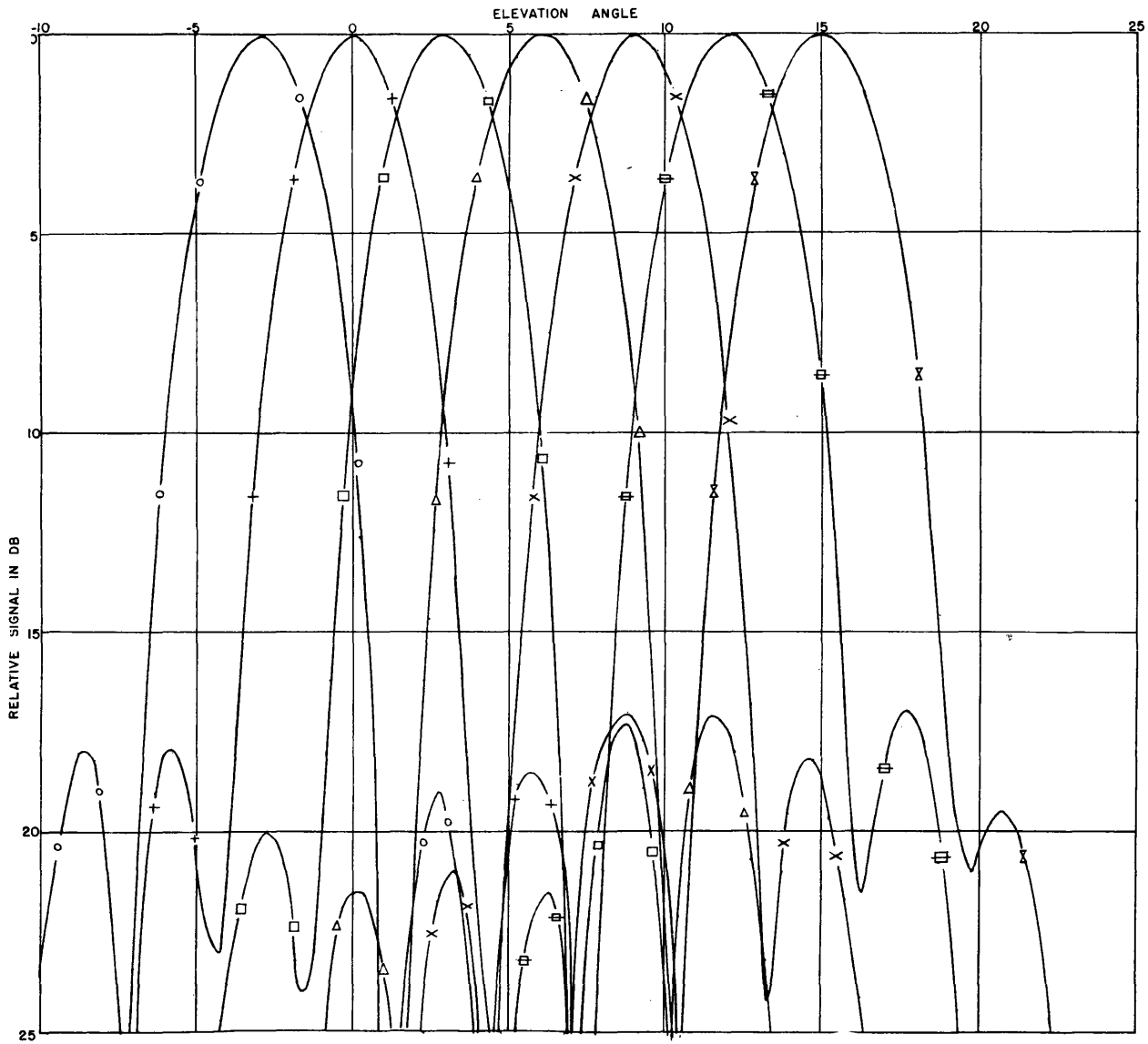

Fig. 64 - Vertical patterns of antenna of Figure 60

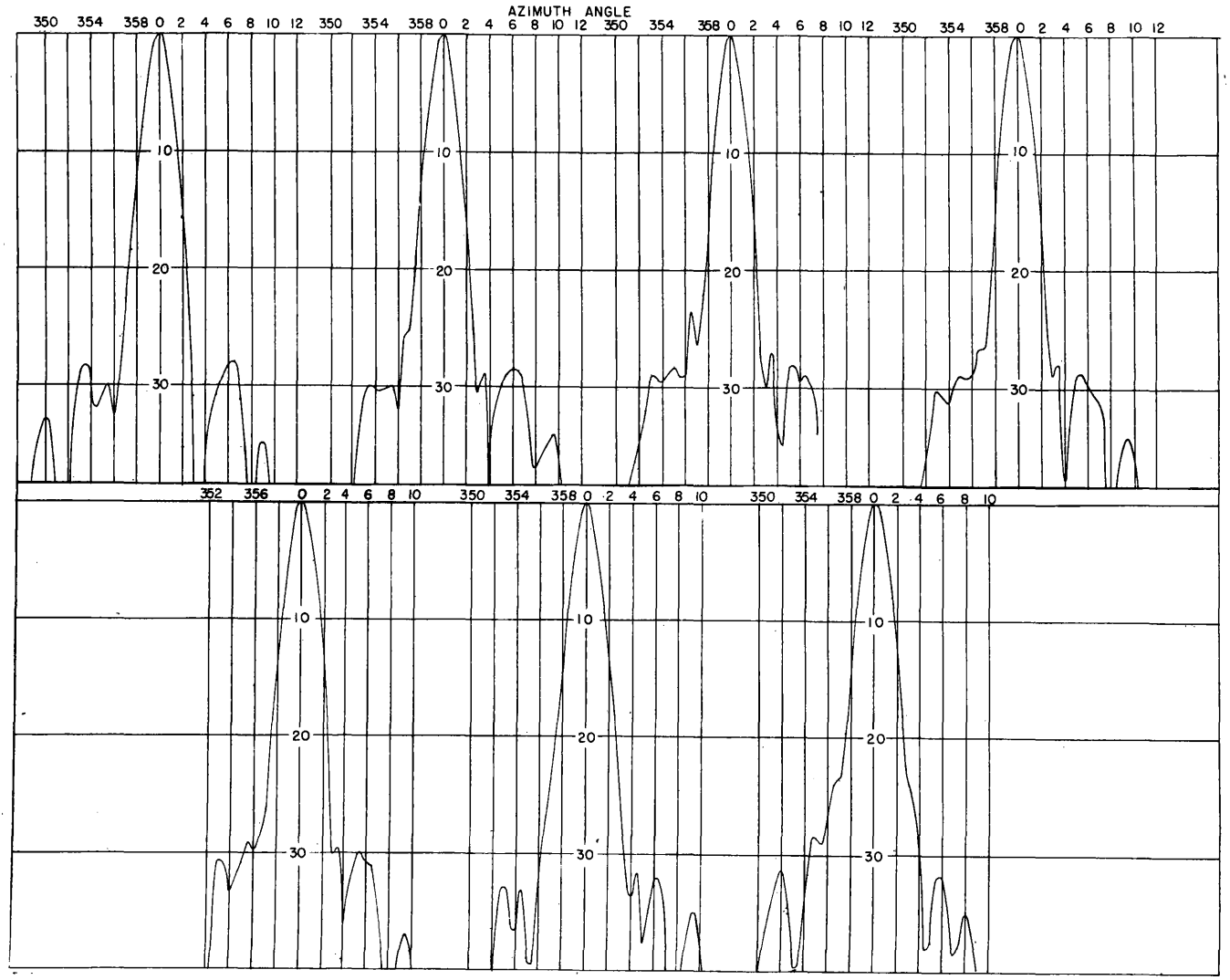

Fig. 65 - Horizontal patterns of antenna of Figure 60

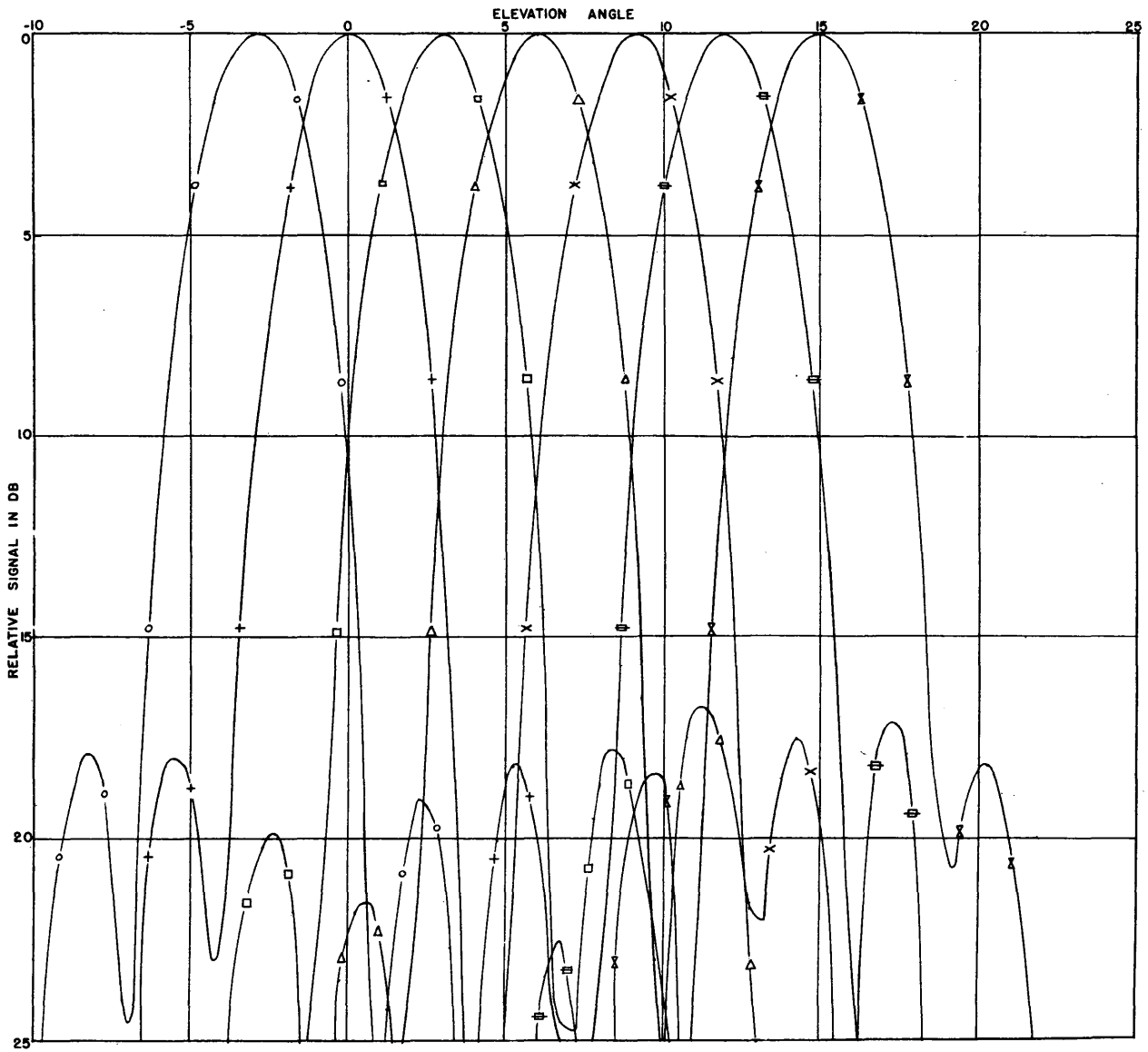

Fig. 66 - Vertical patterns of antenna of Figure 61

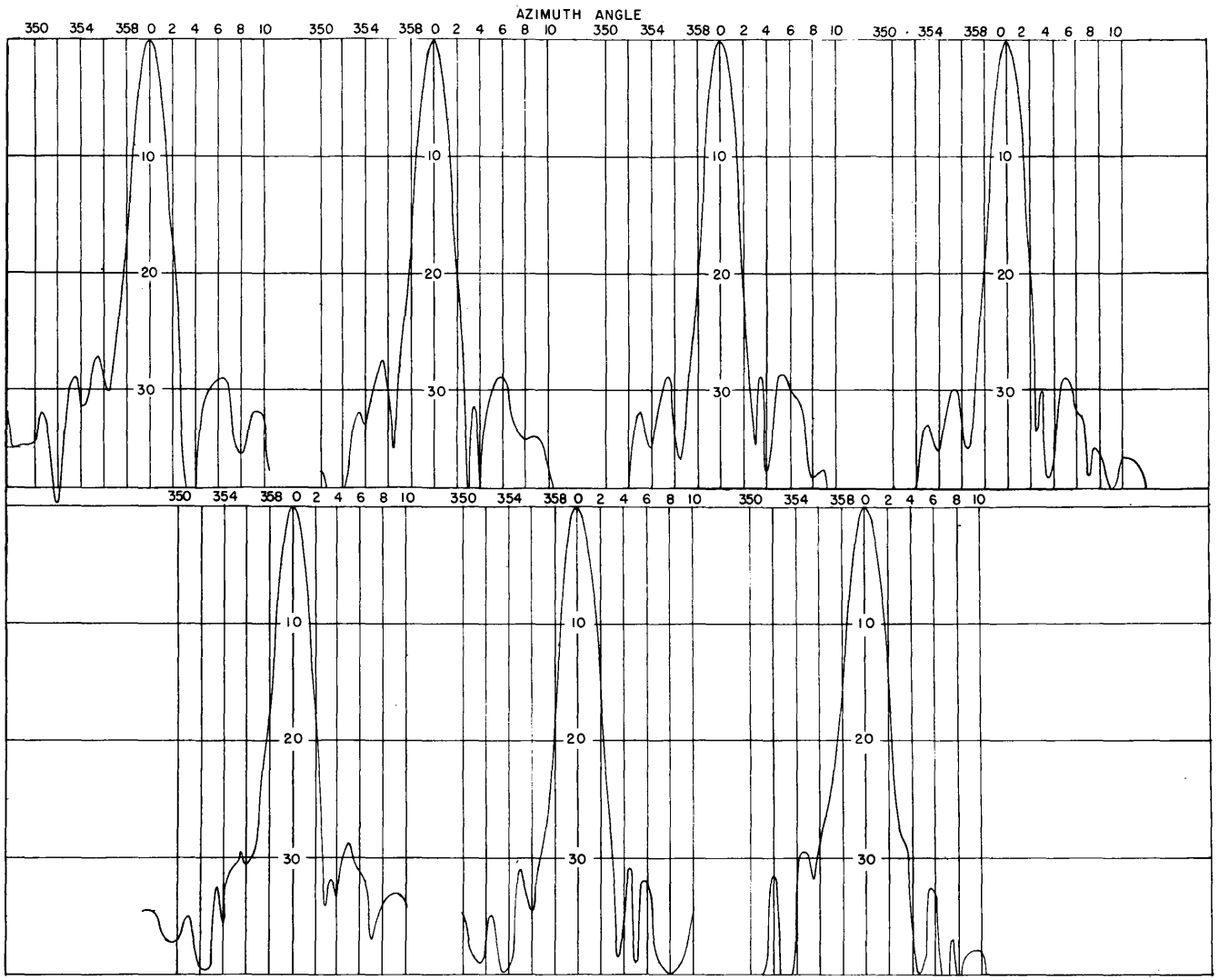

Fig. 67 - Horizontal patterns of antenna of Figure 61

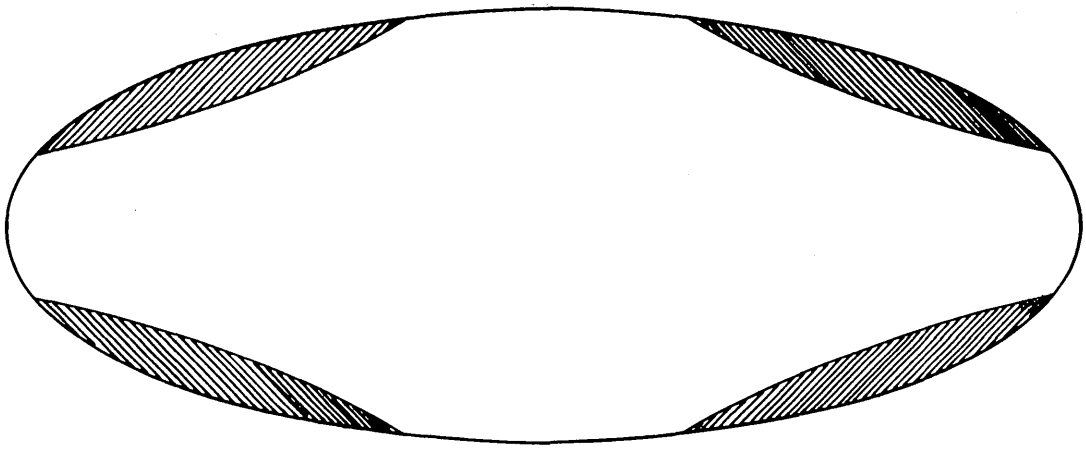

Fig. 68 - Modification of reflector contour

Alteration of the Reflector Contour

One worthwhile means of lowering the side lobes in the vertical plane was discovered when the dish contour was altered as shown in Figure 68. The vertical pattern (Figure 69) had lobes of 23 db compared with the usual 18 db. Unfortunately, the azimuth pattern was affected adversely (Figure 70).

Deformation of the Phase Front

Another method, which has not yet been thoroughly investigated, involves deforming the phase front in some systematic manner. In this way the secondary beam is broadened, and a larger feed horn may be used, reducing the spillover loss and the side-lobe level.

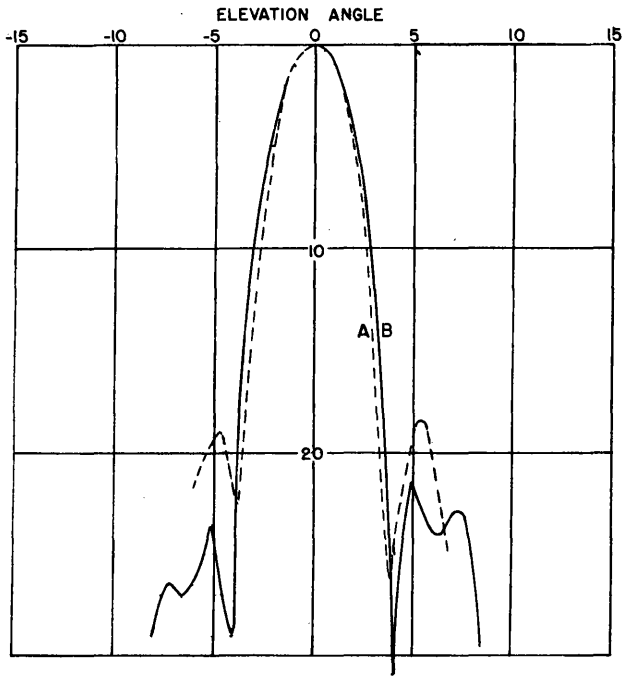

Fig. 69 - Effect on vertical pattern of reflector modification of Figure 68: A - On-axis pattern from Figure 62, B - Pattern with modified reflector

The only disadvantage is a reduction in aperture efficiency. Phase distortion may be obtained in one plane only by the use of a bifocal reflector. A simpler scheme (proposed by Dr. L. C. Van Atta of the Antenna Research Section) consists of making a horizontal cut through the center of a paraboloid and inserting a thin parabolic cylinder between the two halves. The vertical cross section of such an antenna is shown in Figure 71, together with an indication of the phase variation across the aperture. Preliminary theoretical and experimental patterns show that the first side lobe merges into the main beam and broadens it at a level which increases with the height of the parabolic cylinder. Since the remaining side lobes are very low, this method may prove to be valuable, particularly in the case of the single-frequency system already mentioned.

PRELIMINARY X-BAND DESIGN OF THE AN/SPS-2 ANTENNA

After careful consideration of the special feeds and reflector designs described in the preceding two sections, it has been concluded that the most practical antenna for the AN/SPS-2 is a simple paraboloid of elliptical contour fed by an array of ordinary horns. The factor given most weight in this evaluation is the degree of illumination taper consistent with a 2-db crossover; but simplicity, power-handling capacity, and impedance match have also been considered, along with the desirability of using the same polarization on all beams and of keeping the frequency differences between them small.

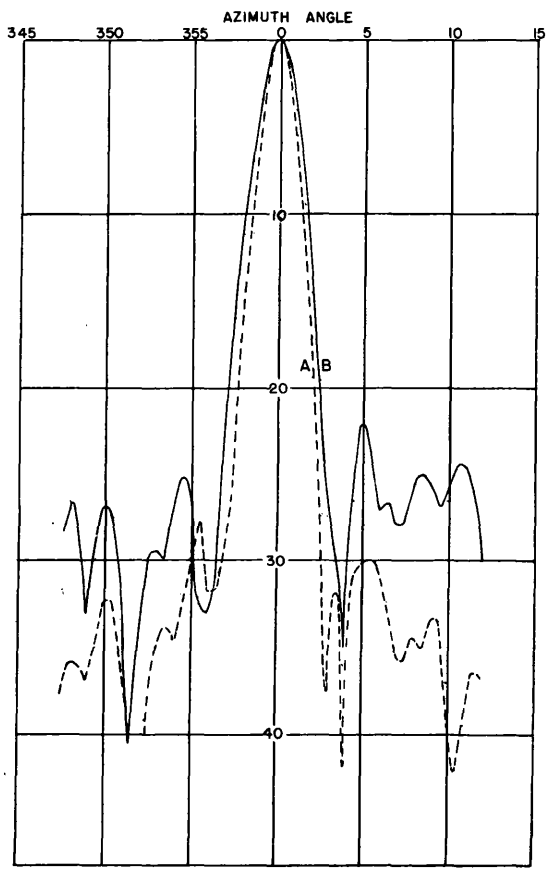

Fig. 70 - Effect on horizontal pattern of reflector modification: A - On-axis pattern from Figure 63, B - Pattern with modified reflector

A straightforward stacked-beam antenna has been designed and constructed to meet the following specifications:

Horizontal beam width	1.5°
Vertical beam width	3.2°
Crossover level	2.0 db
Coverage	0 to 20°

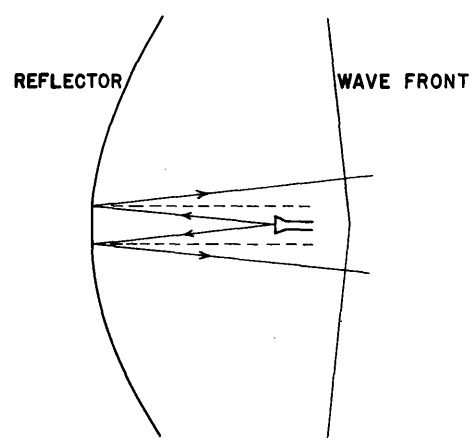

Fig. 71 - Wavefront of split-dish antenna

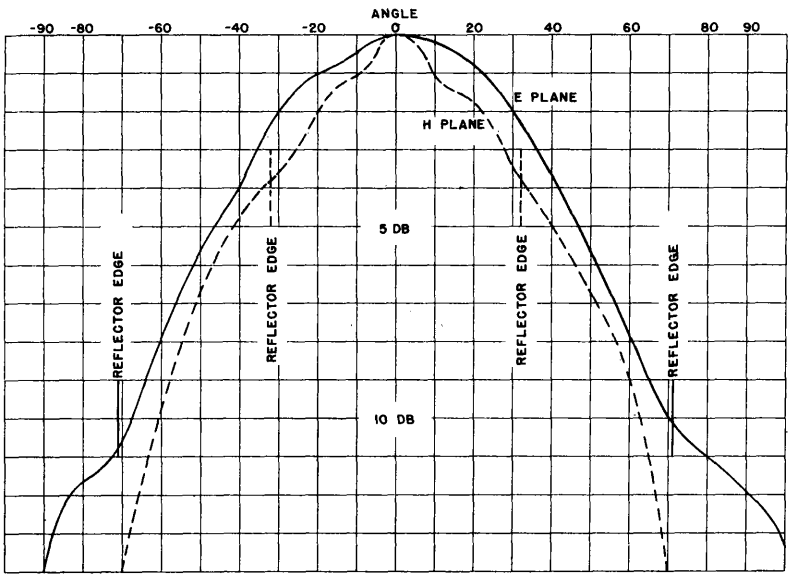

Fig. 72 - Primary patterns of 0.8 x 1.06-inch horn in array

The model frequency, 3.2 cm, has a scaling factor of 7.21 to 1300 Mc, the center of the band allotted to this radar.

After some preliminary measurements, the reflector width and height were set at 60-3/4 and 24 inches respectively. The beam widths finally obtained, 1.55 and 3.15 degrees, are related to the aperture dimensions by the formulas

$$\text{Horizontal beam width} = 75^\circ \ \lambda/D$$
$$\text{Vertical beam width} = 60^\circ \ \lambda/D.$$

The difference in constants shows the dependence of beam width on illumination taper. A focal length of 21.1 inches was chosen from those available in spun aluminum dishes. It gives an f/D ratio of 0.88, a good compromise between illumination taper and coupling between horns as indicated by the arrows in Figure 25. By referring to Figure 20 it is seen that the H-plane horn dimension appropriate to a 2-db crossover is 0.84 wavelength or 1.06 inches. However, some allowance must be made for wall thickness, and the available aperture in the final array is 1.047 inches. The E-plane dimension was made 0.8 inches ID to provide an illumination taper of 14 db, including 3.6-db space attenuation, as shown by one of the curves of Figure 72.

Figure 73 is a view of the complete antenna, and the feed system is shown in Figure 74. The dielectric horn enclosure of the first figure is described later.

Method of Pattern Calculation

It has been shown that the requirement of 2-db crossover severely restricts control of the illumination in the H-plane. Thus, the illumination at the upper and lower edges of the dish may be no more than 3 or 4 db down from the value at the center. One must expect high side lobes in the vertical plane and, in addition, some gain reduction arising from spillover. It is therefore desirable to calculate the performance to be expected from the various primary patterns available, and formulas for the patterns and gain of a reflector of elliptical outline have been derived for this purpose.

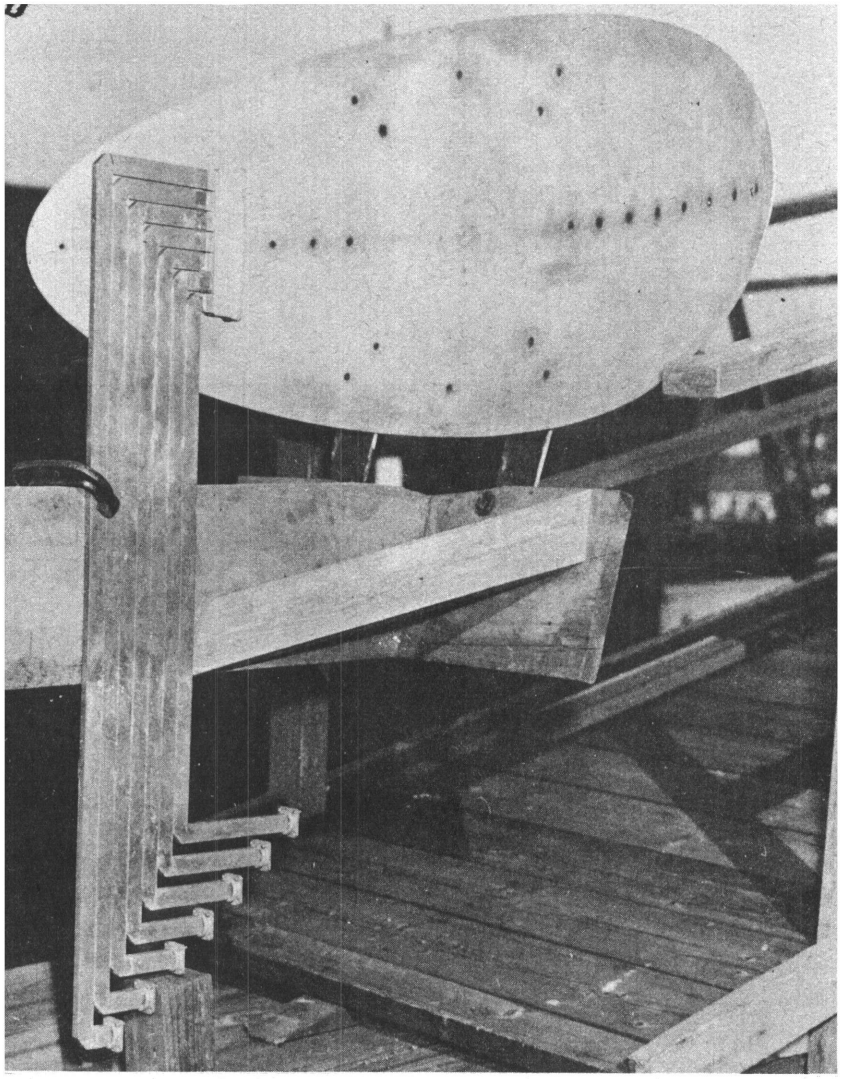

Fig. 73 - Front view of X-band model of AN/SPS-2 antenna

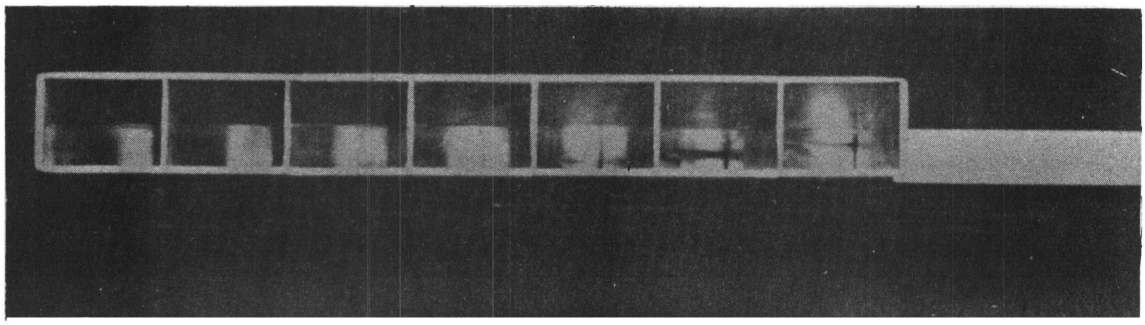

Fig. 74 - Feed system with pressurizing cover removed

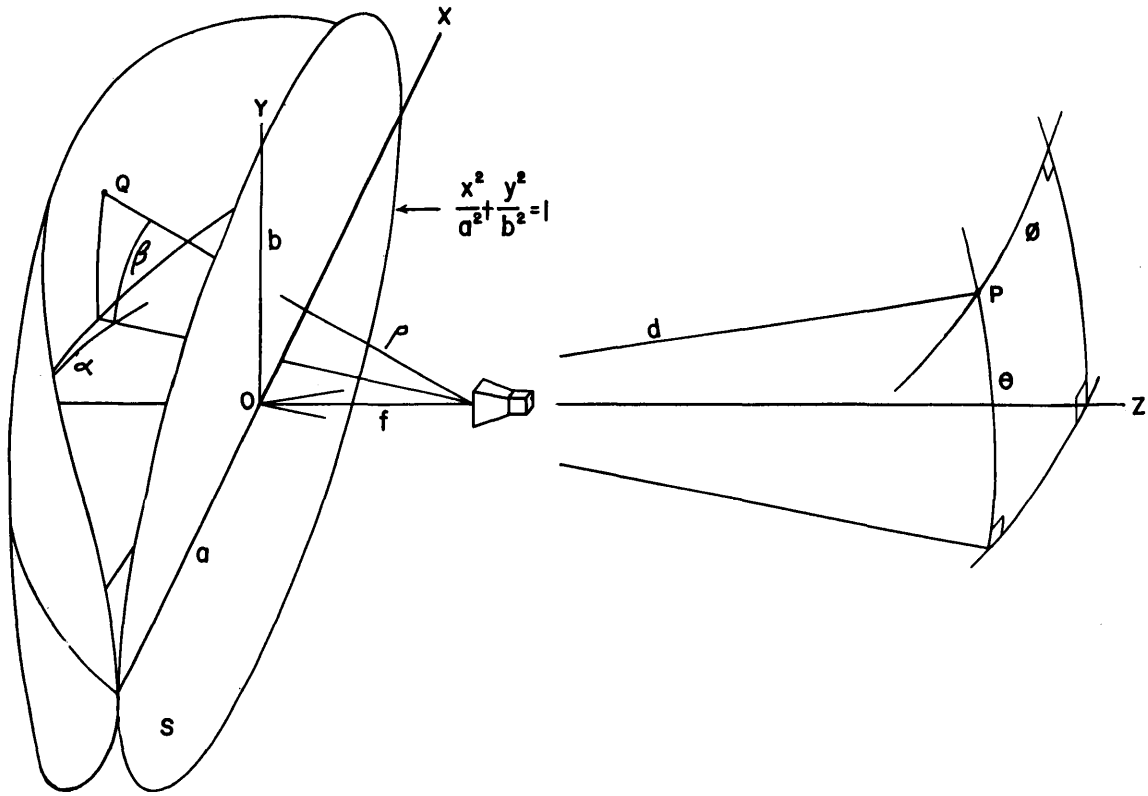

Fig. 75 - Parameters involved in pattern calculation

Derivation of Pattern Expression. To find the radiation pattern of the reflector of Figure 75, let the field strength in the aperture plane be given by

$$E\,(x,y) = E_0\, A(x\,,y)\; e^{i\,\psi\,(x,y)}, \tag{8}$$

where E_0 is the maximum value of the field, and A and ψ are the amplitude and phase distribution respectively. The field strength at a distant point P which lies at a small angle to the axis is given by[15]

$$E(d,\phi,\theta) = \frac{E_0 i e^{-ikd}}{\lambda\, d} \int_S A(x,y) e^{i\,[k(x\,\sin\phi\, + y\,\sin\,\theta)\, + \psi\,(x,y)]}\; dS \tag{9}$$

where $k = 2\pi/\lambda$. The quantity preceding the integral sign is independent of the angles ϕ and θ and therefore has no effect on the pattern. If the phase is constant over the aperture, the factor $e^{i\psi}$ may also be dropped.

The amplitude function may ordinarily be expressed as the product of the amplitude distributions along the two axes,

$$A(x,y) = X(x)\;\; Y(y), \tag{10}$$

---

[15] H. T. Friis and W. D. Lewis, Bell System Tech. J., 26; 219-317, April 1947.

and these in turn may be calculated from the corresponding primary patterns of the horn taking into account the space attenuation. For example, X(x) can be obtained from the E-plane pattern, $\overline{E}_e(\alpha)$, from the parametric equations

$$\left.\begin{aligned} \text{Relative amplitude} &= \overline{E}_e(\alpha)\frac{f}{\rho} = \overline{E}_e(\alpha)\cos^2\frac{\alpha}{2} \\ x &= 2f\tan\frac{\alpha}{2} \end{aligned}\right\} \tag{11}$$

With these simplifications, the pattern is given by the integral in Equation (9), which may be written

$$F(u_1,u_2) = \int_{-a}^{a}\int_{-b\sqrt{1-(\frac{x}{a})^2}}^{b\sqrt{1-(\frac{x}{a})^2}} X(x)\,Y(y)\,e^{i\left[u_1\frac{x}{a}+u_2\frac{y}{b}\right]}\,dy\,dx \tag{12}$$

where

$$u_1 = ak\sin\phi$$
$$u_2 = bk\sin\theta.$$

The integral may be approximated by representing the functions X and Y by the first few terms of a Fourier series:

$$\left.\begin{aligned} X(x) &= \sum_{r=0}^{m} a_r\cos r\pi\frac{x}{a} \\ Y(y) &= \sum_{s=0}^{n} b_s\cos s\pi\frac{y}{b} \end{aligned}\right\} \tag{13}$$

Only cosine terms are needed, since the illumination in a symmetrically cut reflector may be assumed symmetrical about both axes. The coefficients a_r and b_s are obtained by solving a set of simultaneous equations which match the experimental illumination curve at a number of equally spaced points across the aperture. The evaluation of the integral in terms of these coefficients is carried out in Appendix III, with the result

$$F(u_1,u_2) = \pi ab\sum_{r=0}^{m}\sum_{s=0}^{n} a_r\,b_s\,G_{rs}(u_1,u_2). \tag{14}$$

$G_{rs}(u_1,u_2)$ is given by:

$$\begin{aligned} 4G_{rs}(u_1,u_2) = {} & \Lambda_1\left(\sqrt{(r\pi-u_1)^2+(s\pi-u_2)^2}\right) + \Lambda_1\left(\sqrt{(r\pi-u_1)^2+(s\pi+u_2)^2}\right) \\ & + \Lambda_1\left(\sqrt{(r\pi+u_1)^2+(s\pi-u_2)^2}\right) + \Lambda_1\left(\sqrt{(r\pi+u_1)^2+(s\pi+u_2)^2}\right), \end{aligned} \tag{15}$$

where[16]

$$\Lambda_1(x) = 2\frac{J_1(x)}{x}.$$

[16] E. Jahnke and F. Emde, "Tables of Functions with Formulae and Curves," Dover Publications, (1945), p. 128 and Table on p. 181.

The principal plane patterns are easier to compute. For example, the vertical pattern involves only

$$G_{rs}(0_1, u_2) = \frac{1}{2}\Lambda_1\left(\sqrt{(r\pi)^2 + (s\pi - u_2)^2}\right) + \frac{1}{2}\Lambda_1\left(\sqrt{(r\pi)^2 + (s\pi + u_2)^2}\right), \tag{16}$$

while the horizontal pattern contains

$$G_{rs}(u_1, 0) = \frac{1}{2}\Lambda_1\left(\sqrt{(r\pi - u_1)^2 + (s\pi)^2}\right) + \frac{1}{2}\Lambda_1\left(\sqrt{(r\pi + u_1)^2 + (s\pi)^2}\right). \tag{17}$$

The coefficients of Equation (17) can be obtained from those of Equation (16) through the relation

$$G_{rs}(u,0) = G_{rs}(0,u). \tag{18}$$

In Table III are listed values of $G_{rs}(0,u)$ for r and s running from 0 to 3 and for u running from 0 to 7π. This permits the use of as many as four terms in fitting the illumination functions.

Conclusions. The approximations involved in Equation (14) enter through Equations (10) and (13), and the first of these is undoubtedly the more serious. The assumption of separability of the illumination function A(x,y) has been examined for a similar antenna. In Figure 76, the full line curves represent the measured contours of illumination while the dashed curves indicate the illumination obtained by the approximation of Equation 10. It is seen that the two families of curves differ only in a restricted region of the aperture where the illumination is low. The errors introduced by the Fourier analysis can be reduced by taking a sufficient number of terms and can be visualized by plotting the synthesized illumination curve alongside the experimental one.

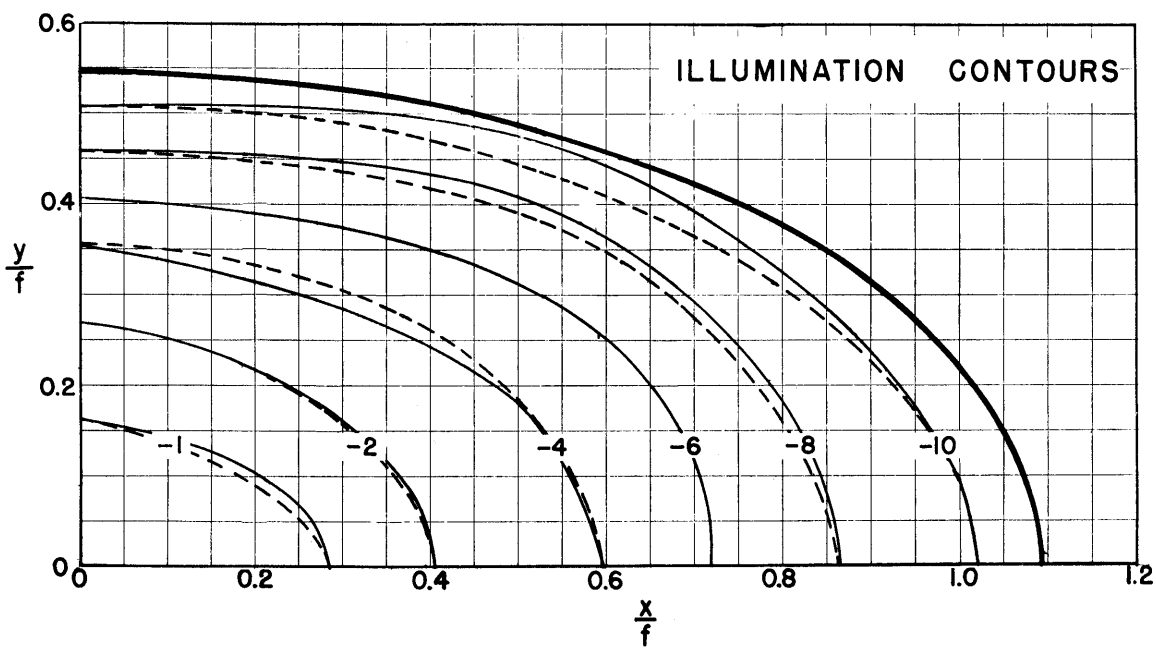

Fig. 76 - Illumination contours on antenna aperture

TABLE III

u	πG_{00}	πG_{01}	πG_{02}	πG_{03}	πG_{10}	πG_{11}	πG_{12}	πG_{13}	πG_{20}	πG_{21}	πG_{22}	πG_{23}	πG_{30}	πG_{31}	πG_{32}	πG_{33}
0.000π	3.1416	0.5688	-0.2124	0.1178	0.5688	-0.3042	0.0032	0.0378	-0.2124	0.0032	0.1820	-0.1200	0.1178	0.0378	-0.1200	0.0004
0.250π	2.9042	0.6753	-0.1882	0.0961	0.4764	-0.2369	-0.0224	0.0398	-0.1980	0.0042	0.1576	-0.0935	0.1132	0.0339	-0.1087	-0.0020
0.500π	2.2674	0.9460	-0.1032	0.0342	0.2366	-0.0637	-0.0808	0.0393	-0.1522	0.0069	0.0934	-0.0252	0.0984	0.0232	-0.0768	-0.0091
0.750π	1.4112	1.2569	0.0686	-0.0550	-0.0606	0.2029	-0.1319	0.0234	-0.0864	0.0020	0.0126	0.0581	0.0734	0.0099	-0.0309	-0.0199
1.000π	0.5692	1.4646	0.3435	-0.3042	-0.3042	0.2855	-0.1332	-0.0184	0.0032	-0.0152	-0.0584	0.1226	0.0396	-0.0012	0.0191	-0.0323
1.250π	-0.0606	1.4590	0.7028	-0.1937	-0.4132	0.3148	-0.0652	-0.0801	0.0948	-0.0424	-0.1019	0.1448	-0.0056	-0.0054	0.0628	-0.0419
1.500π	-0.3754	1.2182	1.0834	-0.1539	-0.3640	0.2195	0.0565	-0.1403	0.1690	-0.0687	-0.1117	0.1191	-0.0520	-0.0016	0.0909	-0.0438
1.625π	-0.4154	1.0259	1.2478	-0.0873	-0.2912	0.1366	0.1239	-0.1599	0.1918	-0.0766	-0.1069	0.0917	-0.0740	0.0030	0.0973	-0.0405
1.750π	-0.3904	0.8045	1.3901	0.0132	-0.1980	0.0444	0.1850	-0.1670	0.2020	-0.0780	-0.0975	0.0580	-0.0934	0.0086	0.0987	-0.0340
2.000π	-0.2124	0.3435	1.5312	0.3124	0.0022	-0.1332	0.2649	-0.1350	0.1820	-0.0584	-0.0746	-0.0139	-0.1202	0.0191	0.0867	-0.0119
2.250π	0.0141	-0.0331	1.4536	0.7048	0.1532	-0.2415	0.2571	0.0417	0.1132	-0.0113	-0.0552	-0.0743	-0.1240	0.0233	0.0614	0.0191
2.500π	0.1690	-0.2380	1.1679	1.1085	0.2024	-0.2438	0.1600	0.1485	0.0178	0.0504	-0.0430	-0.1075	-0.1016	0.0157	0.0214	0.0511
2.750π	0.1978	-0.2572	0.7491	1.4194	0.1494	-0.1512	0.0093	0.2076	-0.0696	0.1024	-0.0326	-0.1131	-0.0562	-0.0046	0.0054	0.0754
3.000π	0.1178	-0.1448	0.3124	1.5496	0.0378	-0.0184	-0.1350	0.2699	-0.1200	0.1226	-0.0139	-0.0992	0.0004	-0.0323	-0.0119	0.0847
3.250π	-0.0056	0.0085	-0.0311	1.4527	-0.0698	0.0955	-0.2180	0.2457	-0.1174	0.1004	0.0163	-0.0765	0.0522	-0.0572	-0.0204	0.0771
3.500π	-0.1006	0.1187	-0.2129	1.1533	-0.1236	0.1429	-0.2122	0.1414	-0.0682	0.0435	0.0546	-0.0526	0.0834	-0.0686	-0.0241	0.0554
3.750π	-0.1240	0.1424	-0.2279	0.7313	-0.1064	0.1143	-0.1296	-0.0058	0.0030	-0.0242	0.0869	-0.0288	0.0842	-0.0593	-0.0279	0.0271
4.000π	-0.0772	0.0867	-0.1274	0.3015	-0.0390	0.0360	-0.0134	-0.1397	0.0632	-0.1755	0.0980	-0.0009	0.0556	-0.0306	-0.0343	-0.0008
4.250π	0.0030	-0.0036	0.0076	-0.0343	0.0378	-0.0463	0.0841	-0.2118	0.0876	-0.0898	0.0791	0.0308	0.0096	0.0085	-0.0415	-0.0223
4.500π	0.0684	-0.0755	0.1041	-0.2134	0.0834	-0.0920	0.1243	-0.2003	0.0692	-0.0640	0.0339	0.0637	-0.0356	0.0436	-0.0446	-0.0368
4.750π	0.0870	-0.0857	0.1246	-0.2161	0.0792	-0.0838	0.0992	-0.1191	0.0212	-0.0126	-0.0204	0.0874	-0.0624	0.0609	-0.0377	-0.0428
5.000π	0.0556	-0.0598	0.0758	-0.1201	0.0342	-0.0340	0.0313	-0.0096	-0.0310	0.0386	-0.0625	0.0911	-0.0616	0.0536	-0.0195	-0.0456
5.250π	-0.0016	0.0021	-0.0032	0.0073	-0.0228	0.0264	-0.0401	0.0788	-0.0622	0.0663	-0.0753	0.0692	-0.0352	0.0253	0.0066	-0.0448
5.500π	-0.0504	0.0538	-0.0660	0.0975	-0.0604	0.0648	-0.0801	0.1162	-0.0598	0.0596	-0.0549	0.0263	0.0038	0.0116	0.0319	-0.0398
5.750π	-0.0654	0.0692	-0.0829	0.1163	-0.0612	0.0641	-0.0733	0.0916	-0.0282	0.0250	-0.0121	-0.0223	0.0376	-0.0408	0.0460	-0.0283
6.000π	-0.0424	0.0447	-0.0525	0.0706	-0.0290	0.0295	-0.0302	0.0282	0.0140	-0.0180	0.0317	-0.0586	0.0516	-0.0505	0.0423	-0.0103
6.250π	0.0012	-0.0012	0.0018	-0.0030	0.0150	-0.0166	0.0211	-0.0387	0.0450	-0.0477	0.0564	-0.0685	0.0410	-0.0371	0.0220	0.0113
6.500π	0.0392	-0.0409	0.0472	-0.0614	0.0462	-0.0485	0.0567	-0.0743	0.0500	-0.0507	0.0520	-0.0489	0.0124	-0.0079	-0.0068	0.0306
6.750π	0.0514	-0.0536	0.0609	-0.0768	0.0490	-0.0507	0.0565	-0.0677	0.0288	-0.0277	0.0231	-0.0099	-0.0192	0.0227	-0.0314	0.0402
7.000π	0.0338	-0.0351	0.0395	-0.0485	0.0248	-0.0252	0.0264	-0.0275	-0.0050	0.0071	-0.0141	0.0295	-0.0394	0.0403	0.0413	0.0354

Subject to the limitations just mentioned, the following conclusions may be drawn regarding the patterns of a paraboloid cut to an elliptical contour:

(1) The ratio of the axes of the ellipse has no effect on the patterns, provided the distribution of illumination along the two axes is not changed.

(2) The horizontal pattern depends on the distribution of illumination along the vertical axis, though to a lesser degree than on the distribution along the horizontal axis, and vice versa. The effect is in the direction of reducing the side lobes in the horizontal pattern if the illumination in the vertical plane becomes more uniform.

Method of Gain Calculation

The gain of an antenna is defined[17] as

$$G = \frac{P}{P_o} \tag{19}$$

where P is the power flow per unit area at a distant point in the direction of maximum signal, and P_o is the power flow per unit area that would exist at that point if the same total power were fed into an omnidirectional antenna. In the notation of Equation (9),

$$P = \frac{[E\,(d,0,0)]^2}{120\pi} = \frac{E_o{}^2\,[F\,(0,0)]^2}{120\pi\,\lambda^2 d^2}\,. \tag{20}$$

But

$$P_o = \frac{\text{Total power radiated from feed horn}}{4\pi d^2}$$

$$= \frac{P_{max}}{4\pi d^2} \int_{\Sigma} |\bar{E}_e(\alpha)|^2 \; |\bar{E}_h(\beta)|^2 \; d\Omega \tag{21}$$

where P_{max} is the power per unit solid angle radiated in the direction of the vertex of the reflector by the feed horn, $\bar{E}_e(\alpha)$ and $\bar{E}_h(\beta)$ are the E- and H-plane primary patterns, and Σ is a sphere with its center at the feed. Since

$$P_{max} = f^2 \frac{E_o{}^2}{120\pi}\,, \tag{22}$$

$$P_o = \frac{f^2 E_o{}^2}{120\pi} \cdot \frac{1}{4\pi d^2} \cdot 4 \int_0^{\pi} \int_0^{\pi/2} |\bar{E}_e(\alpha)|^2 \, |\bar{E}_h(\beta)|^2 \quad \cos\beta \, d\beta \, d\alpha$$

$$= \frac{f^2 E_o{}^2 I_e \; I_h}{120\,\pi \cdot \pi d^2}\,, \tag{23}$$

where $I_e = \int_0^{\pi} |\bar{E}_e\,(\alpha)|^2 d\alpha$ and $I_h = \int_0^{\pi/2} |\bar{E}(\beta)|^2 \cos\beta \, d\beta$.

These quantities may be evaluated graphically from the primary patterns.

---

[17] Friis and Lewis, op. cit.

Then

$$G = \frac{\pi\,[F(0,0)]^2}{\lambda^2\, f^2\, I_e\, I_h} \tag{24}$$

Pattern Calculation for Final Model

Illumination of Reflector. Horizontal and vertical patterns have been calculated for the final version of the antenna by means of Equation (14) and Table III and compared with typical measured patterns. The reflector dimensions were 60-3/4 x 24 x f = 21.1 inches throughout this work, and the feed used was the "on-axis" horn of a vertically stacked array, each horn of which had an E-plane aperture of 0.8 inch and an H-plane aperture of 1.06 inches. Primary patterns of this horn, measured with adjacent wave guides "open," are shown in Figure 72; the illumination across the two axes of the reflector aperture, as calculated from these patterns, is shown in Figures 77 and 78, together with four-term Fourier-series approximations to these curves. The numerical values of the coefficients are:

E-Plane				H-Plane			
a_0	a_1	a_2	a_3	b_0	b_1	b_2	b_3
0.596	0.378	0.017	0.006	0.799	0.174	-0.007	0.030

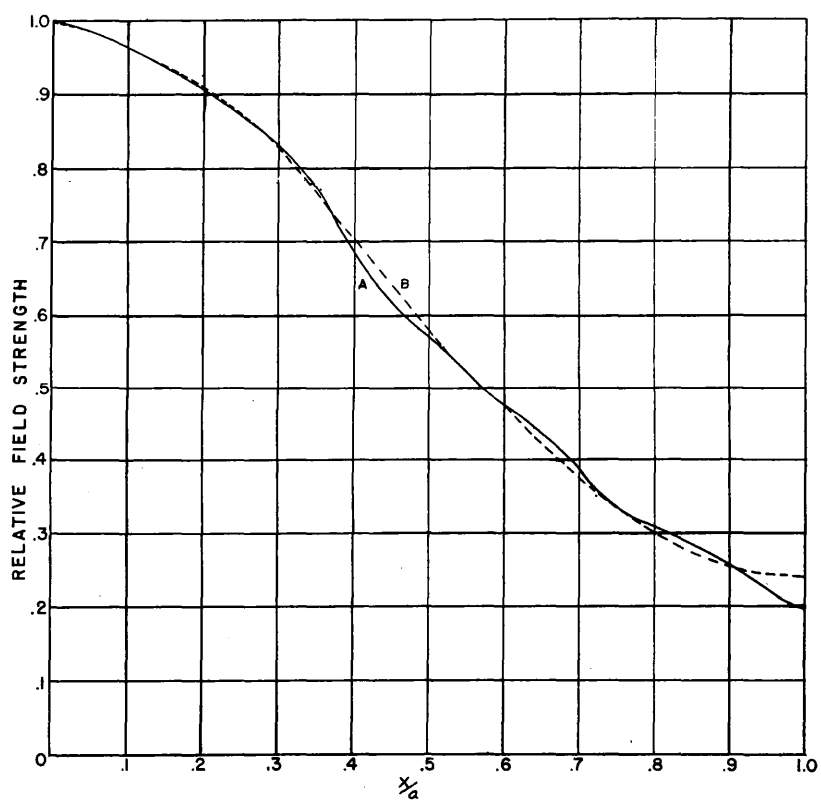

Fig. 77 - Aperture illumination in the E-plane: A - Calculated from primary pattern, B - Fourier series approximation

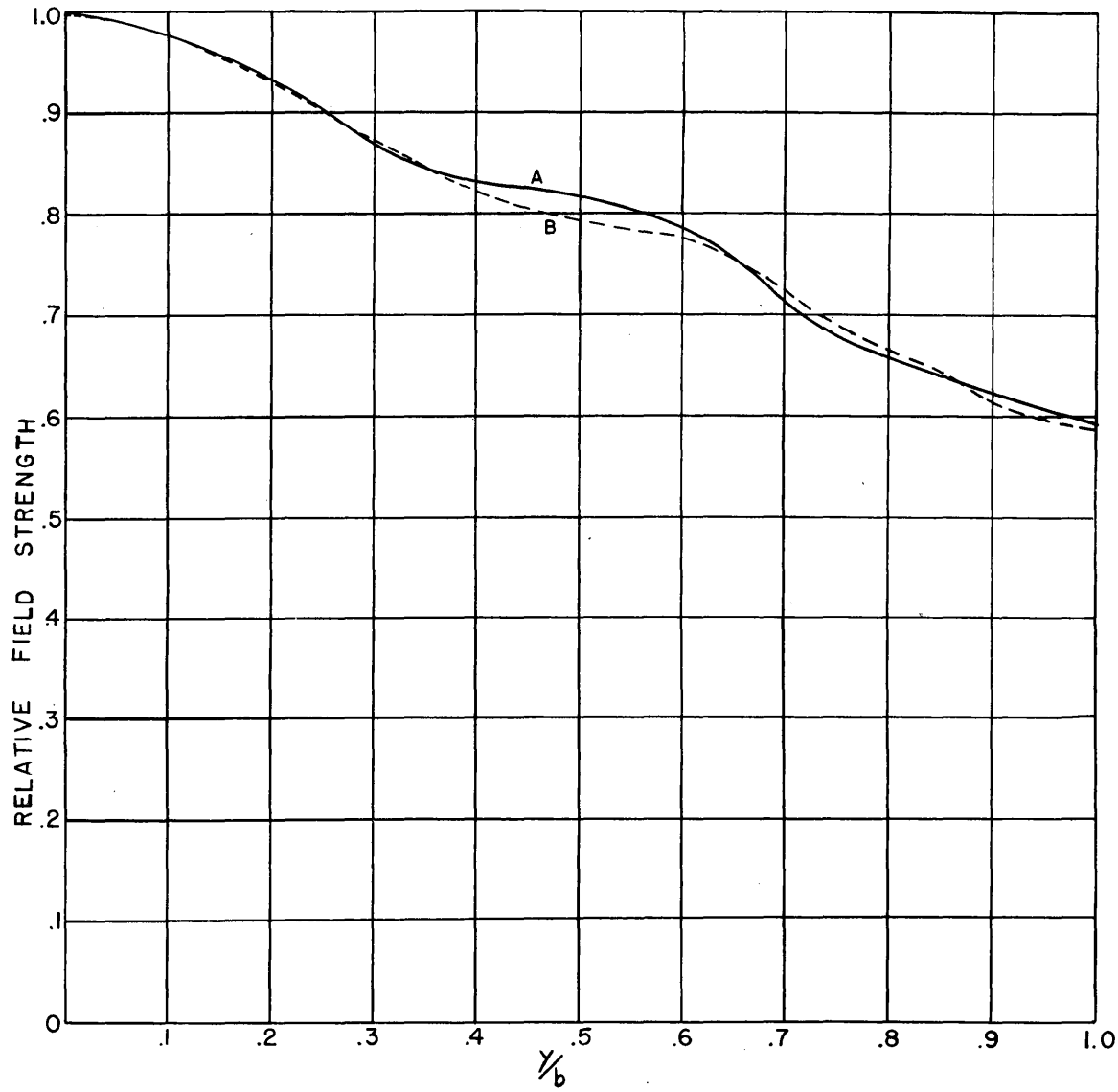

Fig. 78 - Aperture illumination in the H-plane: A - Calculated from primary pattern, B - Fourier series approximation

Horizontal Pattern. The calculated horizontal pattern of Figure 79 includes a correction for shading by the feed horns based on the following reasoning: The actual pattern may, by superposition, be regarded as that of the entire unobstructed aperture, minus the pattern of a fictitious source the same size as the feed assembly, and having the same illumination as that falling back onto the feed. The latter component is essentially omnidirectional in the horizontal plane, since the E-plane dimension of the horns is only 0.9 inch, and so becomes a constant correction term to be subtracted from the first pattern. Its relative magnitude is given by the ratio of the integral of the field

strength over the area obstructed by the feed to a similar integral extended over the entire aperture, that is, by

$$\frac{0.9 \int_{-12}^{1.8} \left(\sum_{s=0}^{3} b_s \cos \frac{s\pi y}{12} \right) dy}{F(0,0)} .$$

The result is 0.0183 for the final antenna, and this value has been subtracted from the normalized pattern to obtain the solid curve of Figure 79. The dashed curve is a measured pattern. It is apparent that the theory predicts the beam width and side-lobe level quite well, but since the experimental pattern is unsymmetrical in the angular position of the lobes, there is some disagreement on this point. A detailed comparison is made in Table IV.

Vertical Pattern. In the calculated vertical pattern (solid curve of Figure 80), no account was taken of obstruction by the feed because in the vertical plane the feed structure extends more than half way across the reflector. If it went all the way across, the correction pattern would be almost exactly the same as that of the reflector itself. Actually, the correction pattern is somewhat broader, and it would have to be calculated in detail. This work does not appear justified in view of the high side lobes already present in the pattern. Unfortunately the measured pattern (dashed curve of Figure 80) was extended only through the first side lobe. To obtain a rough check of the theory it was necessary to plot in (as + marks) the position of the second and third side lobes observed under slightly different conditions, that is, with a feed horn whose H-plane aperture was 1.18 rather than 1.06 inches as assumed in the calculations. In spite of these defects in the calculation and measurement, there is a fairly satisfactory agreement. Table IV summarizes the data pertinent to the patterns shown in Figures 79 and 80.

TABLE IV

	Horizontal Pattern			Vertical Pattern		
	Calculated	Measured		Calculated	Measured	
Beam Width (3 db)	1.54°	1.55°		3.14°	3.15°	
First Side Lobe		L	R		L	R
Intensity (db)	40	--	--	19.7	18.2	18.6
Position	2.4°	--	--	4.9	5.0	5.0
Second Side Lobe						
Intensity	31.1	30.5	30.8	22.4	(24.1)	(21.7)
Position	4.5	4.2	4.5	8.1	(8.0)	(7.7)
Third Side Lobe						
Intensity	32.5	33.0	35.5	29.8	(28.2)	(24.9)
Position	6.8	6.8	6.7	11.25	(11.0)	(11.0)

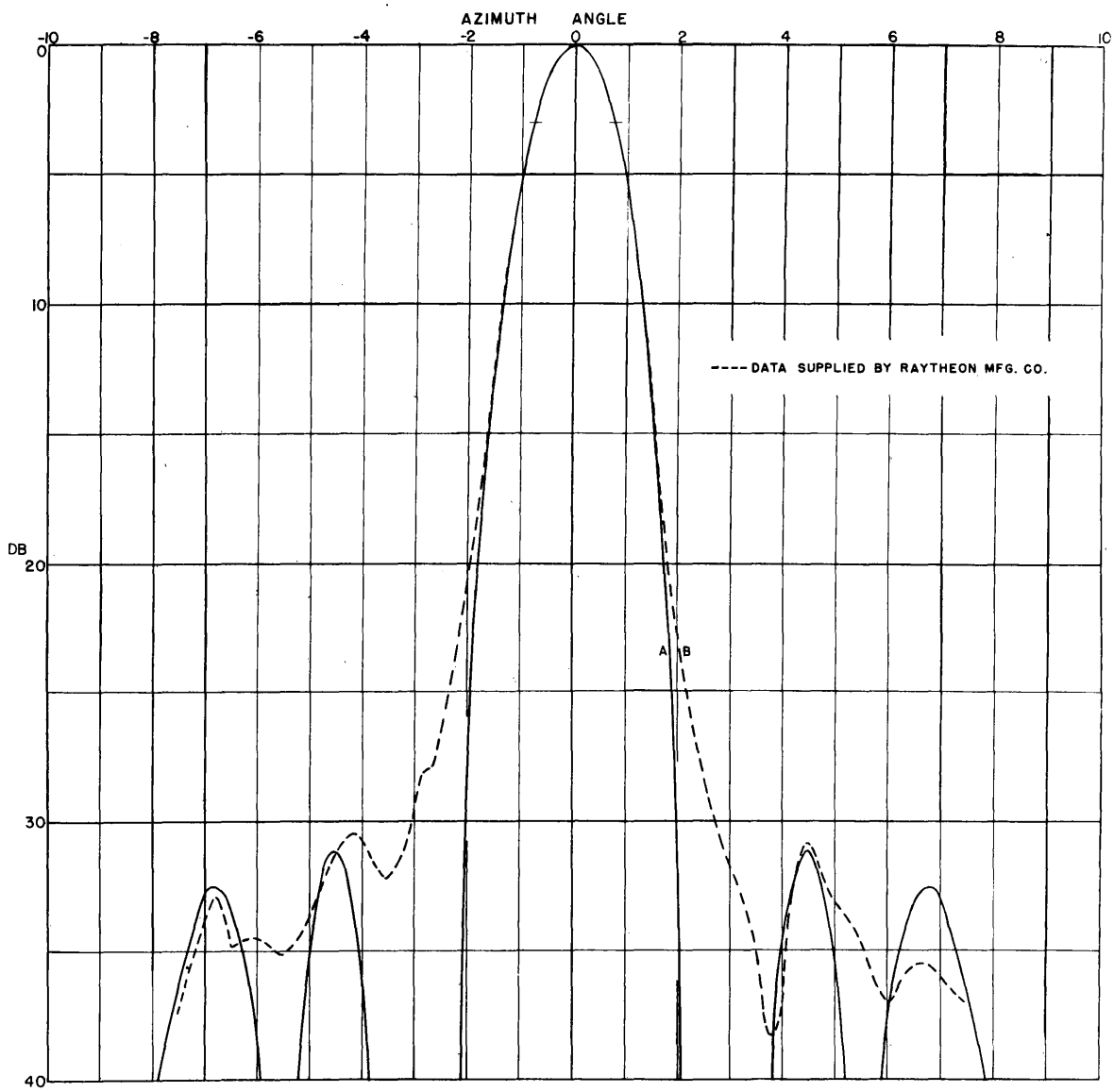

Fig. 79 - Azimuth pattern of on-axis beam: A - Calculated, B - Measured

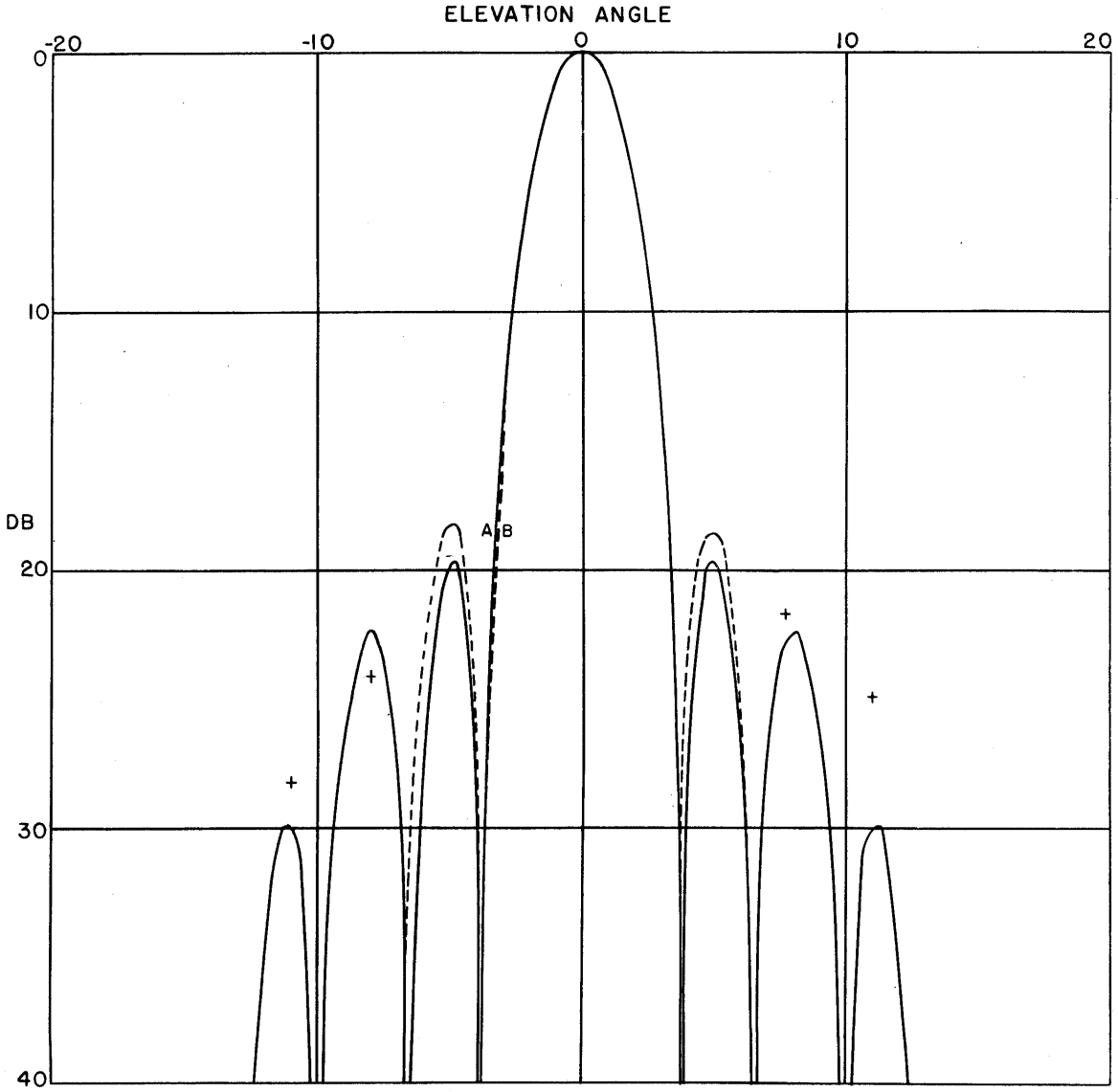

Fig. 80 - Vertical pattern of on-axis beam: A - Calculated, B - Measured

Experimental Patterns

Vertical Patterns. A set of eleven vertical patterns of the antenna is shown in Figure 81, although beam number 5 will be the lowest one used. The gain and side lobe level for each channel are:

Beam Number	Horn Number	Gain	Maximum Side Lobe
5	1	36.5 db	17.5 db
6 (on axis)	2	35.9	18.2
7	3	36.3	18.5
8	4	35.7	18.5
9	5	35.5	20.0
10	6	34.8	21.8
11	7	34.1	17.0

The Raytheon Manufacturing Company has taken a set of vertical patterns (Figure 82) with a dielectric feed enclosure in place. The results may be summarized as follows:

Horn Number	Gain	Maximum Side Lobe
1	35.9 db	17.1 db
2	36.1	17.3
3	35.9	18.5
4	35.6	17.6
5	35.4	19.1
6	35.3	20.0
7	34.4	19.6

Horizontal Patterns. The only horizontal pattern that has been taken is that of the on-axis horn (Curve A of Figure 83), but it is quite similar to the one obtained with 0.8 x 1.18-inch horns (Curve B). Thus the series of patterns taken earlier for horns of this size (Figure 63) may be considered representative of the final antenna.

Gain Calculations

Before calculating the gain to be expected of the final antenna, the formula (Equation 24) was checked against the empirical rule

$$G = 0.65 \frac{4\pi A}{\lambda^2} ,$$

which is based on an illumination taper of approximately 10 db to the edges of the reflector. Accordingly, actual primary patterns were chosen which fit this condition for the 60-3/4 x 24 x f = 21.1-inch reflector, and the gain was worked out. The results are in excellent agreement with the empirical rule.

Case	Edge Illumination		$\frac{F(0,0)}{ab}$	I_e	I_h	Gain, db		
	E	H				Calc.	Meas.	$0.65 \frac{4\pi A}{\lambda^2}$
1.	10 db	10 db	1.7102	0.8979	0.3223	37.76	--	37.70
2.	13.6	11.5	1.4867	0.7452	0.2891	37.82	37.40	--
3.	13.8	4.6	1.6754	0.7024	0.4722	36.99	36.46	--

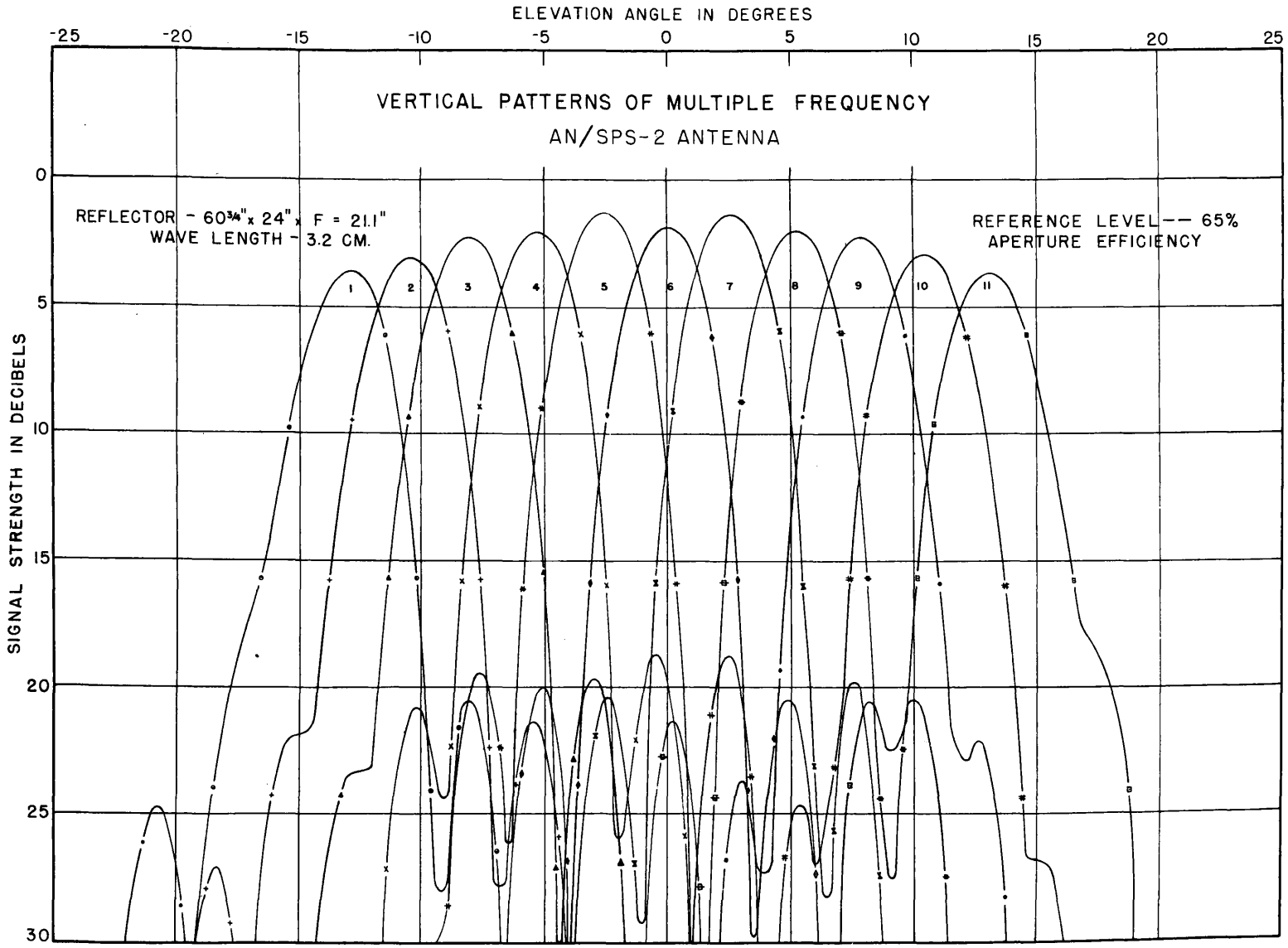

Fig. 81 - Vertical patterns illustrating off-axis performance of the antenna

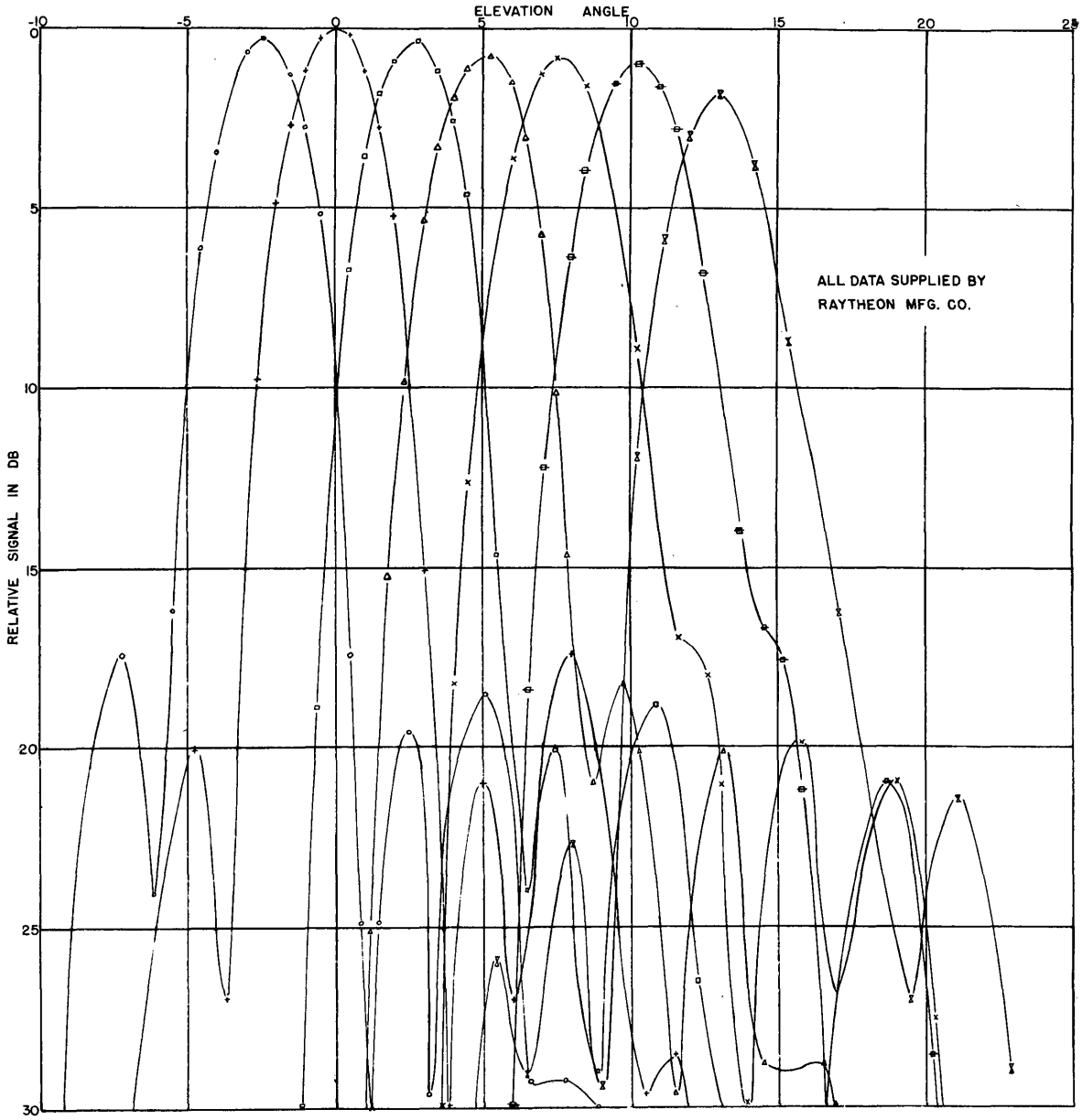

Fig. 82 - Vertical patterns of the complete X-band model

The second line shows calculated and measured gain under illumination conditions that give nearly optimum radiation patterns in a single beam antenna, and the third line refers to the final model. The following conclusions may be drawn:

(1) Although the gain of the final model is 1.3 db below the maximum theoretically attainable, it is less than 1 db down from what would be realized in practice if this reflector were used to generate a single beam.

(2) This theory predicts a gain reduction between cases 2 and 3 of 0.83 db, as compared with a measured gain reduction of 0.94 db. The fact that the measured gains are both low suggests the possibility of defects in the parabolic contour of the reflector.

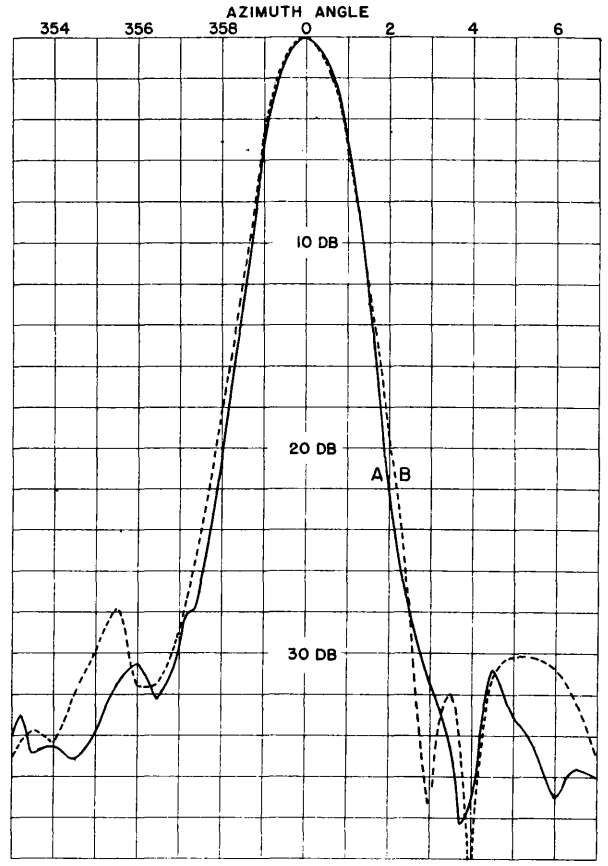

Fig. 83 - Effect of H-plane horn dimension on azimuth pattern: A - 0.8 x 1.06-inch horns, B - 0.8 x 1.18-inch horns

Impedance Match of Horn Feed

Most of the work on impedance matching has been performed on an array of 0.8 x 1.18-inch horns. The H-plane dimension was later decreased to 1.06 inches as dictated by pattern requirements, and preliminary results are given for this case.

Mismatch Due to Reflector. Two factors contribute to the mismatch of an antenna of this type: The reflection coefficient of the horn, Γ_h, and that due to the reflector, Γ_r. The second effect will be considered first. In a symmetrically cut paraboloid, some of the reflected energy is intercepted by the horn, setting up a standing wave in the feed line. This may be calculated from the formula:

$$|\Gamma_r| = \frac{g\lambda}{4\pi f}$$

where g is the power gain of the horn and f is the focal length of the reflector. By comparison with a standard, the gain of an 0.8 x 1.18-inch horn was found to be 7.4. Since the focal length is 21.1 inches, $|\Gamma_r| = 0.035$.

In checking Γ_r experimentally, the horn was first mounted in free space and matched with probes as well as possible. Then the horn was directed into the dish and the new standing wave ratio observed. In the following tabulation these readings have been converted to equivalent reflection coefficients.

Wavelength	Reflection Coefficient	
	Free Space, $\lvert\Gamma_h\rvert$	In Reflector, $\lvert\Gamma_h+\Gamma_r\rvert$
3.15 cm	0.006	0.011
3.20	.011	.017
3.25	.006	.011
3.30	.011	.006
3.35	.017	.017
Average	.009	.012

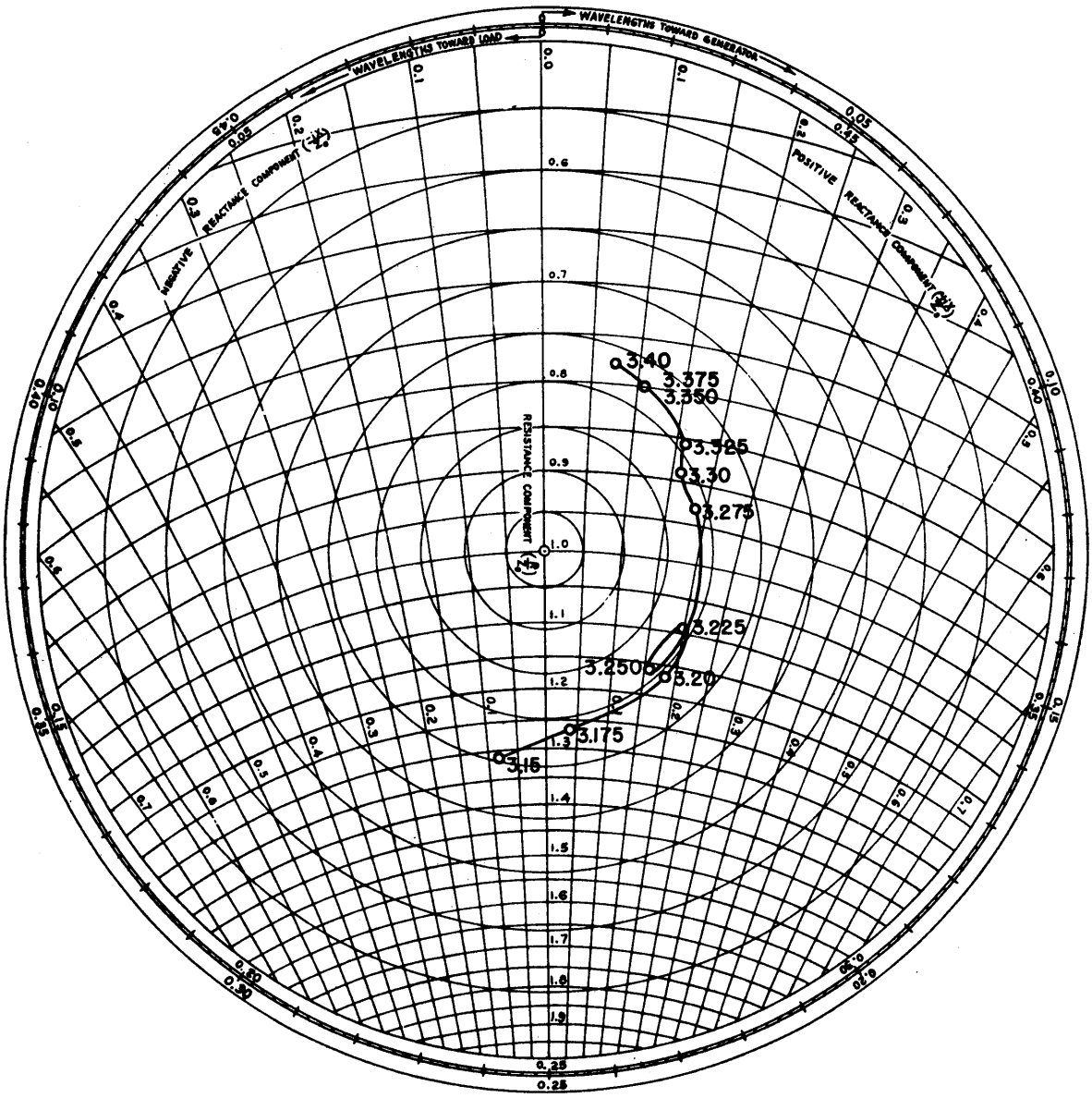

Fig. 84 - Impedance at throat of 0.8 x 1.18-inch horn

If it is assumed that $|\Gamma_h|$ and $|\Gamma_r|$ are essentially constant, and that the data are sufficient to indicate the average resultant of Γ_h and Γ_r for all possible phase relations between them, it can be shown[18] that $|\Gamma_r|$ is approximately 0.01. Since the measured value is even less than the calculated one, it is concluded that the contribution of the reflector to horn mismatch may safely be neglected.

Mismatch at Mouth of Horn. The free-space impedance of a typical horn in the array has been approximated by measuring the center element of a three-horn group of the type already used to study primary patterns (Figure 21). Under these conditions, the impedance seen at the throat of an 0.8 x 1.18-inch horn is plotted in Figure 84. As the wavelength increases from 3.15 to 3.40 cm, the phase angle decreases some 85 degrees. If it is assumed that the reflection originates at the mouth of the horn, the phase shift should be 65-1/2 degrees:

$$\delta = 360^\circ \; \frac{L}{\lambda_g} \cdot \frac{\Delta\lambda_g}{\lambda_g},$$

where

L = length of horn taper, 2 inches
λ_g = average guide wavelength thru taper = 1.59 inches
$\Delta\lambda_g$ = 0.23 inches

This checks fairly well, indicating the assumption is correct. Since the average SWR is 2 db, the reflection coefficient referred to the mouth of the horn is $\Gamma_h = -0.115$.

Electrical Design of Dielectric Cover. A convenient method of overcoming this mismatch involves the use of a dielectric enclosure around the horn aperture. By proper choice of thickness of material and spacing, the reflection coefficient of the cover may be made to cancel that from the horn mouth. Polystyrene has proved to be entirely satisfactory from an r-f standpoint; but owing to the high temperatures likely to be encountered near the stacks, and to the considerable weight and dimensions of the cover when scaled to L-band, a more rugged material is required. Fiberglas laminates, made up of layers of glass cloth impregnated with a thermosetting resin, have many desirable mechanical properties. They are nearly impervious to moisture, will withstand temperatures up to 350°F without deformation, and exhibit high tensile and impact strength. In addition, certain combinations of cloth and resin have excellent r-f characteristics.[19] For example, the type used in this application, Fiberglas ECC-14-128 bonded with Selectron 5003, has a dielectric constant of 4.06 and a loss tangent of only 0.006 at X band.

Using plane-wave theory, it may be shown[20] that the reflection coefficient at the mouth of a horn due to a dielectric cover is given by

$$\Gamma_d = \frac{\frac{1}{2}\left(\sqrt{\epsilon} - \frac{1}{\sqrt{\epsilon}}\right) \sin kt\sqrt{\epsilon}}{\sqrt{1 + \frac{1}{4}\left(\sqrt{\epsilon} - \frac{1}{\sqrt{\epsilon}}\right)^2 \sin^2 kt\sqrt{\epsilon}}} \; e^{i\left\{\pi + \cot^{-1}\left[\frac{1}{2}\left(\sqrt{\epsilon} + \frac{1}{\sqrt{\epsilon}}\right) \tan kt\sqrt{\epsilon} - 2kd\right]\right\}}, \quad (25)$$

---

18 $\overline{|\Gamma_r + \Gamma_h|}/|\Gamma_h| = \frac{2}{\pi}(x+1)\,E\left(\frac{2\sqrt{x}}{x+1}\right)$, where $x = |\Gamma_r|/|\Gamma_h|$, and E(k) is the complete elliptic integral of the second kind.

19 T. J. Suen and E. M. Everhart, "Dielectric Constants and Loss Tangents of Random Materials," MIT Radiation Laboratory Report 483-25, January 11, 1946.

20 Keary and Bohnert, op. cit.

where

ϵ = Dielectric constant of the cover material
t = Thickness of the cover
$k = 2\pi/\lambda$
d = Distance from horn aperture to cover inner face.

If Γ_d is set equal to $-\Gamma_h$, i.e., to $|\Gamma_h|$, the equation may be solved for t and d:

$$\left.\begin{aligned} t &= \frac{\lambda\,|\Gamma_h|}{\pi(\epsilon-1)}, \\ d &= \frac{\lambda}{4} + \frac{\lambda}{4\pi}\cot^{-1}\left[\frac{\epsilon+1}{\epsilon-1}\quad|\Gamma_h|\right], \\ \text{provided}\quad t &\ll \frac{\lambda}{4\sqrt{\epsilon}} \end{aligned}\right\} \qquad (26)$$

With $\epsilon = 4$ and $\lambda = 3.2$ cm, t = 0.015 inches and d = 0.453 inches. A cover constructed of 0.022-inch material (three plies) was found to have proper phasing at d = 0.375 inches, in fair agreement with the calculations. Figure 85 shows that this cover reduces the mismatch from 2 db to a maximum of 0.3 db over the 7.6-percent band tested.

Several cover shapes were tried, and it was found that any deviation from a flat face tended to increase the t and d dimensions. This is undesirable for mechanical reasons, and in addition the primary patterns are less affected if the spacing is kept small. The final design is shown in Figure 86, and Figures 87 and 88 show its influence on the E- and H-plane primary patterns. It will be noticed that there is a slight narrowing of the beam in the E-plane and that the H-plane pattern is somewhat more irregular with the cover in place, but the illumination taper is changed very little.

Mechanical Design of Dielectric Cover. Conventional flange mounting of the pressurizing cover increases the feed silhouette, particularly when the flare angle of the horn is small. In Figure 86 the mounting plates are flush with the horn aperture, and the cover is held in place with cement and screws.

Final Feed System. After this design had been completed, the horn dimensions were changed to 0.8 x 1.06 inches. The reflection coefficient of such a

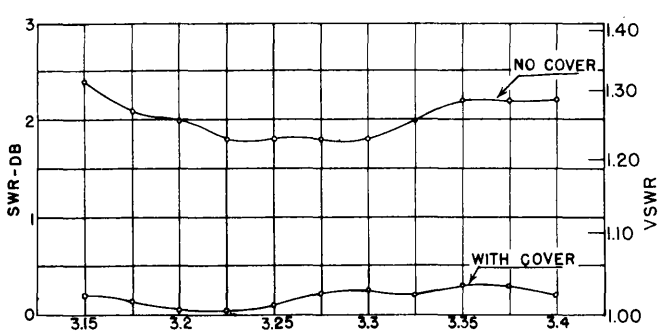

Fig. 85 - Standing wave ratio of 0.8 x 1.18-inch horn

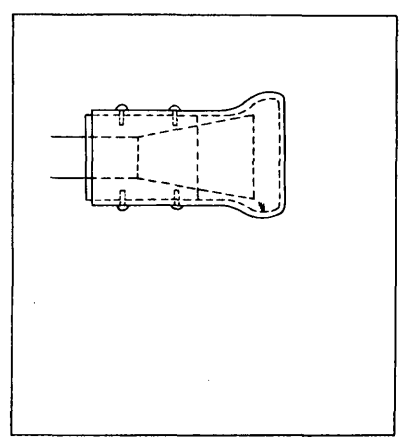

Fig. 86 - Design of pressurizing cover

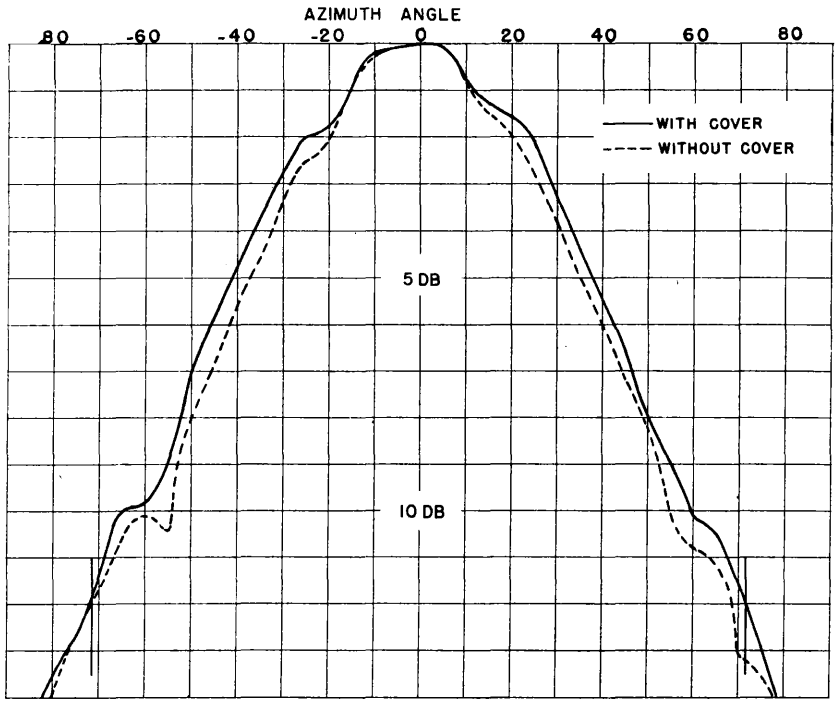

Fig. 87 - Effect of cover on E-plane primary pattern

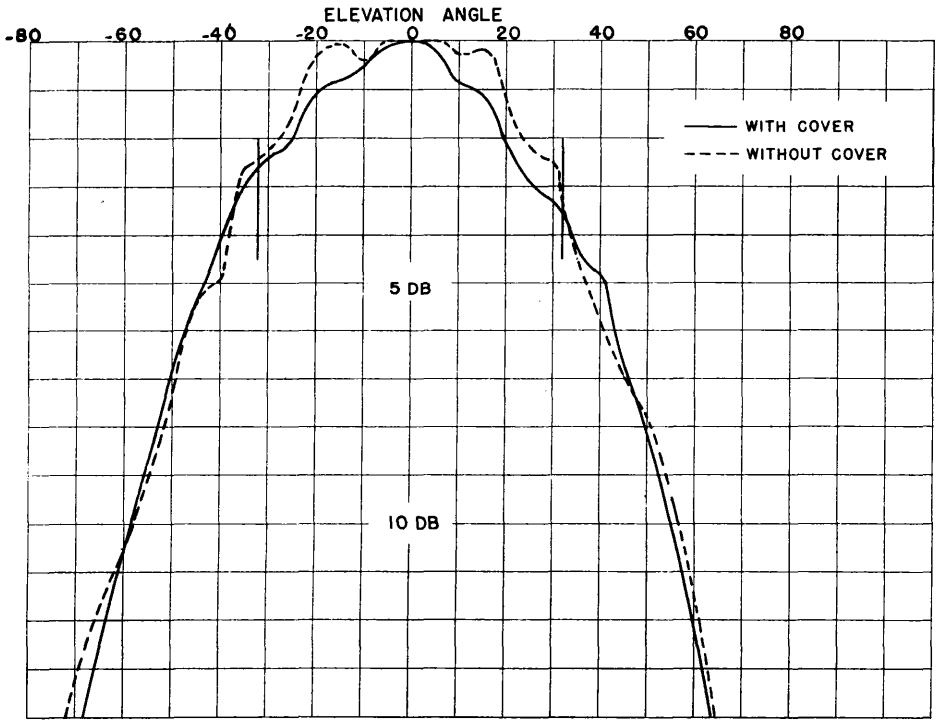

Fig. 88 - Effect of cover on H-plane primary pattern

horn has an average value of 0.084 at wavelengths of 3.15 to 3.40 cm, so that the cover thickness required for matching is approximately 0.022 x (0.084 / 0.115) = 0.016 inches. A new cover is being fabricated; meanwhile experiments have been performed on the old one to check its effect on standing wave ratio (Figure 89), primary patterns (Figure 90), and the coupling between horns (Figure 91).

It is evident from the first of these figures that the thickness of the dielectric is not the correct one for proper matching, although some of the vagaries of these curves may result from the series of mitered H-bends through which the standing wave ratio was measured. A comparison of the dotted and dashed curves shows that the contribution of the reflector to the mismatch is quite small in most cases.

Final adjustment of the cover thickness and spacing must be made at L-band, but there is every reason to believe, on the basis of these tests, that the standing wave ratio can be held well below 2 db over the band. At Raytheon, P. Hines has made up a single L-band horn of the final dimensions and matched it to better than 0.5 db from 1200 to 1350 Mc with a Fiberglas laminate cover 1/8-inch thick. This is equivalent to about 0.017 inches in the X-band model.

Effect of Cover on Primary Patterns. A set of H-plane primary patterns is shown in Figure 90. The cover has an adverse effect on the illumination taper of the first three

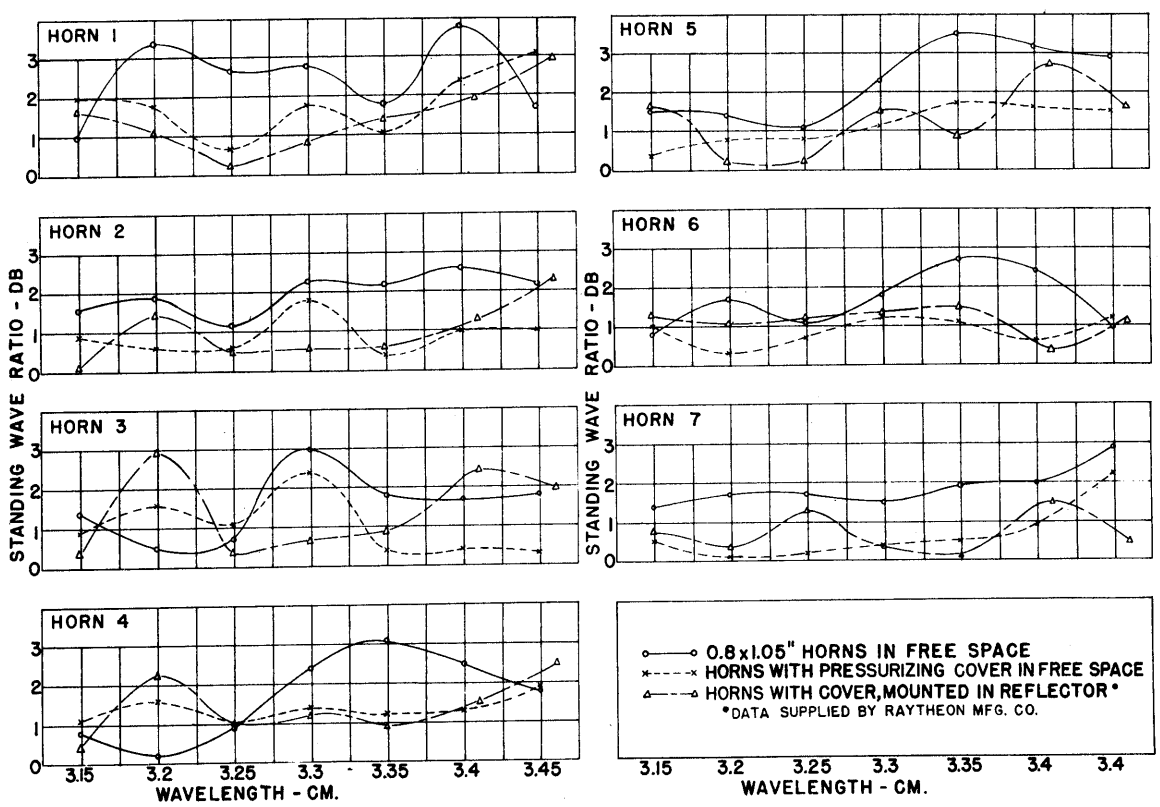

Fig. 89 - Standing wave ratio of complete feed system

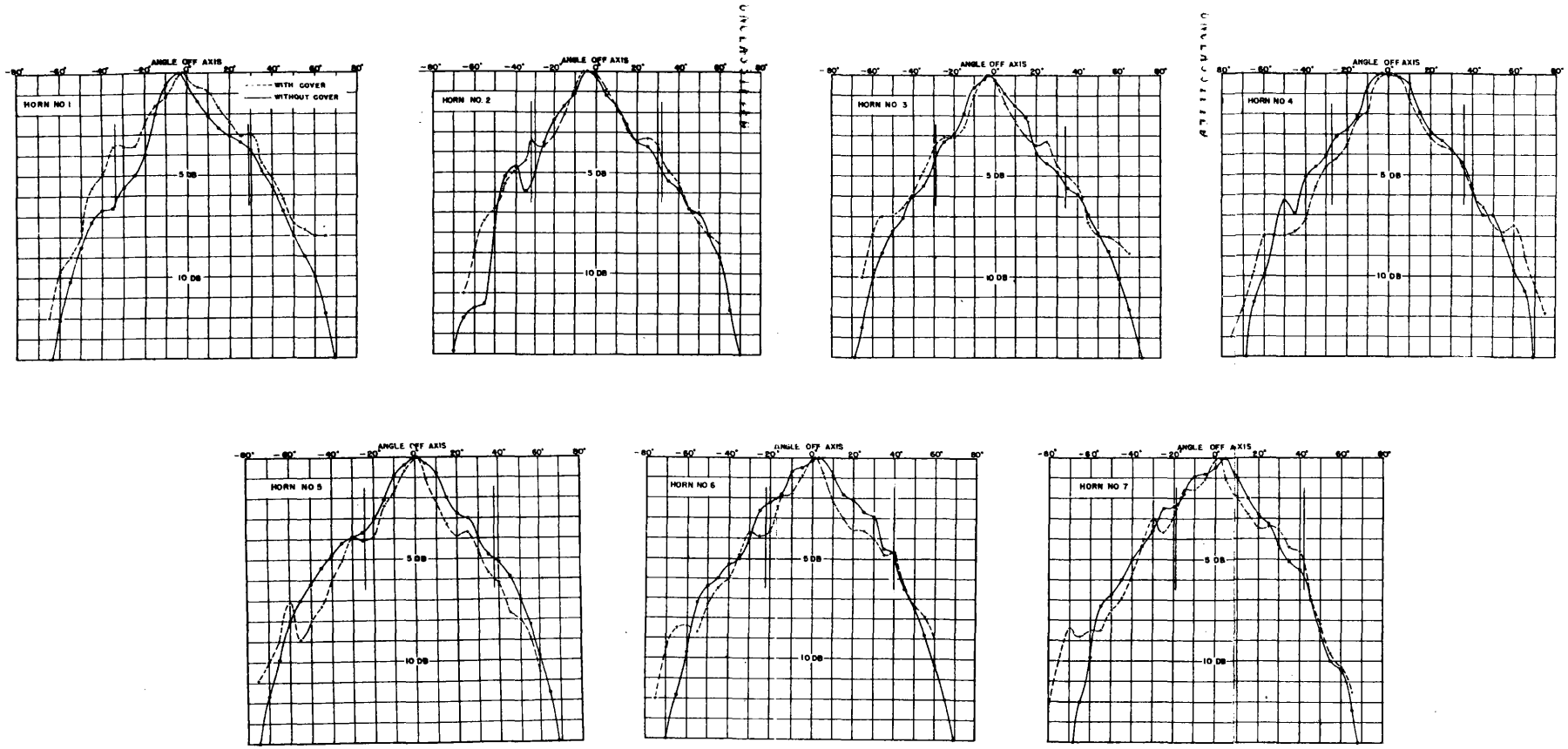

Fig. 90 - Effect of pressurizing cover on primary patterns

This page intentionally left blank.

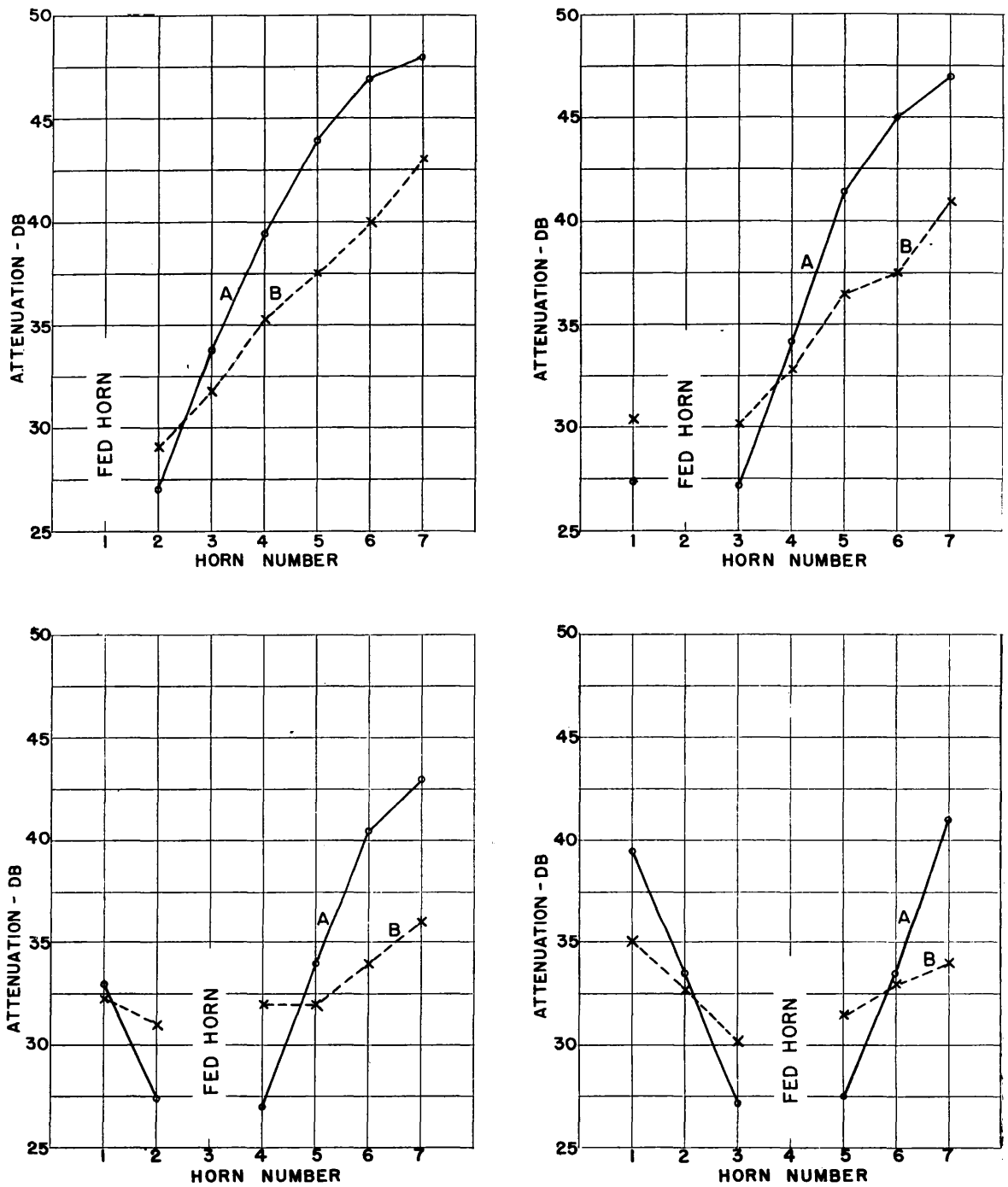

Fig. 91 - Coupling between horns of feed system: A - Without cover, B - With cover

horns but improves the others:

Horn Number	Illumination Taper to Lower Edge		Illumination Taper to Upper Edge	
	Cover Off	Cover On	Cover Off	Cover On
1	6.3 db	3.5 db	3.7 db	3.0 db
2	5.5	3.4	4.9	4.3
3	4.1	3.5	5.5	4.9
4	3.5	4.4	4.6	4.8
5	3.7	4.1	5.0	6.0
6	2.4	3.8	4.8	4.7
7	2.3	2.6	5.9	5.2

A systematic variation of this type suggests mechanical imperfections in the cover.

Effect of Cover on Coupling. Figure 91 indicates that the degree of coupling between horns of the final array is some 27 db without the cover but generally less than 30 db with it in place. The effect of coupling on the vertical patterns, when the cover is removed from the feed, is shown in Figure 92. The two curves represent the limits of the variations that can be produced by adjustable shorting plungers in neighboring wave guides. Pattern stability of the complete antenna should be much better.

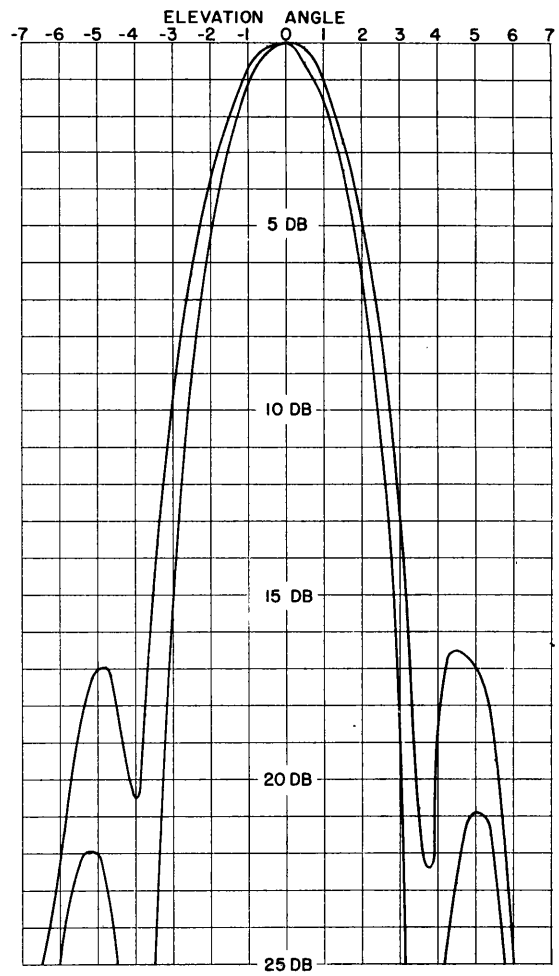

Fig. 92 - Effect of coupling on vertical secondary pattern, cover removed

PRELIMINARY L-BAND DESIGN OF THE AN/SPS-2 ANTENNA

By scaling the X-band model described in the previous section, an AN/SPS-2 antenna has been designed for a center frequency of 1300 Mc. This is shown in Figure 93 with feed system details in Figure 94. A tilt angle of 4.1 degrees is required to put the 3-db point of the lowest beam on the horizon. In order to avoid an increase of height, the feed lines are set side by side in their horizontal run. If this results in pattern deterioration, the guides can be covered with harp material.

These sketches were submitted to the Raytheon Mfg. Co. in July 1948, and it is anticipated that the antenna will be ready for flight tests in June 1949.

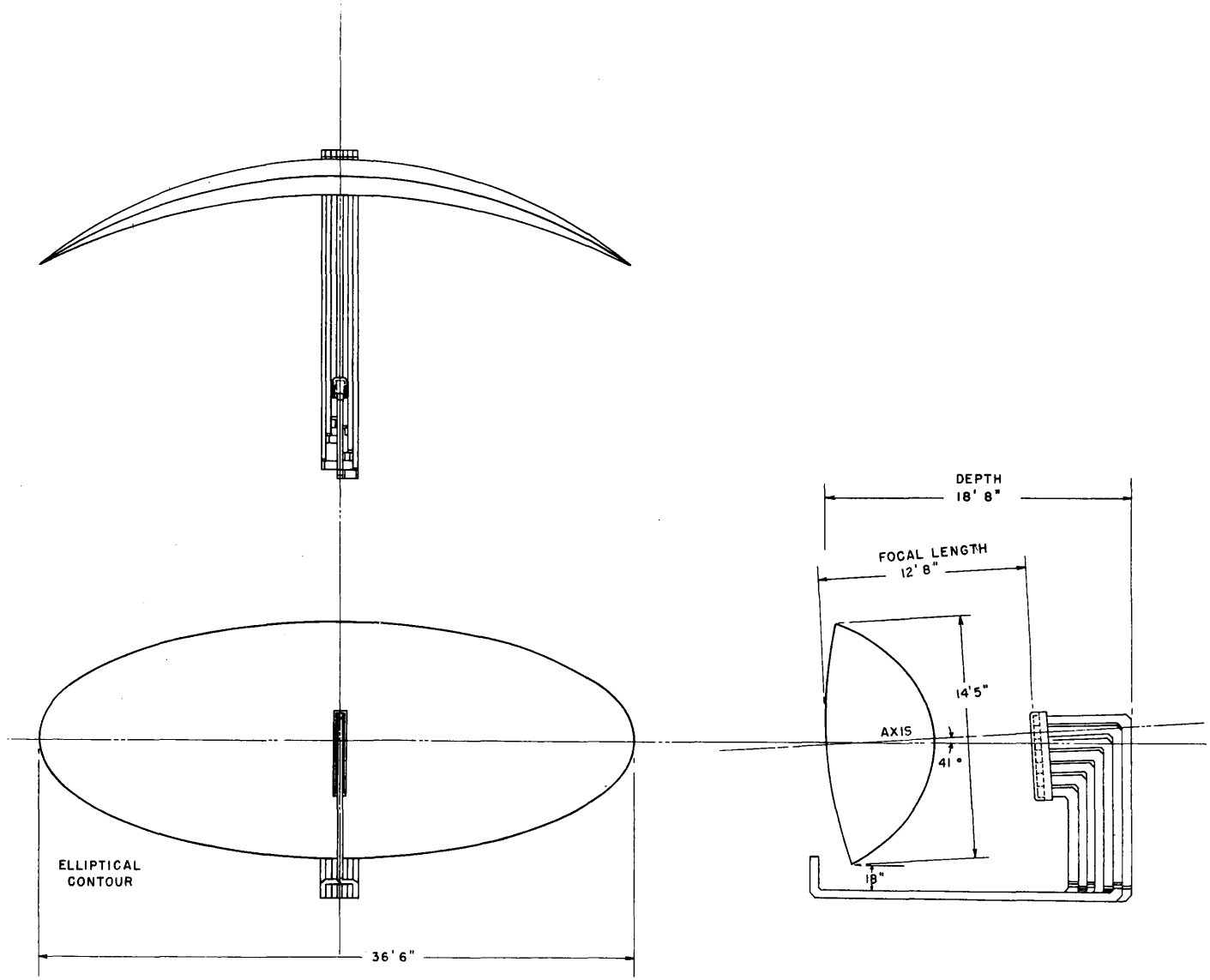

Fig. 93 - Dimensions of L-band model of antenna

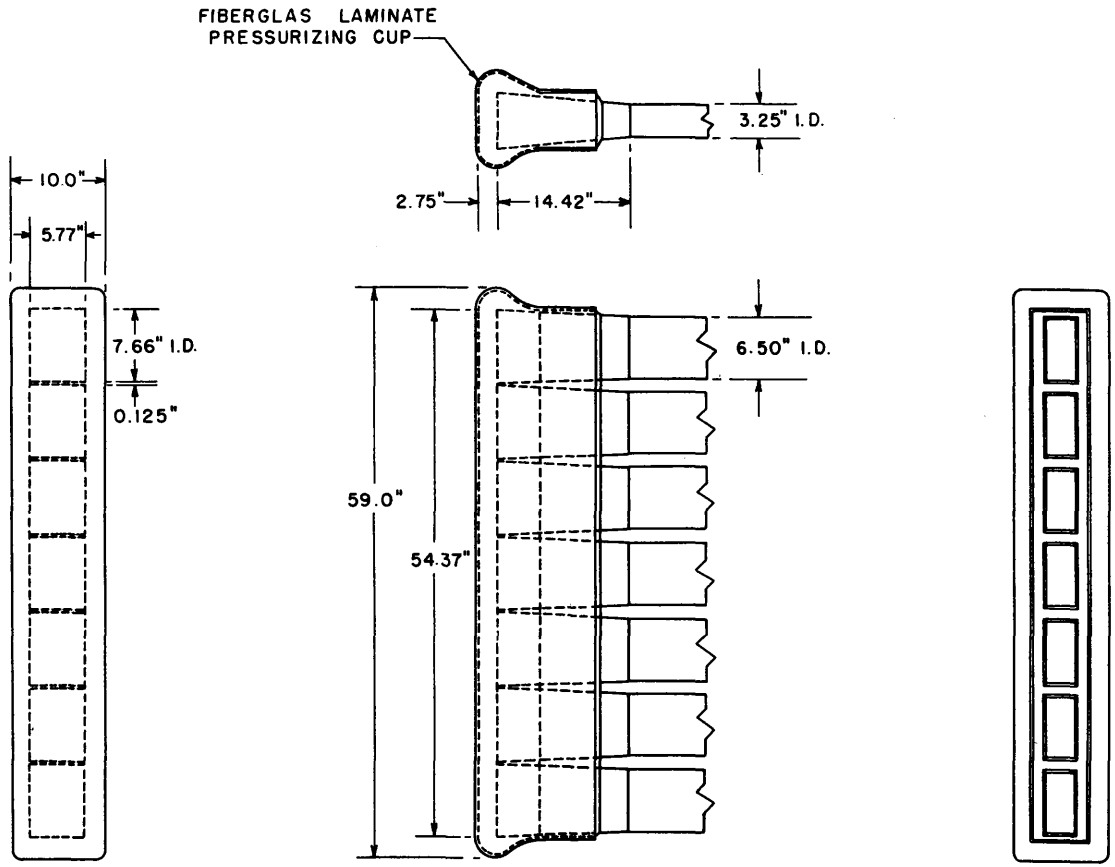

Fig. 94 - Feed system for L-band model

ACKNOWLEDGMENT

The authors wish to express their appreciation to A. A. Varela for his helpful suggestions throughout the course of this work, and to L. C. Van Atta for many stimulating discussions. A large part of the measurements were carried out by W. I. Taylor, and H. D. Fleming was of great assistance in the preparation of this report. Thanks are also due C. W. Price of the Countermeasures Section, Radio Division II, for assistance on the weight estimates.

* * *

This page intentionally left blank.

APPENDIX I

Number of Steps in a Lens of Given f/D and D/λ

It is easily shown[21] that the equation of the mth step of a metal-plate lens is

$$(1-n^2)\left[x+\frac{(m-1)\lambda}{1-n}\right]^2 - 2\left[f+\frac{(m-1)\lambda}{1-n}\right](1-n)\left[x+\frac{(m-1)\lambda}{1-n}\right]+y^2=0, \qquad (27)$$

where the origin is at the vertex of the lens, and x is measured along the axis. At the outer edge of this step, x has the value $\lambda/(1-n)$. If y is set equal to D/2, its value at the edge of the lens, Equation (27) may be used to determine the number of steps in the entire lens. Thus

$$(1-n^2)\frac{(m\lambda)^2}{1-n} - 2\left[f+\frac{(m-1)\lambda}{1-n}\right](1-n)\frac{(m\lambda)}{1-n} + (D/2)^2 = 0 \qquad (28)$$

Divide through by f^2 to obtain

$$(\lambda/f)^2 m^2 + (\lambda/f)\left(2-\frac{\lambda/f}{1-n}\right) m - 1/4\,(D/f)^2 = 0. \qquad (29)$$

This is the exact relation between m, the f/D ratio, and the aperture in wavelengths, D/λ. However, if $(\lambda/f) \ll 1$, the second term reduces to $2(\lambda/f)m$; and if $m(\lambda/f) \ll 1$, the term in m^2 can be neglected. This leads to the simple result:

$$m \approx \frac{1}{8}\,\frac{D/\lambda}{f/D}\,. \qquad (30)$$

* * *

[21] Kock, op. cit.

This page intentionally left blank.

APPENDIX II

Weight Estimates of L-Band Antennas

Weight estimates for a metal-plate lens and two types of parabolic reflectors at L-band have been carried out on the basis of the sketches in Figures 95, 96 and 97. In each case the aperture is elliptical, 14-1/2 feet high by 36-1/2 feet wide. It is assumed that the structure is welded from aluminum alloy 61ST.

The lens (Figure 95) contains 31 horizontal plates of 1/8-inch material; their width varies between 8 and 31 inches, and they are braced at 18-inch intervals by vertical plates of varying width that conform to the lens profile. The entire assembly is supported by a box beam fabricated from 1/4-inch material and formed into an ellipse of the required aperture. The depth of this beam is 36 inches; its height varies from 18 inches at the top to 36 inches at the pedestal, and it is internally braced by transverse plates at 18-inch intervals. Numerous holes reduce the weight of the plates by 1/4 and of the beam by 1/3. The calculated weights are:

Plates	3130 lbs.
Beam	2360
Mounting Brackets	50.
Total	5540 lbs.

One possible reflector design is shown in Figure 96. A horizontal box beam carries 8 main formers that are braced by a network of tubing; light weight formers support the screen wire at 12-inch intervals. The main beam is of 3/16-inch material. It is 36 inches high, and the depth tapers from 36 inches at the pedestal to 12 inches at the ends. The

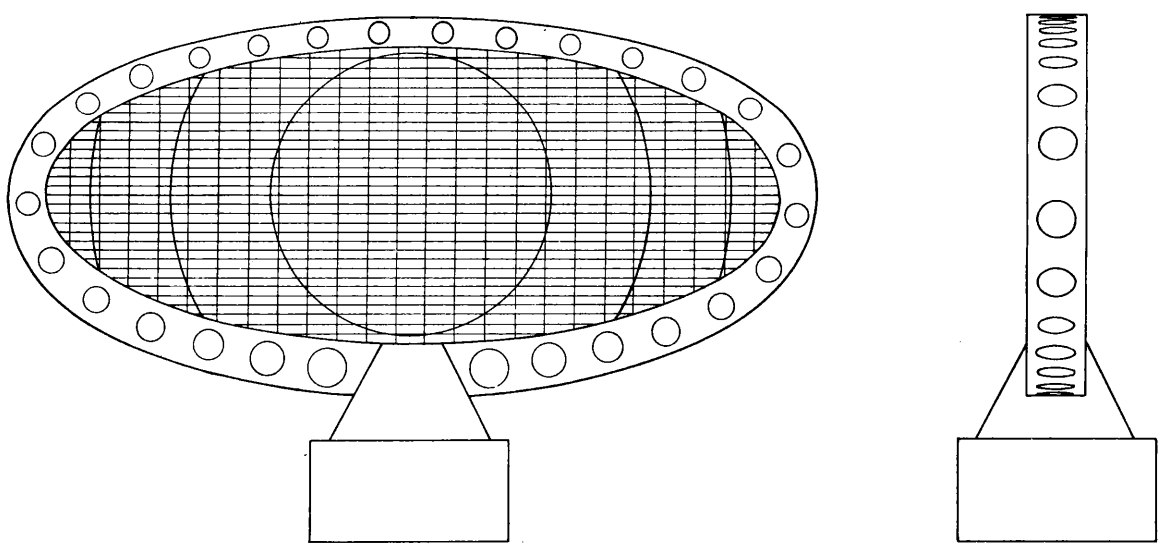

Fig. 95 - L-band metal-plate lens

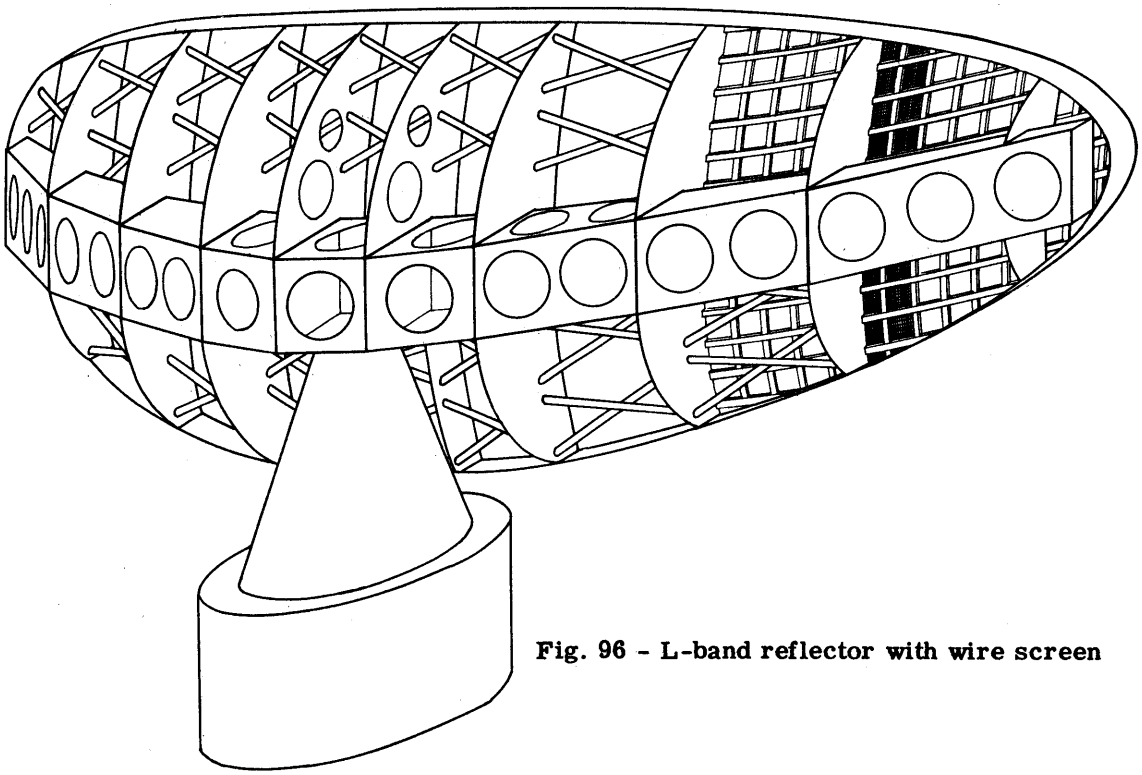

Fig. 96 - L-band reflector with wire screen

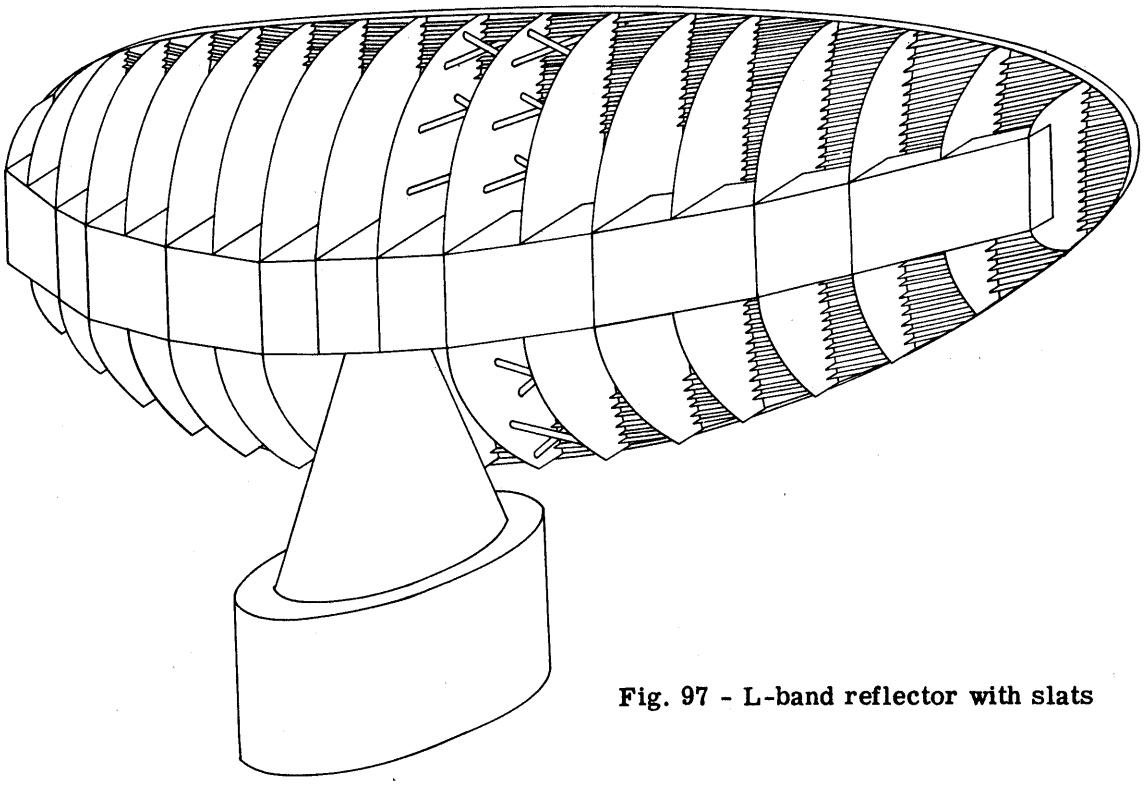

Fig. 97 - L-band reflector with slats

main formers are 3/16-inch plate, the light formers are channel sections 3 x 1 x 3/64 inches, the braces are tubing 2 inches OD x 1/16-inch wall, the rim is a box tube 2 x 4 inches x 1/16-inch wall, and the screen consists of 0.080-inch wire with 1-inch mesh. The weights have been calculated as follows:

Main Beam	1060 lbs.
Main Formers	370
Light Formers	175
Braces	150
Rim	70
Screen	75
Mounting Brackets	50
Total	1950 lbs.

A second type of reflector, sketched in Figure 97, employs slats instead of screening. There are 54 slats at 3-3/16-inch spacing, each 1/8 inch thick and 4 inches wide, supported from 18 main formers at 24-inch intervals. The advantages of this design are ease of construction and reduced wind loading, but the weight is somewhat greater:

Horizontal Beam	1060 lbs.
Formers	560
Slats	760
Braces	150
Rim	70
Brackets	50
Total	2650 lbs.

The weight of a reflector 14-1/2 x 36-1/2 feet has also been estimated by extrapolation from existing antennas on the assumption that the weight varies as the three-halves power of the aperture area.

Antenna Type	Weight	Scaling Factor	Estimated Weight
SX	240 lbs.	$\left(\frac{14\frac{1}{2}}{5} \times \frac{36\frac{1}{2}}{15}\right)^{3/2}$	4500 lbs.
SC/R	200	$\left(\frac{14\frac{1}{2}}{7\frac{1}{2}} \times \frac{36\frac{1}{2}}{14}\right)^{3/2}$	2300
AN/CPS-5	1000	$\left(\frac{14\frac{1}{2}}{14} \times \frac{36\frac{1}{2}}{25}\right)^{3/2}$	1850
Giant Wurzburg	1400	$\left(\frac{14\frac{1}{2}}{25} \times \frac{36\frac{1}{2}}{25}\right)^{3/2}$	1100

Finally, the weight has been estimated by the Raytheon Mfg. Co., under contract to build an experimental XDQ antenna, as between 1500 and 2000 lbs. This design is based on an expanded aluminum screen of 3/4 x 1-1/2-inch mesh.

* * *

This page intentionally left blank.

APPENDIX III

Evaluation of Diffraction Pattern Integral

To evaluate the integral

$$F(u_1,u_2) = \int_{-a}^{a}\int_{-b\sqrt{1-(\frac{x}{a})^2}}^{b\sqrt{1-(\frac{x}{a})^2}}\left(\sum_{r=o}^{m} a_r\cos r\pi\frac{x}{a}\right)\left(\sum_{s=o}^{n} b_s\cos s\pi\frac{y}{b}\right)e^{i\left[u_1\frac{x}{a}+u_2\frac{y}{b}\right]}dy\,dx \qquad (31)$$

Let $x/a = \xi$, $y/b = \eta$, and transform to

$$F(u_1, u_2) = 4ab\int_0^1\int_0^{\sqrt{1-\xi^2}}\left(\sum_0^m a_r\cos r\pi\xi\right)\cos u_1\xi\left(\sum_0^n b_s\cos s\pi\eta\right)\cos u_2\eta\, d\eta d\xi \qquad (32)$$

The integration in η is then carried out

$$F(u_1, u_2) = 2ab\int_0^1\left(\sum_0^m a_r\cos r\pi\xi\right)\cos u_1\xi\ \Sigma b_s\left[\frac{\sin(s\pi-u_2)\sqrt{1-\xi^2}}{s\pi-u_2}+\frac{\sin(s\pi+u_2)\sqrt{1-\xi^2}}{s\pi+u_2}\right]d\xi. \qquad (33)$$

Replace ξ by $\sin\theta$, $d\xi$ by $\cos\theta\, d\theta$, and use the identity

$$2\cos r\pi\xi\cdot\cos u_1\xi = \cos(r\pi-u_1)\xi+\cos(r\pi+u_1)\xi$$

to obtain

$$F(u_1, u_2) = ab\int_0^{\pi/2}\sum_0^m\sum_0^n a_r b_s\left\{\left[\cos[(r\pi-u_1)\sin\theta]+\cos[(r\pi+u_1)\sin\theta]\right]\times\right.$$
$$\left.\left[\frac{\sin[(s\pi-u_2)\cos\theta]}{s\pi-u_2}+\frac{\sin[(s\pi+u_2)\cos\theta]}{s\pi+u_2}\right]\right\}\cos\theta\ d\theta. \qquad (34)$$

It is shown below that

$$\int_0^{\pi/2}\cos(p_1\sin\theta)\frac{\sin(p_2\cos\theta)}{p_2}\cos\theta\ d\theta = \frac{\pi}{4}\Lambda_1\left(\sqrt{p_1^2+p_2^2}\right) \quad . \qquad (35)$$

The substitution of Equation (35) into (34) leads directly to formulas (14) and (15) of the text.

To establish Equation (35), note that the integrand, which may be denoted by $f(\theta)$, is an even function, so that its integral from 0 to $\pi/2$ is just half the integral from $-\pi/2$

to $+\pi/2$. Further, $f(\theta+\pi) = f(\theta)$, and the integral may be written

$$\frac{1}{4}\int_{-\frac{\pi}{2}}^{\frac{3\pi}{2}} f(\theta)\, d\theta\ .$$

If θ is replaced by $(\theta - \pi/2)$, the interval can be changed to $(0,2\pi)$:

$$\frac{1}{4}\int_{0}^{2\pi} \cos(p_1 \cos\theta)\,\frac{\sin(p_2 \sin\theta)}{p_2}\ \sin\theta\, d\theta.$$

Let

$$p_1 = p\sin\gamma;\ p_2 = \cos\gamma$$

where $$p = \sqrt{p_1^2 + p_2^2};\quad \tan\gamma = p_1/p_2.$$

Then by a trigonometric simplification, the integral becomes

$$\frac{1}{8p_2}\int_{0}^{2\pi} \left\{\sin\left[p\sin(\theta+\gamma)\right] + \sin\left[p\sin(\theta-\gamma)\right]\right\}\sin\theta\, d\theta. \tag{36}$$

But

$$\sin\left[p\sin(\theta+\gamma)\right] = 2\left\{J_1(p)\sin(\theta+\gamma) + J_3(p)\sin 3(\theta+\gamma) + \ldots\right\}$$

When this infinite series is multiplied by $\sin\theta$ and integrated from 0 to 2π, the only non-vanishing term is the one containing $\sin\theta$, and its contribution is

$$2\pi\, J_1(p)\cos\gamma.$$

The second term of Equation (36) leads to the same result, so that the value of the integral in Equation (35) is

$$\frac{\pi}{2p_2}\ J_1(p)\cos\gamma = \frac{\pi}{2}\ \frac{J_1(p)}{p} = \frac{\pi}{4}\ \Lambda_1(p). \tag{37}$$

* * *